# Analyses and Historical Reconstruction of Groundwater Flow, Contaminant Fate and Transport, and Distribution of Drinking Water Within the Service Areas of the Hadnot Point and Holcomb Boulevard Water Treatment Plants and Vicinities, U.S. Marine Corps Base Camp Lejeune, North Carolina

## Chapter A–Supplement 7
## Source Characterization and Simulation of the Migration of Light Nonaqueous Phase Liquids (LNAPLs) in the Vicinity of the Hadnot Point Industrial Area


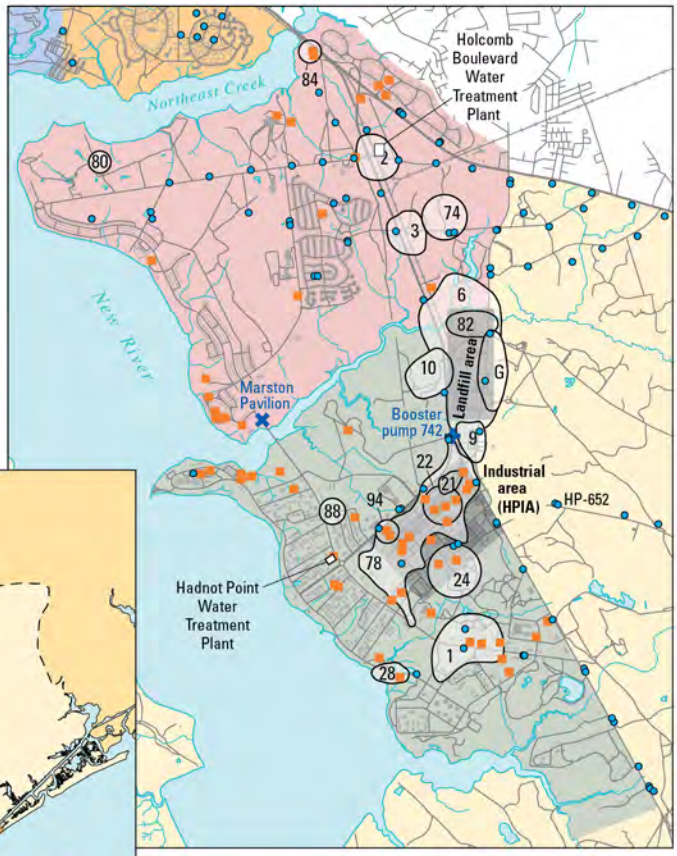


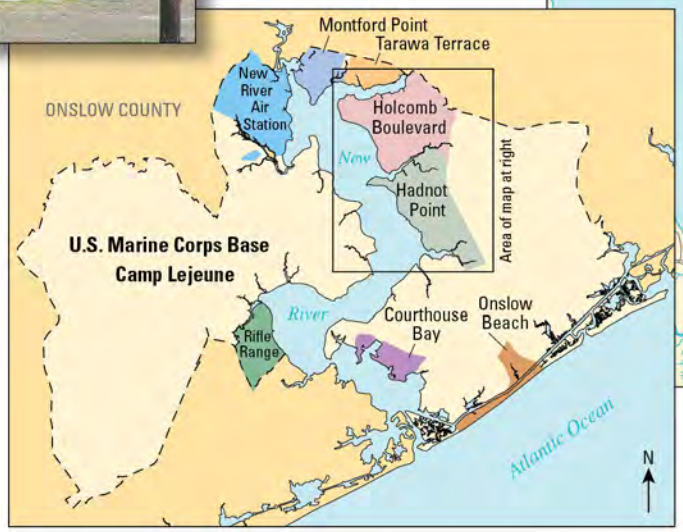


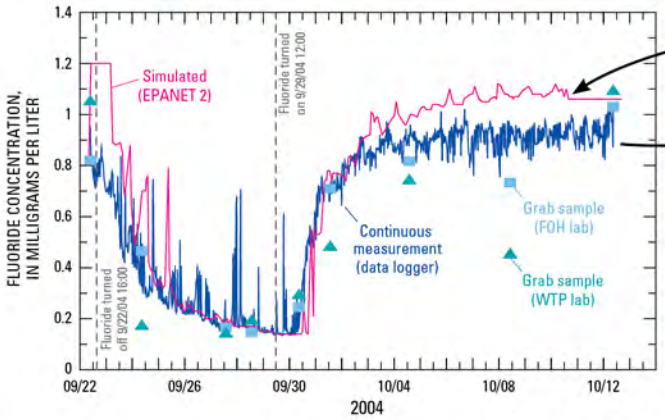


ATSDR
AGENCY FOR TOXIC SUBSTANCES AND DISEASE REGISTRY

Atlanta, Georgia – March 2013

***Front cover:*** Historical reconstruction process using data, information sources, and water-modeling techniques to estimate historical contaminant concentrations.

*Maps:* U.S. Marine Corps Base Camp Lejeune, North Carolina; Holcomb Boulevard and Hadnot Point areas showing extent of sampling at Installation Restoration Program sites (white numbered areas), above-ground and underground storage tank sites (orange squares), and water-supply wells (blue circles).

*Photograph (upper):* Hadnot Point water treatment plant (Building 20).

*Photograph (lower):* Well house building for water-supply well HP-652.

*Graph:* Measured fluoride data and simulation results for Paradise Point elevated storage tank (S-2323) for tracer test of the Holcomb Boulevard water-distribution system, September 22–October 12, 2004; simulation results obtained using EPANET 2 water-distribution system model assuming last-in first-out plug flow (LIFO) storage tank mixing model. [WTP lab, water treatment plant water-quality laboratory; FOH lab, Federal Occupational Health Laboratory]

# Analyses and Historical Reconstruction of Groundwater Flow, Contaminant Fate and Transport, and Distribution of Drinking Water Within the Service Areas of the Hadnot Point and Holcomb Boulevard Water Treatment Plants and Vicinities, U.S. Marine Corps Base Camp Lejeune, North Carolina

## Chapter A–Supplement 7
## Source Characterization and Simulation of the Migration of Light Nonaqueous Phase Liquids (LNAPLs) in the Vicinity of the Hadnot Point Industrial Area

By Wonyong Jang, Barbara A. Anderson, Rene J. Suárez-Soto, Mustafa M. Aral, and Morris L. Maslia

Agency for Toxic Substances and Disease Registry
U.S. Department of Health and Human Services
Atlanta, Georgia

March 2013


ATSDR
AGENCY FOR TOXIC SUBSTANCES AND DISEASE REGISTRY

# Authors

**Wonyong Jang, PhD, PE**
*Senior Research Engineer*
Georgia Institute of Technology
School of Civil and Environmental Engineering
Multimedia Environmental Simulations Laboratory
Atlanta, Georgia

**Barbara A. Anderson, MSEnvE, PE**
*Environmental Health Scientist*
Agency for Toxic Substances and Disease Registry
Division of Community Health Investigations
Atlanta, Georgia

**René J. Suárez-Soto, MSEnvE, EIT**
*Environmental Health Scientist*
Agency for Toxic Substances and Disease Registry
Division of Community Health Investigations
Atlanta, Georgia

**Mustafa M. Aral, PhD, PE, Phy**
*Director and Professor*
Georgia Institute of Technology
School of Civil and Environmental Engineering
Multimedia Environmental Simulations Laboratory
Atlanta, Georgia

**Morris L. Maslia, MSCE, PE, D.WRE, DEE**
*Research Environmental Engineer and Project Officer*
Agency for Toxic Substances and Disease Registry
Division of Community Health Investigations
Atlanta, Georgia

For additional information write to:

Project Officer
Exposure-Dose Reconstruction Project
Division of Community Health Investigations
Agency for Toxic Substances and Disease Registry
4770 Buford Highway, Mail Stop F-59
Atlanta, Georgia 30341-3717

**Suggested citation**

Jang W, Anderson BA, Suárez-Soto RJ, Aral MM, and Maslia ML. Source Characterization and Simulation of the Migration of Light Nonaqueous Phase Liquids (LNAPLs) in the Vicinity of the Hadnot Point Industrial Area—Supplement 7. In: Maslia ML, Suárez-Soto RJ, Sautner JB, Anderson BA, Jones LE, Faye RE, Aral MM, Guan J, Jang W, Telci IT, Grayman WM, Bove FJ, Ruckart PZ, and Moore SM. Analyses and Historical Reconstruction of Groundwater Flow, Contaminant Fate and Transport, and Distribution of Drinking Water Within the Service Areas of the Hadnot Point and Holcomb Boulevard Water Treatment Plants and Vicinities, U.S. Marine Corps Base Camp Lejeune, North Carolina—Chapter A: Summary and Findings. Atlanta, GA: Agency for Toxic Substances and Disease Registry; 2013.

# Contents

# Figures

## Tables

# Abbreviations and Mathematical Symbols

Conversion factors and definitions of common terms and abbreviations used throughout the Chapter A report series are listed in the front of the Chapter A report. Definition of terms and abbreviations that are specific to this report are listed below.

**—A—**

AAN-Well Semi-analytical method for LNAPL volume estimation using apparent LNAPL thickness

**—C—**

$C$ Contaminant concentration [$ML^{-3}$]

**—D—**

$\boldsymbol{D}$ Dispersion tensor [$L^2T^{-1}$]

$D_{gwn}$ Depth to the top boundary of an LNAPL pool in the soil

$D_{gn}$ Depth to a gas–LNAPL interface within an LNAPL pool in the soil

$D_{nw}$ Depth to an LNAPL–water interface at the bottom of an LNAPL pool in the soil

$D_{well}^{gn}$ Depth to a gas–LNAPL interface in a monitoring well

$D_{well}^{nw}$ Depth to an LNAPL–water interface in a monitoring well

**—E—**

$e_z$ Unit vector in the positive $z$-direction

**—F—**

$f$ Mobile fluid

**—G—**

$g$ Gravitational constant [$LT^{-2}$]

**—H—**

HSSM Semi-analytical hydrocarbon spill screening model (Weaver et al. 1996)

HSSM-KO The LNAPL transport module of HSSM (Weaver et al. 1996)

**—I—**

$I_{BT}$ Bio-transformation of contaminants between phases [$ML^{-3}T^{-1}$]

$I_{MT}$ Partitioning processes of contaminants between phases [$ML^{-3}T^{-1}$]

$I_{source}$ Source/sink [$ML^{-3}T^{-1}$]

IML++ Iterative sparse matrix solver

**—K—**

$\boldsymbol{k}$ Intrinsic permeability tensor for soil media [$L^2$]

$k_r$ Relative permeability

$K_D$ Sorption coefficient [$L^3M_{soil}^{-1}$]

**—N—**

NI-Soil Numerical integration method for LNAPL volume estimation using real LNAPL thickness

NI-Well Numerical integration method for LNAPL volume estimation using apparent LNAPL thickness

**—P—**

$P$ Phase pressure [$ML^{-1}T^{-2}$]

PARDISO Pardiso sparse matrix solver

**—Q—**

$\boldsymbol{q}$ Darcy flux [$LT^{-1}$]

$Q$ Strength of sources/sinks [$T^{-1}$]

**—S—**

$S$ Degree of saturation, typically combined with a subscript indicating the fluid phase (i.e., $w$, water; $g$, gas; or $n$, non-aqueous phase liquid)

$S$-$cP$ Saturation-capillary pressure

SpillCAD Data management and decision support model for hydrocarbons spills (ES&T 1993)

**—T—**

$t$ Time [$T$]

TechFlowMP Three-dimensional multispecies, multiphase mass transport model developed by the Multimedia Environmental Simulations Laboratory at the Georgia Institute of Technology, Atlanta, Georgia

TechNAPLVol LNAPL volume estimation code developed by the Multimedia Environmental Simulations Laboratory at the Georgia Institute of Technology, Atlanta, Georgia

$T_{soil}^{w+n}$ Thickness of liquid-saturated zone in the soil

$T_{well}^{n}$ LNAPL thickness in a monitoring well

**—V—**

$v$ Pore velocity of mobile fluid

$V_{napl}$ Volume of LNAPL

VSZ Variably saturated zone

**—Z—**

$Z_{gwn}$ Elevation of the top boundary of an LNAPL pool

$Z_{gn}$ Elevation of gas–LNAPL interface within an LNAPL pool

$Z_{nw}$ Elevation of LNAPL–water interface at the bottom of an LNAPL pool

**—Other mathematical symbols—**

$x, y, z$ Directions in a Cartesian coordinate system

$\alpha$ Surface tension

$\alpha_L$ Longitudinal dispersivity of soil media

$\alpha_T$ Transversal dispersivity of soil media

$\beta$ Fluid-pair-dependent scaling coefficient

$\delta$ Kronecker delta

$\lambda$ First-order coefficient of mass transfer [$T^{-1}$]

$\mu$ Dynamic viscosity [$ML^{-1}T^{-1}$]

$\rho$ Density [$ML^{-3}$]

$\tau$ Tortuosity of porous media

$\phi$ Porosity (dimensionless)

$\psi$ Water-equivalent pressure head [$L$]

$\psi_c$ Inter-phase capillary pressure head [$L$]

# Analyses and Historical Reconstruction of Groundwater Flow, Contaminant Fate and Transport, and Distribution of Drinking Water Within the Service Areas of the Hadnot Point and Holcomb Boulevard Water Treatment Plants and Vicinities, U.S. Marine Corps Base Camp Lejeune, North Carolina

## Chapter A–Supplement 7
## Source Characterization and Simulation of the Migration of Light Nonaqueous Phase Liquids (LNAPLs) in the Vicinity of the Hadnot Point Industrial Area

By Wonyong Jang,[1] Barbara A. Anderson,[2] Rene J. Suárez-Soto,[2] Mustafa M. Aral,[3] and Morris L. Maslia[2]

## Introduction

As outlined in Maslia et al. (2013), the Agency for Toxic Substances and Disease Registry (ATSDR) is conducting epidemiological studies to evaluate the potential for health effects from exposures to volatile organic compounds (VOCs) in finished water[4] supplied to family housing units at U.S. Marine Corps Base (USMCB) Camp Lejeune in North Carolina. The core study period for the epidemiological studies is 1968–1985. Because historical exposure data—measured contaminant concentrations in finished water—are limited, ATSDR is using water modeling techniques to reconstruct the history of contaminants in the groundwater, in selected water-supply wells, and in associated water-distribution systems.

For the overall project, the area of interest is the entire Hadnot Point–Holcomb Boulevard (HPHB) study area (Figures A1 and A12 in Maslia et al. 2013). The focus for the modeling and analyses described in this report is an area of the Base designated the Hadnot Point Industrial Area (HPIA; Figure S7.1). Various fuels, solvents, and other chemicals were stored, used, and inadvertently released during routine operations in the HPIA. Of particular interest in this study is the historical presence and subsequent fate and transport of subsurface light nonaqueous phase liquid (LNAPL) associated with fuel storage system releases in the HPIA. Results from the analyses described herein are integrated with the results from other models and approaches as part of the overall project objective to produce estimates and uncertainty bounds for the concentration of contaminants over time in selected water-supply wells and water-distribution systems.

[1] Georgia Institute of Technology, School of Civil and Environmental Engineering, Multimedia Environmental Simulations Laboratory, Atlanta, Georgia; now with Itasca Denver, Inc., Lakewood, Colorado.

[2] Agency for Toxic Substances and Disease Registry, Atlanta, Georgia.

[3] Georgia Institute of Technology, School of Civil and Environmental Engineering, Multimedia Environmental Simulations Laboratory, Atlanta, Georgia.

[4] For this study, finished water is defined as groundwater that has undergone treatment at a water treatment plant and was subsequently delivered to a family housing unit or other facility. Throughout this report, the term finished water is used in place of terms such as finished drinking water, drinking water, treated water, or tap water.

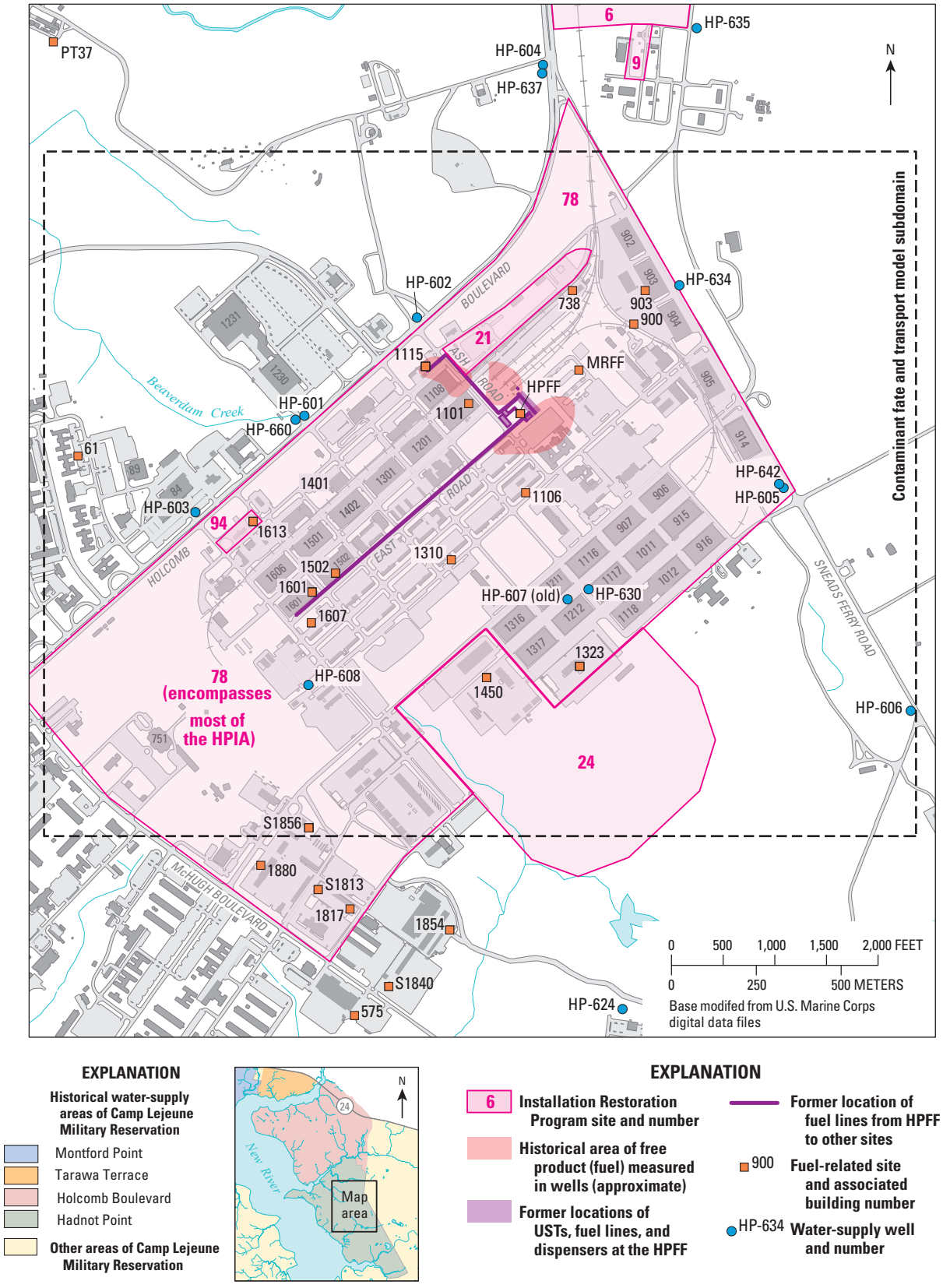


**Figure S7.1.** Hadnot Point Industrial Area (HPIA) and vicinity, selected water-supply wells, fuel-related sites, and contaminant fate and transport model subdomain boundary, Hadnot Point–Holcomb Boulevard study area, U.S. Marine Corps Base Camp Lejeune, North Carolina. [HPFF, Hadnot Point fuel farm; MRFF, Michael Road fuel farm; UST, underground storage tank]

## Objectives

The objectives of this study are to

1. investigate the migration and distribution of fuel-related LNAPL released in the unsaturated zone above a shallow aquifer for a hypothetical scenario,
2. estimate the volume and distribution of LNAPL in the subsurface at the HPIA using historical field data for LNAPL (free product) thickness measured over time in site monitor wells, and
3. analyze the dissolution of benzene and total xylenes from the LNAPL source areas and the subsequent dissolved phase fate and transport of these contaminants under unsteady hydrologic conditions (variable water-supply well pumping) in the underlying groundwater system within the HPIA.

The purpose of the hypothetical scenario is to illustrate and explore the behavior of LNAPL in a multiphase environment and provide insight about the potential variability of results involving LNAPL movement. LNAPL movement is just one component of the overall fate and transport process for the applied analysis at the HPIA. For the HPIA analysis, LNAPL movement and estimates of LNAPL distribution in soil are integrated within the TechFlowMP model with the LNAPL dissolution process and subsequent transport of the dissolved phase contaminants in the groundwater. The ultimate goal of the integrated analysis is to evaluate contaminant arrival at water-supply wells in the area.

Modeling tools used for multiphase flow and multispecies transport in the subsurface included public-domain and newly developed codes, including HSSM[5] [a semi-analytical model developed by the U.S. Environmental Protection Agency (USEPA)], MODFLOW-2005[5] [a three-dimensional finite-difference groundwater-flow model developed by the U.S. Geological Survey (USGS)], TechNAPLVol[6] (an LNAPL volume estimation model), and TechFlowMP[6] (a multiphase flow and multispecies contaminant transport model). The HSSM and TechFlowMP models were used to investigate the migration of LNAPL in the unsaturated zone and at the water table and to explore the distribution of LNAPL saturation in soil over time. Using LNAPL thickness data measured in monitor wells, the TechNAPLVol model code was used to estimate the spatial distribution of LNAPL saturation and the volume of LNAPL in a three-dimensional subsurface domain within the HPIA. The TechFlowMP model used the saturation profiles from the LNAPL analysis as a starting point for modeling the dissolution of benzene and total xylenes from free-phase LNAPL and the subsequent fate and transport of dissolved phase benzene and total xylenes in the underlying groundwater system.

## Background

USMCB Camp Lejeune is a military base located in the Coastal Plain of North Carolina, in Onslow County, southeast of the City of Jacksonville (Figure S7.1; Figure A1 in Maslia et al. 2013). Operations began at USMCB Camp Lejeune during the 1940s. The Base covers approximately 236 square miles and includes 14 miles of coastline. The HPIA, located in the central interior of the Base, has historically included maintenance shops, refueling stations, administrative offices, printing shops, warehouses, painting shops, storage yards, a steam generation plant, and other light industrial facilities. Historical groundwater contamination in the HPIA occurred as a result of the storage, use, and inadvertent releases of fuels, such as gasoline and diesel, and various chlorinated solvents, including trichloroethylene and tetrachloroethylene (Baker Environmental, Inc. 1999). A brief history of contaminated sites identified within the HPIA and a summary of the environmental site investigations and remediation activities conducted within the HPIA are provided in Faye et al. (2010) and Faye et al. (2012). Relevant information about the geohydrologic framework of the area is provided in Faye (2012).

[5] Public-domain software.

[6] Specialized model code developed by the Multimedia Environmental Simulations Laboratory at the School of Civil and Environmental Engineering, Georgia Institute of Technology. Refer to Maslia et al. (2013), "Availability of Input Data Files, Models, and Simulation Results" for details.

## Fuel-Related Sites Within the Hadnot Point Industrial Area (HPIA)

There are numerous sites within the HPIA that stored or dispensed fuel (Figure S7.1). Based on historical environmental investigations, three of these fuel-related sites had significant subsurface LNAPL contamination: (1) the Hadnot Point fuel farm (HPFF), (2) the Building 1115 fuel service station, and (3) the Building 1613 fuel service station. Each of these sites maintained multiple underground storage tank (UST) systems containing primarily gasoline, although records indicate at least one tank may have held kerosene:

- Fourteen USTs (5,000–12,000 gallon [gal] capacity) were installed at the HPFF in 1941 (O'Brien and Gere Engineers, Inc. 1988; CH2M HILL, Inc. 2001). There were also at least five 1,000-gal USTs associated with above-ground fuel dispenser islands at the site. The UST system piping at the HPFF was extensive and included a bank of fill piping to the north of the site to offload fuel from incoming rail cars; a piping manifold that interconnected the main storage tanks; numerous piping runs, fittings, and associated components that connected the main storage tanks to the 1,000-gal USTs associated with the dispenser islands; a 3-inch-diameter fuel pipeline along Ash Road connecting the HPFF to the Building 1115 USTs; and a 4-inch-diameter fuel pipeline along East Road connecting the HPFF to USTs at Buildings 1502 and 1601 (CH2M HILL, Inc. 2001; OHM Remediation Services Corp. 2001).
- Seven USTs (1,000–5,000 gal capacity) were installed at the Building 1115 area in 1942 (CH2M HILL, Inc. 2001). The site also had multiple above-ground fuel dispensers for vehicle refueling.
- Four USTs (9,000–30,000 gal capacity) were installed at Building 1613 in the 1950s (Richard Catlin and Associates, Inc. 1996, 1998). The site also had multiple above-ground fuel dispensers for vehicle refueling.

Historical environmental investigations confirmed the presence of fuel-related subsurface LNAPL at each of these sites. Consequently, various free product recovery systems, air sparge/soil vapor recovery networks, and other remediation systems were installed and operated to clean up the free-phase LNAPL and resulting dissolved phase contaminant plumes in the groundwater at these sites (O'Brien & Gere Engineers, Inc. 1990; Richard Catlin and Associates, Inc. 1996; OHM Remediation Services Corp. 2000; CH2M HILL, Inc. 2001; Shaw Environmental, Inc. 2009).The HPFF and Building 1115 UST systems were interconnected by an underground pipeline, and subsurface LNAPL contamination and dissolved phase benzene plumes in groundwater are commingled for these two sites (Figure S7.1). Therefore, for the purposes of this report, the HPFF site and the Building 1115 site are often collectively referred to as the "HPFF area."

Detailed site histories, summaries of environmental investigations and remediation activities, and associated data and information for monitor well installations, soil and groundwater sample collection, and soil and groundwater analytical results for the HPFF area sites and Building 1613 are provided in Faye et al. (2010) and Faye et al. (2012). Note that these reports, Maslia et al. (2013), and other historical documentation often refer to the sites using designations from the Installation Restoration Program: the Installation Restoration Site 22 is the HPFF, and Installation Restoration Site 94 is the Building 1613 site.

## Theoretical Framework for Numerical Analyses and Modeling

Nonaqueous phase liquids (NAPLs) are hydrocarbon liquids such as fuel oil, gasoline, and dry cleaning fluids, which exist as a separate, immiscible phase when in contact with water and/or air. Surface spills and leakage of NAPLs associated with human activities are a significant source of groundwater contamination. Based on liquid density, NAPLs are classified into light and dense nonaqueous phase liquids. Light nonaqueous phase liquids (LNAPLs), including hydrocarbon fuel constituents such as benzene, toluene, ethylbenzene, and xylenes (BTEX), have densities less than that of water. Dense nonaqueous phase liquids (DNAPLs), including chlorinated hydrocarbons such as trichloroethylene (TCE) and tetrachloroethylene (PCE), have densities greater than that of water (Newell et al. 1995). This study is concerned with LNAPL associated with hydrocarbon fuel releases from UST systems.

Once LNAPL is released into the subsurface, it moves downward due to gravity through the unsaturated zone until it reaches the water table. At the water table, LNAPL tends to mound above the water-saturated zone and spread out laterally, resulting in a pool or lens of free-phase LNAPL on top of the water table (Figure S7.2) (ASTM 2007). The hydraulic gradient or slope of the water table can generate a pressure gradient for the LNAPL phase, becoming a driving force for the migration of LNAPL (Brost and DeVaull 2000). The movement of LNAPL depends on a variety of factors, including phase saturation, hydraulic gradients, fluid density, viscosity, and displacement entry pressure. When mobile LNAPL migrates, its volume is usually depleted as some fraction of LNAPL is left behind in soil pore spaces due to surface-tension effects (Falta et al. 1989). The entrapped LNAPL becomes immobile residuals in the soil matrix. The depletion of mobile LNAPLs volume in this manner will reduce its relative permeability and, subsequently, the pressure

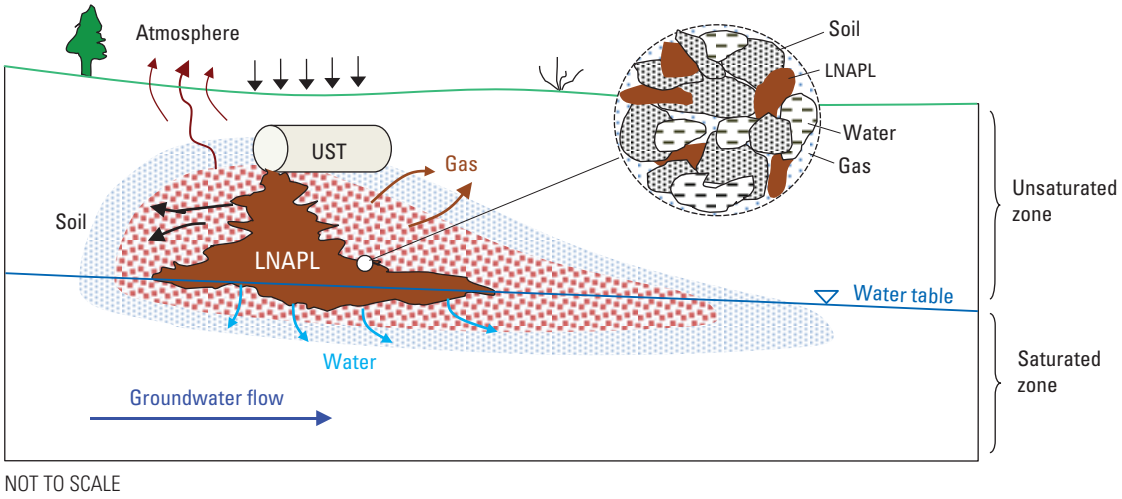


**Figure S7.2.** Subsurface light nonaqueous phase liquid (LNAPL) contamination scenario.
[UST, underground storage tank]

gradient that drives its movement. Thus, the migration of LNAPL can be limited by this depletion mechanism. LNAPL migration can also be limited by physical barriers such as low permeability soil zones (Brost and DeVaull 2000). Over time, LNAPL released in the subsurface will become stationary when hydraulic equilibrium is reached. Stabilization of mobile LNAPL is often reached within 3 to 10 years (Golder Associates 2008; Hawthorne and Kirkman 2011).

When LNAPL is present, the subsurface becomes a multiphase environment consisting of water, LNAPL, and gas phases. The distribution of free-phase LNAPL in the subsurface depends on the pressures of the multiple phases and the properties of the soil matrix and the LNAPL, including porosity, residual water saturation, and surface tension. In the unsaturated and saturated zones, water and LNAPL can coexist in pore spaces of the soil matrix. Under the assumption of a vertical hydraulic equilibrium (or a hydrostatic condition), water and LNAPL saturation profiles can be evaluated using the saturation–capillary pressure ($S-cP$) relations of water–air (or gas)–LNAPL phases (Farr et al. 1990; Lenhard and Parker 1990). The capillary pressure curves describing the $S-cP$ relations require the site-specific fluid densities and surface and interfacial tensions for the water–air–LNAPL combination. At contaminated sites, the distribution of an LNAPL in the subsurface can be estimated using direct core boring samples, cone penetrometer, and geophysical methods for hydrocarbon characterization, including electrical, magnetic, and ground-penetrating radars (Chiang et al. 1992; Newell et al. 1995; Shoop et al. 1996; Kechavarzi et al. 2000; Moroizumi and Sasaki 2008). Monitor wells are often installed at contaminated sites, and LNAPL thickness measured within the wells can be used to estimate the distribution and volume of LNAPL in the soil (Farr et al. 1990; Lenhard and Parker 1990; Lundegard and Mudford 1998).

Immobile LNAPL trapped in the soil matrix will act as a long-term source of contamination as LNAPL constituents dissolve into the groundwater and volatilize into the gas phase until the LNAPL is depleted (Figure S7.2). Fate and transport of dissolved LNAPL chemicals in the aquifer can occur as a result of advection, dispersion/diffusion, partitioning, and biological transformations. In general, advective groundwater flow plays a dominant role in the development of dissolved contaminant plumes (Mendoza and Frind 1990; Auer et al. 1996; Jang and Aral 2007b). LNAPL constituents such as BTEX can be biologically degraded by indigenous microorganisms in the groundwater system under aerobic and anaerobic conditions (Barbaro et al. 1992; Davis et al. 1994; Agency for Toxic Substances and Disease Registry 1995, 2000; Alagappan and Cowan 2004; Andreoni and Gianfreda 2007; Lawrence 2007).

## Multiphase Flow

Multiphase flow in the subsurface refers to the simultaneous flow of groundwater, NAPL, and gas through a porous soil matrix. The generalized governing equation describing the unsteady state flow of water, NAPL, and gas (air) in porous media can be written as follows (Abriola 1989; Rathfelder et al. 2000; Jang and Aral 2007)

$$\frac{\partial\left(\phi S_f \rho_f\right)}{\partial t} + \nabla\cdot\left(\rho_f \boldsymbol{q}_f\right) = I_f + Q_f \ , \tag{S7.1}$$

where

$f$ denotes the fluid phases ($w$ for water, $g$ for gas, or $n$ for NAPL phase),
$\phi$ is the porosity (i.e., total void fraction in a soil matrix is equal to pore volume/bulk volume),
$S_f$ is the fluid saturation of $f$ phase (i.e., $f$ phase volume/pore volume),
$\rho_f$ is the mass density of $f$ phase ($M/L^3$),
$\boldsymbol{q}_f$ is the Darcy flux vector of $f$ phase ($L/T$),
$I_f$ is the rate of inter-phase mass transfer between phases ($M/L^3T$), and
$Q_f$ is the external supply (source/sink) of mass of fluid phase, $f$ ($M/L^3T$) .

In the unsaturated zone, the conventional three-phase flow expressed in Equation S7.1 can be simplified by assuming that the pressure gradient in the soil gas is negligible and the gas pressure remains constant at atmospheric pressure (Faust 1985; Parker et al. 1987; Forsyth et al. 1998; Wu and Forsyth 2001). In addition, it is typically assumed that porous soil media and liquid fluids, i.e., water and NAPLs, are incompressible in shallow aquifers.

In multiphase fluid flow, hydraulic conductivity is a function of fluid saturation, resulting in a nonlinear equation. This nonlinearity has been expressed by a dimensionless relative permeability coefficient, which is also a function of fluid saturation. The generalized form of Darcy's law for multiphase flow is with

$$\boldsymbol{q}_f = -\frac{\mathbf{k}k_{rf}}{\mu_f}\rho_w\, g\cdot\left(\nabla\psi_f - \left(\frac{\rho_f}{\rho_w}\right)e_z\right) \ , \tag{S7.2}$$

$$\psi_f = \frac{P_f}{\rho_w g} \ , \tag{S7.3}$$

where

$\mathbf{k}$ is the intrinsic permeability tensor ($L^2$),
$k_{rf}$ is the relative permeability of $f$ phase in a porous medium,
$\mu_f$ is the dynamic viscosity of $f$ phase ($M/LT$),
$\rho_w$ is the water density ($M/L^2$),
$g$ is the value of gravitational acceleration ($L/T^2$),
$\psi_f$ is the water-height equivalent pressure head ($L$),
$P_f$ is the pressure in $f$ phase ($M/LT^2$), and
$e_z$ denotes a unit vector in the positive $z$-direction in the Cartesian coordinates.

For dimensional convenience, water-height equivalent pressure heads rather than pressures are used. For multiphase flow, Equation S7.1 is linked by capillary pressures existing at interfaces between phases and phase saturation within a soil matrix. The capillary pressures between phases are expressed as follows (Sleep and Sykes 1989; Sale 2001)

$$\psi_{cgw} = \psi_g - \psi_w \ , \tag{S7.4a}$$

$$\psi_{cnw} = \psi_n - \psi_w \ , \tag{S7.4b}$$

$$\psi_{cgn} = \psi_g - \psi_n \ , \tag{S7.4c}$$

where

$\psi_{cgw}$ is the gas–water capillary pressure head;
$\psi_{cnw}$ is the NAPL–water capillary pressure head;
$\psi_{cgn}$ is the gas–NAPL capillary pressure head; and
$\psi_g, \psi_w, \psi_n$ are the pressure heads of gas, water, and NAPL phases, respectively.

The volumetric saturation of three phases (i.e., water, gas, and NAPL) are related by

$$S_w + S_g + S_n = 1 \,, \tag{S7.5}$$

where

$S_w, S_g, S_n$ are the saturation of water, gas, and NAPL phases, respectively.

NAPL saturation $S_n$, which is nonzero only in the region containing NAPL phase, can be specified as an initial condition. The magnitude of NAPL saturation can decrease with time as a result of migration, dissolution, and volatilization. The dissolution NAPL constituents will lead to the reduction in the mass of NAPL as the constituents are transferred into the dissolved phase in groundwater. The dissolution of NAPL can be described with a first-order kinetic,

$$I_n = -\phi S_w \lambda_D (C_{we} - C_w) \,, \tag{S7.6}$$

where

$\lambda_D$ is the first-order coefficients ($T^{-1}$) for dissolution of a NAPL contaminant and
$C_{we}$ and $C_w$ are the maximum (or equilibrium) and current concentrations ($ML^{-3}$) of the contaminant in the groundwater, respectively.

The aforementioned mathematical framework for mulitphase flow was developed for a general case of NAPL. As discussed in the Background section of this report, sites within the HPIA had significant fuel-related subsurface contamination. Therefore, because these fuel products are lighter (less dense) than water, from this point forward, all NAPL terms refer specifically to light nonaqeous phase liquids or LNAPLs.

## Capillary Pressure and Phase Saturation

In a hydrostatic condition, hydraulic head of the groundwater is constant regardless of elevation, while water pressure varies with elevation (Figure S7.3). In the unsaturated zone without LNAPL present, the water pressure above the water table has negative values, but the air pressure is nearly constant at zero (atmospheric pressure).

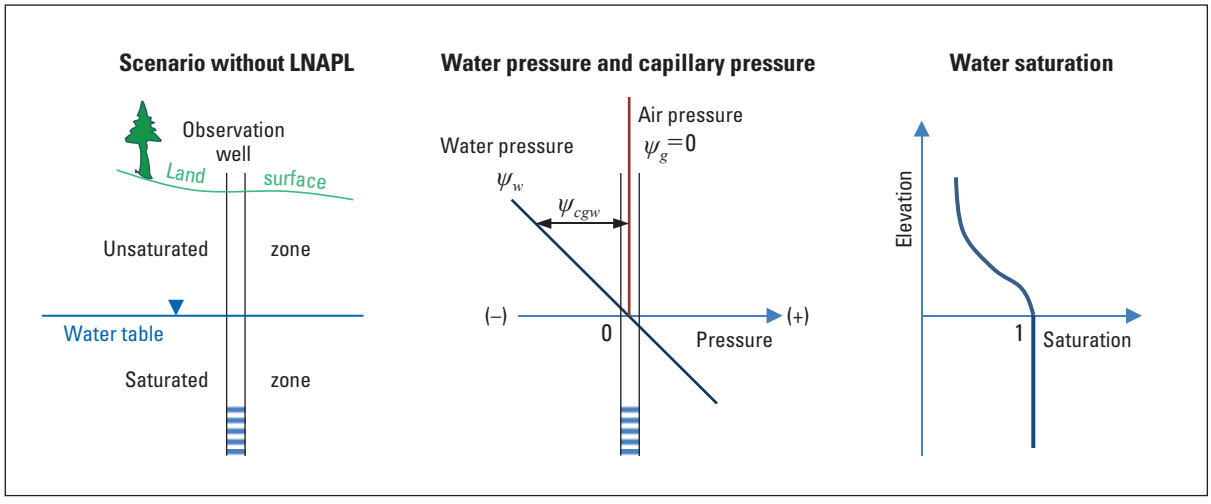


**Figure S7.3.** Water pressure, capillary pressure, and water saturation in an aquifer in the absence of light nonaqueous phase liquid (LNAPL). [See text or Glossary for definition of mathematical symbols]

At contaminated sites, the presence of LNAPL has an effect on the elevation of the water table due to the pressure the LNAPL exerts. The subsurface environment becomes a three-phase system consisting of water, gas, and LNAPL phases (Figure S7.4). The vertical pressure profiles of water and LNAPL are shown in Figure S7.4. In the presence of LNAPL, the capillary pressure heads of phases at the interfaces are written in Equation S7.4. The capillary pressure and LNAPL saturation profiles vary with elevation, as described in Equations S7. 7 and S7. 8. The gas phase in the unsaturated zone is connected with the atmosphere, thus its pressure is assumed to be equal to the constant atmospheric pressure (i.e., $\psi_g=0$).

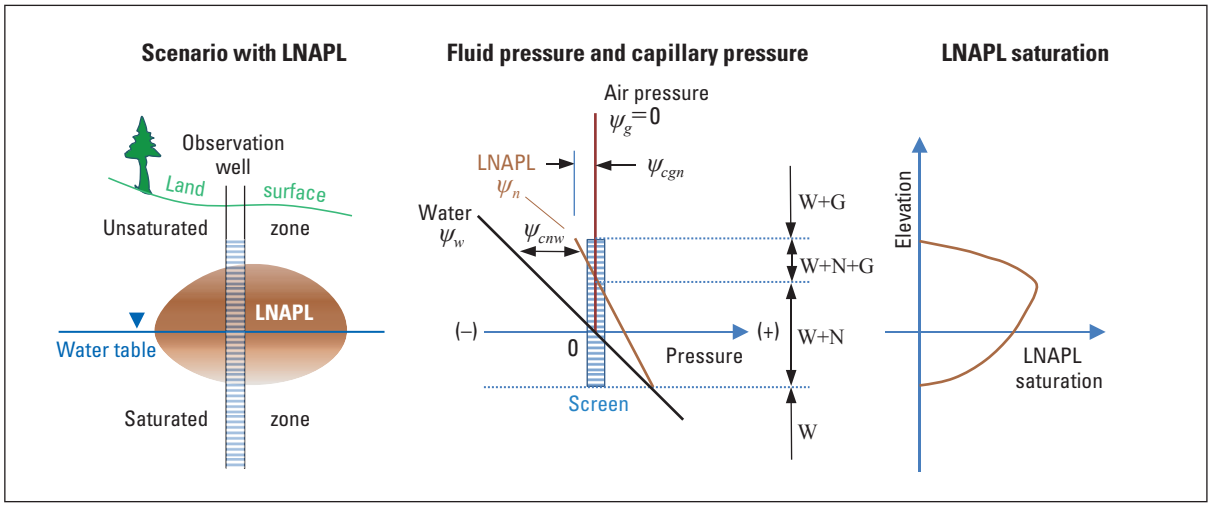


**Figure S7.4.** Pressure distributions of water and free-phase light nonaqueous phase liquid (LNAPL) at the water table (after Charbeneau and Adamski 2011). [W, water; N, LNAPL; G, gas phase; see text or Glossary for definition of mathematical symbols]

The vertical saturation profiles of water and LNAPL can be estimated using the relations for saturation and capillary pressure (*S*-*cP*) (Huntley and Beckett 2002) expressed in the van Genuchten (1980) model and Brooks-Corey (Brooks and Corey 1964, 1966) equations. The Brooks-Corey equations for the saturations of water and LNAPL are

$$S_w=(1-S_{wr})\left[\frac{\psi_d}{\beta_{nw}\,\psi_{cnw}}\right]^{\lambda}+S_{wr},\qquad \psi_{cnw}>\psi_d/\beta_{nw}\ , \tag{S7.7a}$$

$$S_w=1,\qquad \psi_{cnw}\le\psi_d/\beta_{nw}\ , \tag{S7.7b}$$

$$S_t=(1-S_{wr})\left[\frac{\psi_d}{\beta_{gn}\,\psi_{cgn}}\right]^{\lambda}+S_{wr},\qquad \psi_{cgn}>\psi_d/\beta_{gn}\ , \tag{S7.8a}$$

$$S_t=1,\qquad \psi_{cgn}\le\psi_d/\beta_{gn}\ , \tag{S7.8b}$$

with

$$S_t=S_n+S_w\ , \tag{S7.9}$$

where

$S_{wr}$ and $S_t$ are the saturations of irreducible water and total liquid (water and LNAPL) phases, respectively;

$\beta_{nw}$ and $\beta_{gn}$ are the fluid-pair-dependent scaling coefficients;

$\psi_d$ (or $\psi_d^{gw}$) is the air–water displacement (or entry) pressure head ($L$) of the pristine air–water system; and

$\lambda$ is the pore size distribution index for the Brooks-Corey equations.

## Semi-Analytical Volume Estimation of Subsurface LNAPL

The volume of LNAPL in an aquifer can be estimated from measurements of LNAPL thickness in monitor wells, parameters of the soil matrix, and properties of the LNAPL (Farr et al. 1990). Figure S7.5 illustrates the distribution of three phases—water, gas, and LNAPL—in the vicinity of the water table. The vertical saturation profiles of air, water, and LNAPL phases can be used to estimate the volume of LNAPL (Farr et al. 1990).

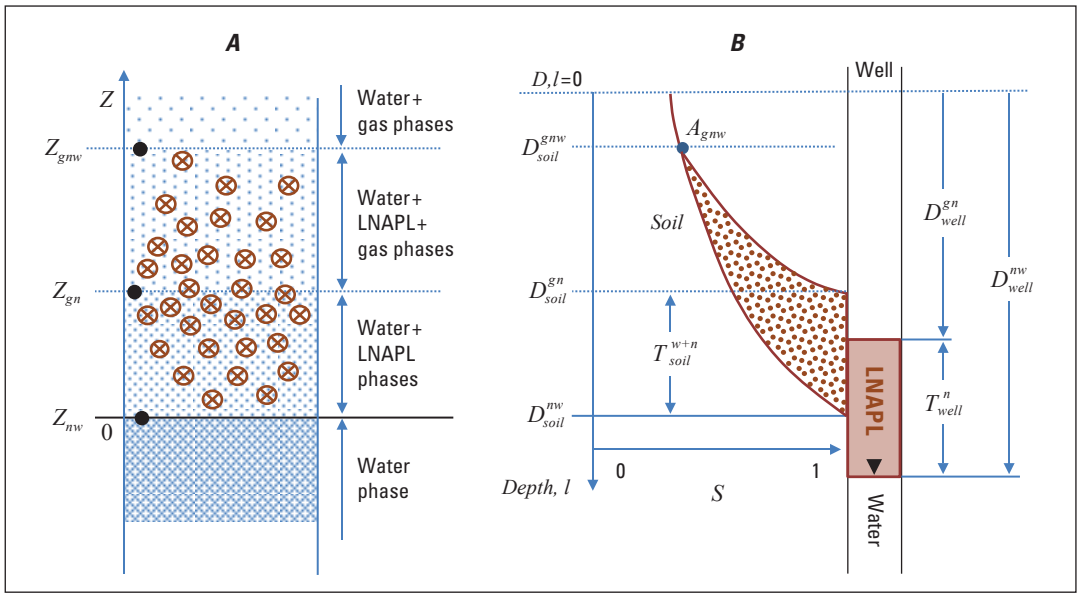


**Figure S7.5.** *(A)* Distribution of light nonaqueous phase liquid (LNAPL) in soil and *(B)* vertical saturation profile of LNAPL in soil and LNAPL thickness in well (after Farr et al. 1990). [See text or Glossary for definition of mathematical symbols]

Farr et al. (1990) developed a semi-analytical equation to evaluate LNAPL volume in this scenario as

$$V_{napl} = \phi \left\{ \int_{D_{soil}^{gnw}}^{D_{soil}^{nw}} \left(1 - S_w\right) dl - \int_{D_{soil}^{gnw}}^{D_{soil}^{gn}} \left(1 - S_w - S_n\right) dl \right\} , \quad \text{(S7.10)}$$

where

$V_{napl}$ is the volume of an LNAPL in the porous medium per unit area ($L$),
$\phi$ is the porosity,
$S_w$ is the water saturation,
$S_n$ is the LNAPL saturation,
$D$ indicates the depth ($L$),
$l$ is the vertical coordinate ($L$) in the downward direction from the ground surface,
$D_{soil}^{gn}$ is the depth ($L$) at which the air–LNAPL capillary pressure is the minimum that is required for continuous air and LNAPL to exist simultaneously,
$D_{soil}^{gnw}$ is the depth ($L$) to the top of the body of continuous LNAPL,
$D_{soil}^{nw}$ is the depth ($L$) at which the LNAPL-water capillary pressure is the minimum that is required for continuous water and LNAPL to exist simultaneously,
$D_{well}^{gn}$ is the depth ($L$) to the top of LNAPL measured in the well,
$D_{well}^{nw}$ is the depth ($L$) to the bottom of LNAPL measured in the well, and
$T_{well}^{n}$ is the thickness of LNAPL in the well.

The relations of saturation-capillary pressures (*S*-*cP*) for multiple phases, e.g., water, gas, and LNAPL, can be written using the Brooks-Corey equations or the van Genuchten model. The depths of phase-interfaces, $D_{soil}^{nw}$, $D_{soil}^{gn}$, and $D_{soil}^{gnw}$, are estimated by using field LNAPL-thickness data and the relations of saturation-capillary pressures of multiple phases. With the Brooks-Corey equations and field data consisting of measured LNAPL thickness in monitor wells, the depth $D_{soil}^{nw}$ in the soil can be calculated as

$$D_{soil}^{nw} = D_{well}^{nw} - \frac{\rho_w}{\left(\rho_w - \rho_n\right)} \psi_d^{nw} \quad , \tag{S7.11}$$

where

$\psi_d^{nw}$ is the LNAPL–water displacement pore entry pressure head (or entry pressure head for LNAPL–water phases) ($L$), $\psi_d^{nw} = \psi_d / \beta_{nw}$; and

$\rho_w$ and $\rho_n$ are the densities ($M/L^3$) of water and LNAPL, respectively.

The depth $D_{soil}^{gn}$ can be expressed as

$$D_{soil}^{gn} = D_{well}^{gn} - \frac{\rho_w}{\rho_n} \psi_d^{gn} \quad , \tag{S7.12}$$

where

$\psi_d^{gn}$ is the air–LNAPL displacement pressure head (i.e., entry pressure head for air–LNAPL phases), $\psi_d^{gn} = \psi_d / \beta_{gn}$.

It is noted that the thickness of a free-phase LNAPL, $T_{well}^{n}$, measured in observation wells can be different from that of a liquid-saturated zone, $T_{soil}^{w+n}$, in the soil matrix (Figure S7.5*B*). This is due to the displacement pressures (or entry pressures) of air–LNAPL and LNAPL–water phases in the soil matrix. The thickness of a liquid-saturated zone, $T_{soil}^{w+n}$, in which $S_w + S_n = 1$ in the subsurface, is calculated by

$$T_{soil}^{w+n} = D_{soil}^{nw} - D_{soil}^{gn} = T_{well}^{n} + \frac{\rho_w}{\rho_n} \psi_d^{gn} - \frac{\rho_w}{\left(\rho_w - \rho_n\right)} \psi_d^{nw} \quad . \tag{S7.13}$$

At point $A_{gnw}$, an LNAPL's saturation becomes zero, suggesting $S_t = S_w$. Using Equations S7.11– S7.13, the depth of point $A_{gnw}$ is calculated by

$$D_{soil}^{gnw} = \left( \frac{\Delta\rho}{\psi_d^{nw}} D_{well}^{nw} - \frac{\rho_n}{\psi_d^{gn}} D_{well}^{gn} \right) \Big/ \left( \frac{\Delta\rho}{\psi_d^{nw}} - \frac{\rho_n}{\psi_d^{gn}} \right) \quad . \tag{S7.14}$$

Finally the integration of Equation S7.11 with $D_{soil}^{nw}$, $D_{soil}^{gn}$, and $D_{soil}^{gmw}$ ($\geq 0$) using the Brooks-Corey equations yields

$$V_{napl} = \frac{\phi\left(1 - S_{wr}\right) D}{1 - \lambda} \left\{ \lambda + \left(1 - \lambda\right)\left(T / D\right) - \left(T / D\right)^{1-\lambda} \right\}, \quad \lambda \neq 1 \quad , \tag{S7.15a}$$

$$V_{napl} = \phi\left(1 - S_{wr}\right) D\{1 - D\left(1 + \ln T\right)\}, \lambda = 1 \quad , \tag{S7.15b}$$

with

$$D = \frac{\psi_d^{nw} \rho_w}{\Delta\rho} - \frac{\psi_d^{gn} \rho_w}{\rho_n} \quad , \tag{S7.16}$$

$$T = D_{well}^{nw} - D_{well}^{gn} \geq \frac{\psi_d^{nw} \rho_w}{\Delta\rho} \quad , \tag{S7.17}$$

where $\Delta\rho = \rho_w - \rho_n$ and $\psi_d^{nw}\rho_w / \Delta\rho$ is the minimum thickness of LNAPL in an observation well to guarantee the presence of an LNAPL layer in the soil (Farr et al. 1990).

## Numerical Integration for the Volume and Distribution of Subsurface LNAPL

The saturation of an LNAPL lens varies as the capillary pressure between phases, i.e., gas–LNAPL and LNAPL–water phases, changes with elevation. The spatial distribution of LNAPL saturation can be computed using *S-cP* relations for the water, gas, and LNAPL phases that are present.

The semi-analytical solution for LNAPL volume estimation, Equation S7.15 developed by Farr et al. (1990), provides the total volume of LNAPL in the subsurface, but cannot provide its spatial distribution in an actual three-dimensional aquifer. To construct the distribution of LNAPL in the groundwater system, it is necessary to calculate LNAPL saturation with elevation (or the vertical saturation profile of LNAPL) within the pool or lens area of LNAPL (Figure S7.6). The vertical saturation profile of LNAPL can be obtained by analyzing interphase capillary pressures along the *z*-axis within the LNAPL lens.

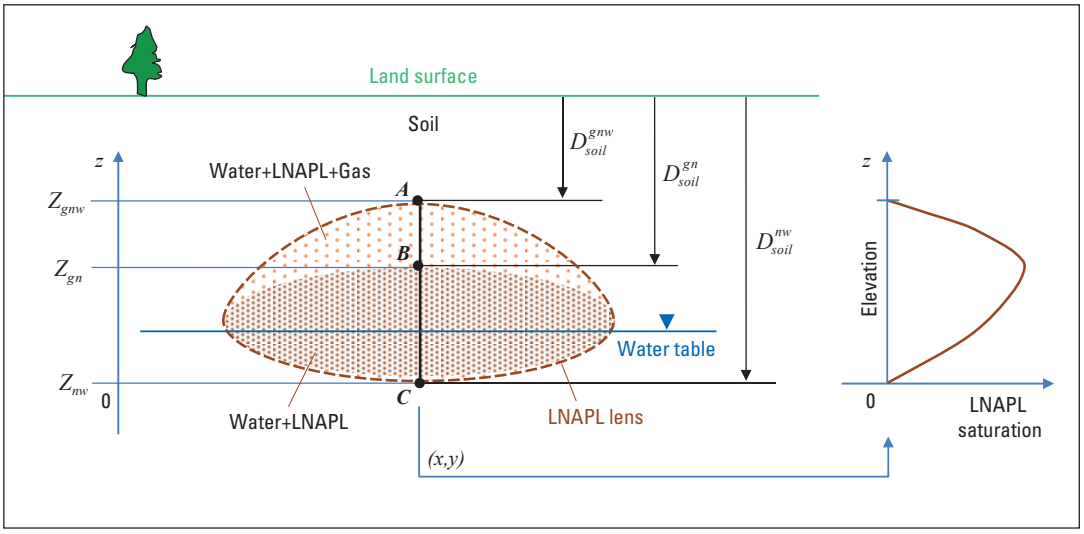


**Figure S7.6.** A light nonaqueous phase liquid (LNAPL) lens and its vertical saturation profile in the subsurface. [See text or Glossary for definition of mathematical symbols]

The depths of the interfaces, $D_{soil}^{nw}$, $D_{soil}^{gn}$, and $D_{soil}^{gnw}$, shown in Equations S7.11, S7.12, and S7.14, can be manipulated to calculate elevations of $Z_{gnw}$ and $Z_{gn}$ along the *z*-axis, which are used in computing interphase capillary pressures and phase saturations. The elevation of $Z_{nw}(x, y)$ is set to be zero at a given location of $(x, y)$. As the LNAPL thickness changes, the elevations of $Z_{gn}(x, y)$ and $Z_{gnw}(x, y)$ vary spatially on a horizontal plane within the LNAPL lens. From the depths of the interfaces, $D_{soil}^{nw}$, $D_{soil}^{gn}$, and $D_{soil}^{gnw}$, the elevations of $Z_{gnw}$ and $Z_{gn}$ can be derived by setting $Z_{nw}(x, y)=0$ as follows:

$$Z_{gn} = D_{soil}^{nw} - D_{soil}^{gn} = D_{well}^{nw} - D_{well}^{gn} - \frac{\rho_w}{(\rho_w - \rho_n)} \psi_d^{nw} + \frac{\rho_w}{\rho_n} \psi_d^{gn} = T_{well}^{n} - \frac{\rho_w}{(\rho_w - \rho_n)} \psi_d^{nw} + \frac{\rho_w}{\rho_n} \psi_d^{gn} , \quad \text{(S7.18)}$$

$$Z_{gnw} = D_{soil}^{nw} - D_{soil}^{gnw} = \frac{\rho_n}{\psi_d^{gn}} T_{soil}^{nw} \Big/ \left( \frac{\rho_n}{\psi_d^{gn}} - \frac{\Delta\rho}{\psi_d^{nw}} \right) . \quad \text{(S7.19)}$$

At a location of $(x,y)$ within the LNAPL lens, LNAPL is present in the interval $0<z<Z_{gnw}(x,y)$. In the interval $0<z<Z_{gn}(x,y)$, the saturation of the water phase and the saturation of the LNAPL phase sum to 1 ($S_w+S_n=1$). In the interval $Z_{gn}(x,y)<z<Z_{gnw}(x,y)$, the saturation of water, gas, and LNAPL sums to 1 ($S_w+S_n+S_g=1$). In the range of $0\le z\le Z_{gn}(x,y)$, for a liquid-saturated zone with only water and LNAPL, the capillary pressure of the two phases and the saturation of the LNAPL are

$$\psi_{cnw}=\frac{\rho_w-\rho_n}{\rho_w}z+\psi_d^{nw},\quad 0\le z\le Z_{gn}\ , \tag{S7.20}$$

$$S_n(x,y,z)=(1-S_{wr})\left(1-\left[\frac{\psi_d^{nw}}{\psi_{cnw}}\right]^{\lambda}\right)\ . \tag{S7.21}$$

Within a range of $Z_{gn}\le z\le Z_{gnw}$ for a three-phase zone with water, LNAPL, and gas phases, the capillary pressures of the phases and the saturation of an LNAPL are as follows:

$$\psi_{cgn}=\frac{\rho_n}{\rho_w}(z-Z_{gn})+\psi_d^{gn},\quad Z_{gn}\le z\le Z_{gnw}\ , \tag{S7.22}$$

$$\psi_{cnw}=\frac{\rho_w-\rho_n}{\rho_w}z+\psi_d^{nw},\quad Z_{gn}\le z\le Z_{gnw}\ , \tag{S7.23}$$

$$S_n(x,y,z)=(1-S_{wr})\left\{\left[\frac{\psi_d^{gn}}{\psi_{cgn}}\right]^{\lambda}-\left[\frac{\psi_d^{nw}}{\psi_{cnw}}\right]^{\lambda}\right\}\ . \tag{S7.24}$$

Using Equations S7.20 through S7.24, the LNAPL saturation can be obtained. The integration of $S_n(x,y,z)$ with respect to $z$ produces the volume of an LNAPL per unit area at a location of $(x,y)$,

$$V_{napl}^{*}(x,y)=\int_0^{Z_{gnw}(x,y)}\phi S_n(x,y,z)\,dz\ , \tag{S7.25}$$

where

$V_{napl}^{*}(x,y)$ is the volume of an LNAPL per unit area at location $(x,y)$.

Total volume of an LNAPL within its lens can be obtained by integrating $S_n(x,y,z)$ in $x$-, $y$-, and $z$-directions as follows:

$$V_{napl}^{Total}=\int_x\int_y\int_0^{Z_{gnw}(x,y)}\phi S_n(x,y,z)\,dx\,dy\,dz\ , \tag{S7.26}$$

where

$V_{napl}^{Total}$ is the total volume of an LNAPL within the lens.

## Contaminant Transport in the Groundwater

The equation for the advective-dispersive transport of multiple contaminant species in multiphase flow can be written as follows (Jang and Aral 2007)

$$\frac{\partial\left(\phi S_f C_f^i\right)}{\partial t} = \nabla\left(\phi S_f \nabla \boldsymbol{D}_f^i\right) - \nabla\left(\boldsymbol{q}_f C_f^i\right) + I_{f,BT}^i + I_{source}\,, \tag{S7.27}$$

where

$i$, $f$ represent the indexes for contaminants and fluid phases, respectively;
$C$ is the chemical concentration ($M/L^3$);
$\boldsymbol{D}$ and $\boldsymbol{q}$ are the dispersion tensor ($L^2/T$) and Darcy flux ($L/T$) terms, respectively; and
$I_{BT}$ and $I_{source}$ indicate the biotransformation/decay and source of a contaminant ($M/L^3T$), respectively.

The dispersion tensor of a species can be defined by

$$\boldsymbol{D}_{f,mm}^i = \alpha\left|v_f\right|\delta_{mm} + \left(\alpha_L + \alpha_T\right)\frac{\left(v_{f,m}\, v_{f,n}\right)}{\left|v_n\right|} + \tau_f D_f^{*i}\delta_{mm}, \quad m,n=x,y,z\ , \tag{S7.28}$$

where

$\alpha_L$ and $\alpha_T$ are the longitudinal and transversal dispersivities of the soil media ($L$), respectively,
$v_f$ is the pore velocity ($L/T$),
$\tau$ is tortuosity,
$D^*$ is a molecular diffusion coefficient ($L^2/T$), and
$\delta_{mm}$ is the Kronecker delta (Bear 1972).

The tortuosity can be estimated using an empirical equation developed by Millington and Quirk (1961):

$$\tau_f = (\phi S_f)^{\frac{7}{3}} / \phi^2\ . \tag{S7.29}$$

The dissolution of LNAPL contaminants can play an important role in determining the concentration of LNAPL constituents in the dissolved phase (groundwater) and also the reduction of LNAPL mass in the source area. The dissolution process—an interphase mass transfer of contaminants from free-phase LNAPL to an aqueous (dissolved) phase—can be described either as equilibrium partitioning or non-equilibrium partitioning (rate-limited mass transfer), with the former expressed as a first-order relationship and the latter requiring non-linear kinetic equations (Abriola and Pinder 1985; Sleep and Sykes 1989; Borden and Kao 1992; Zhu and Sykes 2004; Jang and Aral 2008). Weber and DiGiano (1996) suggested that first-order processes are widely applicable for describing various environmental reactions. This analysis incorporates equilibrium partitioning represented as a first-order process. By applying first-order equations, LNAPL dissolution can be written as follows:

$$I_{source} = \phi S_w \lambda_D \left(C_{we} - C_w\right)\ . \tag{S7.30}$$

The first-order bioreaction process can be written as

$$I_{w,BT}^i = -\phi S_w \lambda_B^i C_w^i\ , \tag{S7.31}$$

where $\lambda_B$ is a first-order biological transformation coefficient ($T^{-1}$).

# Simulation of the Migration of LNAPL

The movement of LNAPL through pore spaces in a soil matrix is a very complicated process involving a range of physical and chemical parameters, including soil permeability, gravity, surface tension, displacement entry pressure, and fluid densities and viscosities. Because many of these parameters depend on specific fluid properties, LNAPL has a velocity and spreading pattern in the unsaturated and saturated zones that is unique and different from that of water. Likewise, different LNAPLs may have their own unique subsurface velocity and migration patterns.

Gravity is a key driving force for the downward migration of LNAPL released in the unsaturated zone. When LNAPL reaches the water table and develops into an LNAPL mound or lens, the pressure inside the lens increases and pressure gradients are generated in a horizontal direction, resulting in lateral spreading of LNAPL. In the capillary fringe, water and LNAPL phases compete to occupy soil pore spaces. Once the capillary pressure between LNAPL and water phases, $\psi_{cnw}$, is greater than the displacement entry pressure of the soil pore spaces, LNAPL will migrate into water-saturated areas of the soil matrix (Mercer and Cohen 1990). LNAPL of relatively higher density will penetrate further into the water-saturated zone than LNAPL of relatively lower density.

Although LNAPL migration is explored independently in the following hypothetical scenario, it is important to note that LNAPL migration, LNAPL dissolution, and dissolved phase constituent fate and transport model components are integrated within the TechFlowMP model for the applied analysis at the HPIA. The purpose of the hypothetical scenario is to illustrate and explore the behavior of LNAPL in a multiphase environment and provide insight about the potential variability of the expected results, which is helpful in the subsequent linked model components for the dissolution of LNAPL and transport of dissolved phase contaminants.

## Methods

For a hypothetical scenario representing an unconfined sandy aquifer (Figure S7.7), two models are used to investigate the downward migration and lateral dispersive spreading of a free-phase LNAPL: (1) TechFlowMP, a numerical model, and (2) HSSM, a semi-analytical model. TechFlowMP is a three-dimensional, Galerkin, finite element model developed by Jang and Aral (2005). In a subsurface system with LNAPL, TechFlowMP incorporates vertically variable water saturation. This means that initial unoccupied pore spaces in a soil matrix (for LNAPL) change with depth, leading to different relative permeabilities of water with depth. This may also result in spatially and temporally varying velocities of LNAPL in the modeling domain. For multiphase flow in TechFlowMP, the Brooks-Corey equation (Brooks and Corey 1964, 1966) is used to describe *S*-*cP* relations in which total liquid saturation depends on a gas–LNAPL capillary pressure, while water saturation relies on NAPL−water capillary pressure when $S_n > 0$. The multiphase flow modeling delineates the variation of phase saturation and pressures in the domain over time.

The expansion of an LNAPL lens can be also evaluated by using HSSM (Weaver et al. 1996). HSSM is a screening-level semi-analytical model for estimating the transport of LNAPL in the unsaturated and saturated zones of a homogeneous aquifer. HSSM-KO, one of two HSSM modules, is used to simulate the downward flow of LNAPL in the unsaturated zone and the subsequent radial spreading of LNAPL at the water table. The HSSM-KO module uses simplified subsurface conditions, including the assumption of a shallow aquifer. HSSM does not consider dispersive spreading of free-phase LNAPL, vertically variable water saturation in the unsaturated zone (i.e., water saturation is uniform in the HSSM), or the effects of groundwater flow (i.e., the water table is a horizontal plane in HSSM).

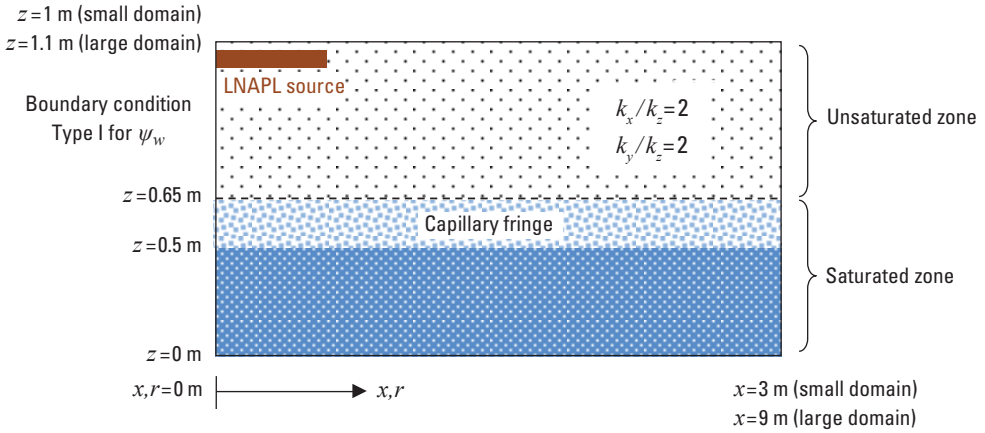


**Figure S7.7.** Hypothetical scenario of a light nonaqueous phase liquid (LNAPL) source release in the unsaturated zone above an unconfined aquifer. [See text or Glossary for definition of mathematical symbols; m, meter; *z*, vertical height or altitude; *x*,*r*, radial distance]

This study incorporates two different source scenarios and two different model grid designs. Because the downward movement of an immiscible LNAPL fluid is dynamic, a dense model grid is needed to improve the stability of numerical solutions of LNAPL transport. A coarse model grid design is also used where applicable to reduce the computational time and resources that are needed for the dense grid design.

## Model Domain and Model Input Parameters

Two different model domains are used to discretize the hypothetical unconfined aquifer scenario illustrated in Figure S7.7. Domain A is a relatively smaller model domain (radius of 3 meters [m] and thickness of 1 m) with a fine, or dense, grid, and Domain B is a relatively larger model domain (radius of 9 m and thickness of 1.1 m) with a coarse grid (Table S7.1). The boundary and initial conditions for the models are listed in Table S7.1. Within the model domain, the groundwater pressure head is zero at an elevation of 0.5 m. However, with a capillary fringe of 0.15 m, the water table in the soil formation is located at $z$=0.65 m, indicating that the water-saturated zone ranges in elevation from 0 m to 0.65 m.

TechFlowMP uses three-dimensional Cartesian coordinates (i.e., $x$-, $y$-, and $z$-axis) and Dirichlet (Type 1) boundary conditions at the outer boundaries of the model domains (model boundary at $r$=3 m for a small domain and $r$=9 m for a large domain). Water saturation within the TechFlowMP model varies according to hydraulic head and could change spatially and temporally due to the movement of LNAPL in the unsaturated zone. In contrast, HSSM uses one-dimensional coordinates (i.e., the $z$-axis) for vertical transport of LNAPL in the unsaturated zone and radial coordinates to map lateral spreading at the water table. HSSM uses simplified subsurface conditions that assume uniform water saturation in the unsaturated zone regardless of elevation above the water table, no groundwater flow in the model domain, and no lateral movement of LNAPL in the unsaturated zone.

Model input parameter values for soil, water, and LNAPL are listed in Table S7.2. The aquifer has a soil porosity of 0.35 and horizontal and vertical permeabilities of $1.675\times10^{-11}$ and $8.375\times10^{-12}$ m$^2$, respectively (Table S7.2). The Brooks-Corey equations are used to define the relations of capillary pressure, effective saturation, and relative permeability. Typically LNAPL movement is observed when residual saturation, $S_{nr}$, is greater than 0.1, and LNAPL dissolution is the dominant process when residual saturation is less than 0.1. As stated previously, although LNAPL migration is explored independently in these hypothetical scenarios, the LNAPL migration, LNAPL dissolution, and subsequent dissolved-phase constituent fate and transport components are integrated within the TechFlowMP model for the applied analysis at the HPIA.

**Table S7.1.** Model domain and boundary conditions for the hypothetical LNAPL release scenario.

[LNAPL, light nonaqueous phase liquid; m, meter]

| Property | Value |
|---|---|
| Boundary conditions | |
| Water hydraulic head | 0.5 m Dirichlet (Type I) |
| Gas pressure | Constant atmospheric pressure |
| LNAPL saturation | No flux/flow boundary |
| Initial conditions | |
| Water hydraulic head | 0.5 m |
| Water saturation | $S_w$ varies with $z$ |
| LNAPL saturation | $S_n$=0 |
| Domain discretization | |
| Domain A (Smaller, dense grid) | $x$=3 m |
| | $z$=1 m |
| | $\Delta x$=0.02 m |
| | $\Delta z$=0.02–0.10 m |
| | 12,080 nodes |
| | 5,850 elements |
| Domain B (Larger, coarse grid) | $x$=9 m |
| | $z$=1.1 m |
| | $\Delta x$=0.16–0.67 m |
| | $\Delta z$=0.02–0.10 m |
| | 1,764 nodes |
| | 820 elements |

**Table S7.2.** Model input parameter values for the hypothetical LNAPL release scenario.

[LNAPL, light nonaqueous phase liquid; m$^2$, square meters; kg/m$^3$, kilograms per cubic meter; Pa s$^{-1}$, Pascals per second; kg/m-s, kilogram per meter per second; cm, centimeter; m, meters]

| Parameter | Value |
|---|---|
| Soil | |
| Horizontal intrinsic permeability | $1.675\times10^{-11}$ m$^2$ |
| Vertical intrinsic permeability | $8.375\times10^{-12}$ m$^2$ |
| Porosity | 0.35 |
| Fluid | |
| Water density | $\rho_w$ = 1,000 kg/m$^3$ |
| LNAPL density | $\rho_n$ = 720 kg/m$^3$ |
| Water viscosity | 0.001 Pa s$^{-1}$ (0.001 kg/m-s) |
| LNAPL viscosity | 0.00045 Pa s$^{-1}$ (0.00045 kg/m-s) |
| Water-surface tension | 70 dyne/cm |
| LNAPL-surface tension | 30 dyne/cm |
| Brooks-Corey equation[1] | |
| Pore-size distribution index | 2 |
| Displacement entry pressure head, $\psi_d$ | 0.15 m |
| Water residual saturation | $S_{wr}$ = 0.1 |
| NAPL residual saturation | $S_{nr}$ = 0.1 |

[1] Brooks and Corey 1964, 1966

Two simulation scenarios that incorporate different source characteristics are used to explore LNAPL movement (Table S7.3). Scenario A uses the dense model grid to delineate the detailed spatial spreading of LNAPL in the domain, while scenario B uses the coarse model grid to evaluate the change in the size (or radius) of the LNAPL plume with time. In both scenarios, LNAPL is introduced into the system at an initial time, $t$=0, and the LNAPL release flux is specified as 0.2 cubic meter per day ($m^3/d$) per unit area. Scenarios A and B each have different LNAPL source sizes (radius), source elevations, and LNAPL release periods (Table S7.3). Note that different LNAPL source elevations for scenarios A and B imply differences in water saturation levels at the release point. Scenario A has a shorter initial time step than scenario B to improve the stability of numerical solutions and the conservation of introduced LNAPL mass; however, both scenarios use the same maximum time step of 1 second.

**Table S7.3.** Simulation scenarios for LNAPL migration.

[LNAPL, light nonaqueous phase liquid; m, meter; $m^3/d$, cubic meter per day; h, hour; d, day; s, second]

| Parameters | Scenario A | Scenario B |
|---|---|---|
| Model domain | Smaller, dense grid (domain A in Table S7.1) | Larger, coarse grid (domain B in Table S7.1) |
| Radius of LNAPL source | 0.5 m | 1.49 m |
| Source elevation | $z$=0.96–0.98 m | $z$=1.04–1.06 m |
| LNAPL source release flux | 0.2 $m^3/d$ per area | 0.2 $m^3/d$ per area |
| LNAPL source release period | 9 h | 6 h |
| Simulation time | 2 d | 10 d |
| Time step ($\Delta t$) | 0.1 s initial<br>1 s maximum | 1 s |

## Numerical Techniques

The selection of primary variables is an important step in solving nonlinear flow equations involving multiphase flow. Pressure head, $\psi$, and saturation, $S$, of water and/or LNAPL phases can be selected as primary variables. Combinations of primary variables also may be considered for multiphase flow systems (Forsyth et al. 1998; Kaluarachchi and Parker 1989; Parker and Lenhard 1989; Wu and Forsyth 2001). Selection of primary variables depends on the sensitivity of the system of flow equations for the subsurface system of interest. Wu and Forsyth (2001) reported that a mixed formulation using water pressure and LNAPL saturation as primary variables yields better performance and accuracy than a pressure-only formulation (i.e., using pressures of both water and LNAPL as primary variables).

In this study, TechFlowMP implements a mixed formulation using water pressure, $\psi_w$, and LNAPL saturation, $S_n$, as primary variables. That facilitates the transition between single-, two-, and three-phase environments (e.g., areas of groundwater-only, air–groundwater, groundwater–LNAPL, and water–gas–LNAPL phases). To analyze the migration of LNAPL, TechFlowMP uses a global implicit scheme to simultaneously solve the flow equations for the water and LNAPL phases. Upwind techniques are incorporated as needed for the multiphase flow modeling.

# Results

For each scenario outlined in Table S7.3, numerical results from the TechFlowMP model are compared with the semi-analytical solutions from the HSSM model.

## Scenario A

TechFlowMP and HSSM model results describing the movement of free-phase LNAPL under scenario A, using a dense model grid, are illustrated in Figure S7.8. The distribution profiles for the LNAPL lens for HSSM results (Figure S7.8*A*) show the constant radius of LNAPL in the unsaturated zone above the water table and its lateral spreading at the water table. Similarly, TechFlowMP results illustrate the evolution of LNAPL saturation and the lateral and vertical spreading of the LNAPL at the water table (Figure S7.8*B*). The modeling results follow the conceptual framework indicating LNAPL mounds at the water table, generating lateral hydraulic (or pressure-head) gradients that in turn drive lateral movement at the water table. The peak LNAPL saturation is observed at the center of the lens. As the LNAPL plume spreads out laterally (i.e., the lens' radius increases), LNAPL saturation at the center of the lens decreases. LNAPL spreading continues until the pressure gradient, which is a driving force for lateral movement, is sufficiently reduced. Note the presence of the LNAPL lens in both the unsaturated and saturated zones.

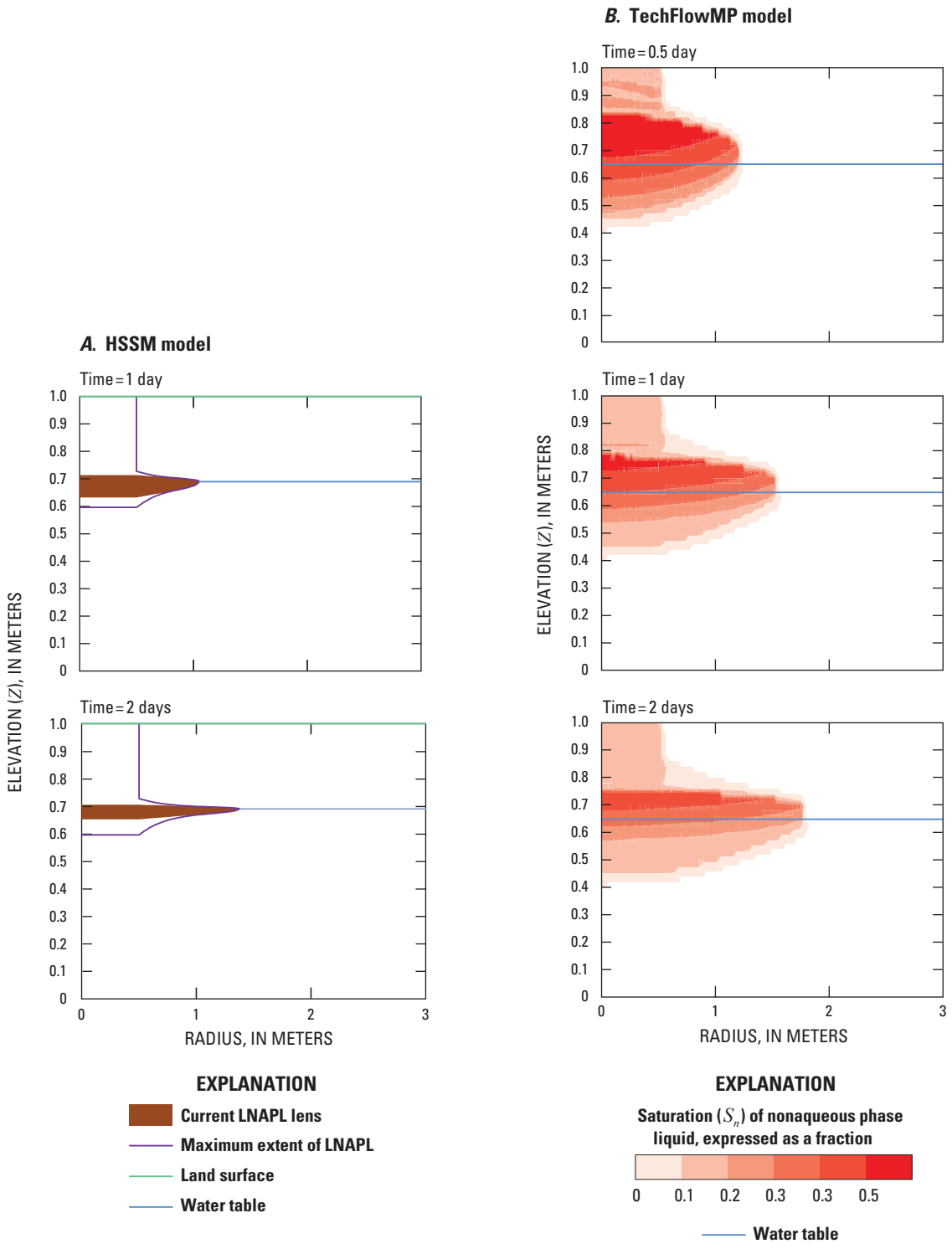


**Figure S7.8.** Simulated distribution of light nonaqueous phase liquid (LNAPL) for scenario A using *(A)* the HSSM model and *(B)* the TechFlowMP model.

## Scenario B

TechFlowMP and HSSM model results describing the movement of free-phase LNAPL under scenario B are illustrated in Figure S7.9. When compared with scenario A, scenario B has a larger model domain with a relatively coarser model grid in *x*- (or *r*-) direction and a larger LNAPL source area (Table S7.3). The lateral extent of the LNAPL lens in scenario B is greater than that in scenario A because of the larger source area and correspondingly greater LNAPL mass introduced into the system in scenario B. HSSM results indicate that as the radius of the LNAPL lens increases with time, the thickness of the LNAPL lens decreases (Figure S7.9*A*). As in scenario A, the peak LNAPL saturation at the center of the lens reduces with lateral expansion the lens at the water table over time (Figure S7.9*B*).

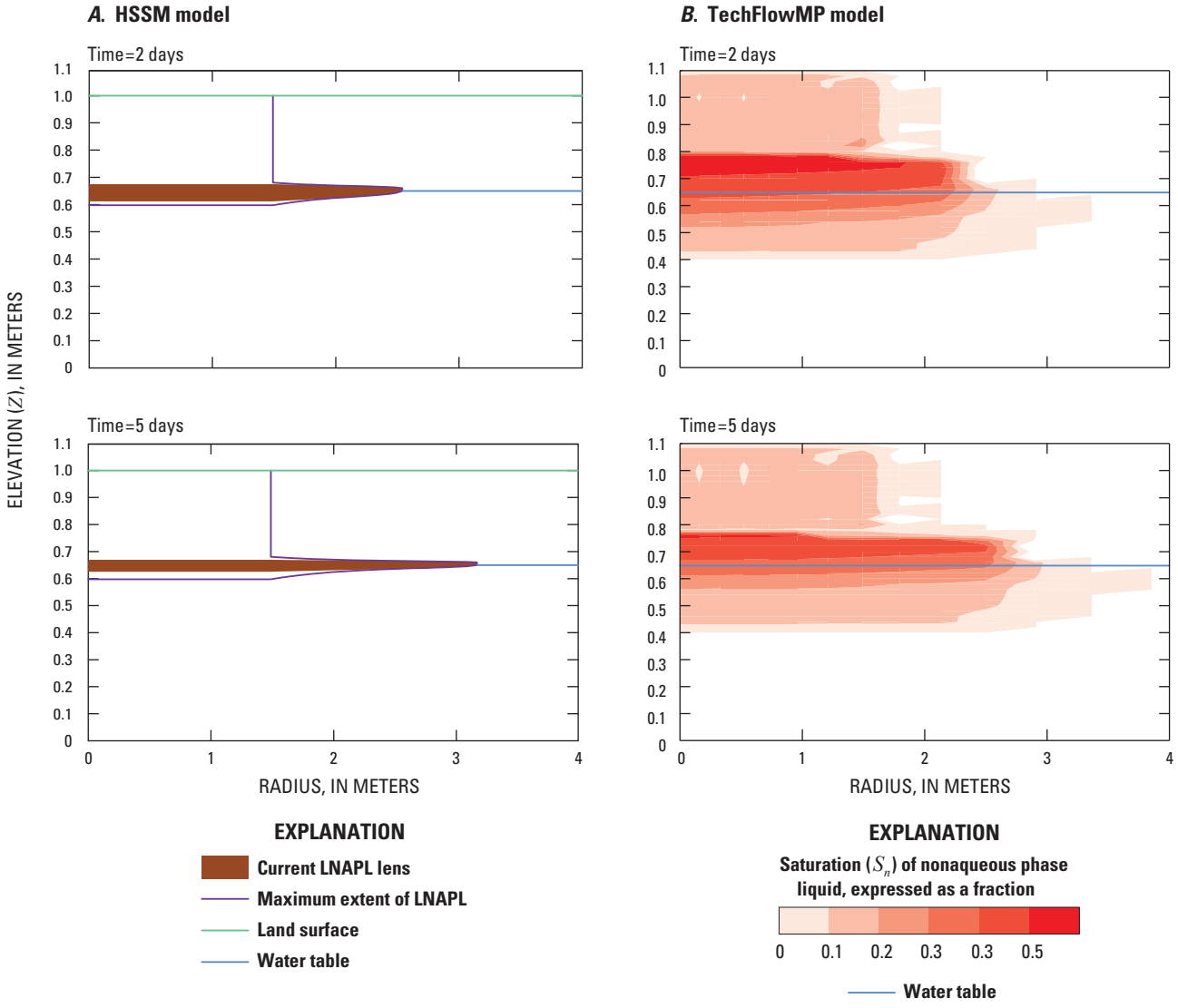


**Figure S7.9.** Simulated distribution of light nonaqueous phase liquid (LNAPL) for scenario B using *(A)* the HSSM model and *(B)* the TechFlowMP model.

The size and configuration of an LNAPL lens could play an important role in determining subsequent transport of dissolved phase contaminants in the groundwater. The source characteristics in scenario B resulted in an LNAPL lens with a larger lateral extent (larger radius) than scenario A; this may lead to greater transfer of LNAPL constituents from the free-phase LNAPL to dissolved phase in the groundwater. Likewise, the vertical extent of an LNAPL lens below the natural groundwater table may be a factor in contaminant transport. As the bottom of an LNAPL lens reaches further below the natural water table, transport of dissolved LNAPL constituents into deeper areas of the aquifer may increase.

Temporal changes in the radius of the LNAPL lens for scenario B are presented in Figure S7.10 for HSSM results and for TechFlowMP results at two different LNAPL saturation levels, $S_n$=0.1 (i.e., LNAPL occupies 10 percent of pore space volume) and $S_n$=0.01 (i.e., LNAPL occupies 1 percent of pore space volume). The results of the two models are consistent. Slight differences in results may be caused by the different approaches (i.e., semi-analytical vs. numerical) and assumptions incorporated into each model. Recall that the HSSM model assumes vertically homogeneous water saturation and only vertical LNAPL movement (no lateral spreading) in the unsaturated zone, whereas the TechFlowMP model incorporates variable water saturation and three-dimensional spreading in the unsaturated and saturated zones.

In the hypothetical scenarios generated for this analysis, LNAPL source characteristics, including release location, duration, and rate of release (source strength), are specified. This is an idealized situation that facilitates the analysis and delineation of the spatial configuration and extent of LNAPL migration over time. In real-world scenarios, documentation about the source of historical LNAPL releases at contaminated sites is often very limited or, in some cases, non-existent. Consequently, uncertainty is inherent with respect to source location, timing, and strength when reconstructing the historical fate and transport of LNAPL in the subsurface. Nonetheless, the spatial and temporal saturation profiles of LNAPL developed for this hypothetical analysis (Figures S7.8–S7.10), are useful in understanding the behavior and migration of free-phase LNAPL released to the subsurface.

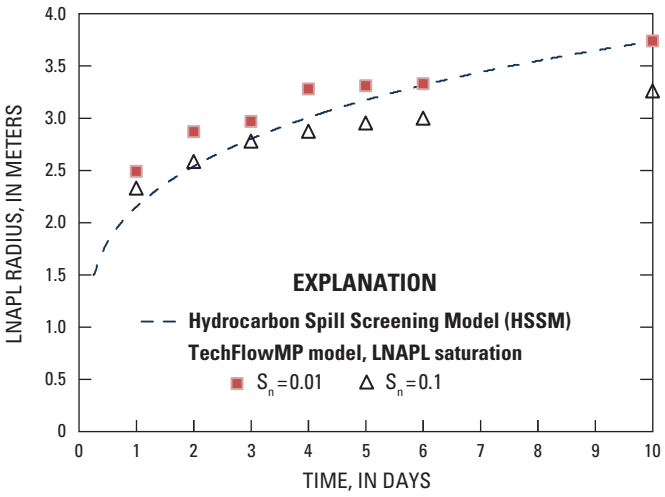


**Figure S7.10.** Simulated results of changes in radii of light nonaqueous phase liquid (LNAPL) lenses over time.

# Subsurface LNAPL Volume and Mass Distribution

This analysis uses field data for LNAPL thickness measured in site monitor wells within the HPIA to estimate subsurface LNAPL volume and mass distribution. LNAPL volume estimates derived from this analysis are compared with the historical fuel-loss, model derived, and fuel-recovery estimates listed in Table S7.4. LNAPL thickness in observation wells typically differs from LNAPL thickness in the surrounding soil (American Petroleum Institute 2003; Deska and Malina 2008). Accordingly, LNAPL thickness measured in wells is commonly referred to as "apparent" LNAPL thickness, whereas LNAPL thickness in soil is referred to as "actual" LNAPL thickness.

Historical environmental investigations in the HPIA identified the presence of free-phase LNAPL in the HPFF area, including Building 1115, and the Building 1613 area (Figure S7.11) (O'Brien and Gere Engineers, Inc. 1988, 1990; Richard Catlin and Associates, Inc. 1996; CH2M HILL, Inc. 2001; Faye et al. 2010, 2012). A summary of free-phase LNAPL thickness measured in monitor wells during 1988–1999 in the HPFF, Building 1115, and Building 1613 areas is listed in Table S7.5. This analysis focused on free product measurements collected prior to 2000, before most of the more extensive remediation systems were installed and operated in the HPFF, Building 1115, and Building 1613 areas. Apparent LNAPL thickness measured in wells varied by location and time (Figure S7.11). The maximum measured thickness of LNAPL in the HPFF and Building 1115 areas was 16 feet (ft) in January 1994. The maximum measured thickness of LNAPL in the Building 1613 area was 6 ft in late 1994. The field data listed in Table S7.5 represent the distribution of LNAPL in the subsurface during a 12-year period when these data were collected. The extent and volume of LNAPL likely changed over time due to variations in fuel release rates, water-supply well operations, and variability in environmental conditions and processes (i.e., precipitation and associated groundwater recharge, dissolution of LNAPL constituents into the groundwater, volatilization and biodegradation of LNAPL constituents). Additionally, the extent and volume of subsurface LNAPL was reduced by engineering activities implemented to remove leaking UST systems, remediate contaminated soil areas, recover free-phase LNAPL, and remediate dissolved phase contaminants in the subsurface source areas (Baker Environmental, Inc. 1996; Catlin Engineers and Scientists 2001; CH2M HILL, Inc. 2001; Faye et al. 2010).

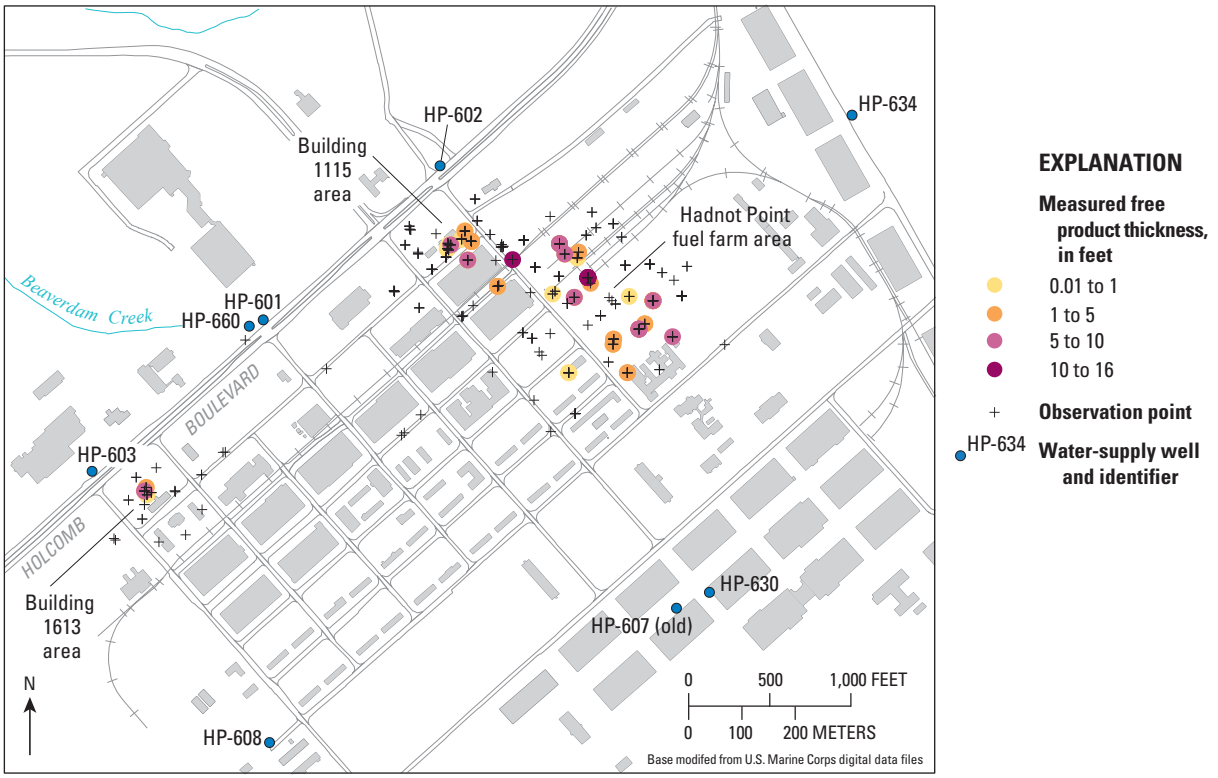


**Figure S7.11.** Distribution of light nonaqueous phase liquid (LNAPL) thickness measured in wells within the Hadnot Point Industrial Area (HPIA), Hadnot Point–Holcomb Boulevard study area, U.S. Marine Corps Base Camp Lejeune, North Carolina.

**Table S7.4.** Estimates of fuel loss, free product in the subsurface, and fuel recovery at the Hadnot Point Industrial Area fuel farm, Hadnot Point–Holcomb Boulevard study area, U.S. Marine Corps Base Camp Lejeune, North Carolina.

[USMCB, U.S. Marine Corps Base; HPFF, Hadnot Point fuel farm; ATSDR, Agency for Toxic Substances and Disease Registry]

| Type of estimate | Volume, in gallons | Reference |
|---|---|---|
| Fuel-loss estimates | | |
| USMC documentation of known release from underground fuel line in 1979 | 20,000–50,000 | Water and Air Research, Inc. (1983) |
| USMC documentation of known fuel releases and inventory losses during 1979–1987 | 23,150–33,150 | O'Brien and Gere Engineers, Inc. (1988, 1990), CH2M HILL (2001) |
| Model-derived estimates | | |
| [1]SpillCAD™ model estimate of free product (LNAPL) in the subsurface using free product measurements collected during 1988–1995 | 830,324–1,061,901 | UST Management Web Portal Files (2010–2012)[2] |
| Order-of-magnitude estimate of total fuel in the subsurface based on available documentation as of 2001 (specific methodology not described) | 400,000–1,100,000 | CH2M HILL (2001) |
| Fuel recovery estimate | | |
| Reported total fuel recovery from HPFF/Building 1115 area remediation systems as of July 2010 | 414,118 | [3]USMCB Camp Lejeune (July 2010) |

[1] SpillCAD™ was developed by Environmental Systems & Technologies (1993)

[2] Draft report by Baker Environmental, Inc., contained in UST Management Web Portal File #01185, p. 526–562

[3] From information presented at the ATSDR-DON Data Mining & Discovery Technical Work Group Meeting, USMCB Camp Lejeune, July 21–22, 2010

**Table S7.5.** Summary of field data for LNAPL thickness measured in monitor wells within the Hadnot Point fuel farm and Building 1613 areas, Hadnot Point–Holcomb Boulevard study area, U.S. Marine Corps Base Camp Lejeune, North Carolina.

[LNAPL, light nonaqueous phase liquid; HPFF, Hadnot Point fuel farm; Bldg, building; —, no data]

| Year | Total observations | Number of monitor wells with free LNAPL | Apparent LNAPL thickness in wells with free LNAPL, in feet | Sites |
|---|---|---|---|---|
| 1988 | 40 | 11 | 0.24–15.3 | HPFF area |
| 1989 | 45 | 8 | 3.07–15.07 | HPFF area |
| 1992 | 45 | 20 | 0.7–13.52 | HPFF area |
| 1993 | 10 | 3 | 0.17–10.18 | Bldg 1115 |
| 1994 | 22 | 7 | 0.160–16 | Bldg 1115, Bldg 1613 |
| 1995 | 75 | 12 | 0.26–4 | HPFF area, Bldg 1115, Bldg 1613 |
| 1997 | 96 | 20 | 0.01–5.29 | HPFF area, Bldg 1115, Bldg 1613 |
| 1998 | 31 | 15 | 0.01–4.24 | HPFF area, Bldg 1115, Bldg 1613 |
| 1999 | 9 | 0 | — | Bldg 1613 |

## Methods

In this analysis, apparent thickness obtained from field measurements and actual LNAPL thickness calculated from apparent thickness measurements are first interpolated to obtain area-wide distributions. Semi-analytical and numerical methods are then used to estimate LNAPL volume in the three-dimensional domain using the interpolated LNAPL thickness distributions (Farr et al. 1990; Lenhard and Parker 1990; Lundegard and Mudford 1998; Mayer and Hassanizadeh 2005). In addition to providing estimates of total LNAPL volume at the site, the numerical methods also are used to generate spatial saturation profiles of LNAPL in the subsurface. The spatial saturation profiles are used in the analysis of contaminant fate and transport with an LNAPL source described later in this report.

The interpolation and integration processes in the analysis are dependent on site-specific parameters and associated uncertainties, such as porosity, soil–LNAPL capillary characteristics, LNAPL density, appropriateness of interpolation techniques, and fluid-saturation history (Lundegard and Mudford 1998; Mayer and Hassanizadeh 2005). The uncertainties associated with soil porosity and variations in the Brooks-Corey equation parameter values (e.g., Table S7.2) are explored in two different model scenarios. Scenario A examines the variation in LNAPL volume estimates for three different soil porosity values and two different sets of fluid-dependent scaling factors, one set corresponding to fresh gasoline and one set corresponding to aged gasoline. Scenario B examines the variation in LNAPL volume estimates for three different sets of Brooks-Corey equation parameter values [air–water displacement (or entry) pressure, $\psi_d^{gw}$, and pore size distribution index, $\lambda$]. For all scenarios, an LNAPL density of 0.74 kilogram per liter (kg/L) (corresponds to gasoline) and residual water saturation of 0.1 are used in calculations.

Three different solution schemes are used in this analysis (Figure S7.12): Scheme 1 uses a semi-analytical solution (Farr et al. 1990) with interpolated apparent LNAPL thickness measured in monitor wells (AN-Well), Scheme 2 uses numerical integration with interpolated apparent LNAPL thickness measured in monitor wells (NI-Well), and Scheme 3 uses numerical integration with interpolated actual LNAPL thickness in the soil (NI-Soil). Step-wise details for the procedures are as follows:

***Step 1. Collect and review relevant field data:*** Field data for LNAPL (free product) thickness and corresponding groundwater elevation measured in monitor wells were assembled from a variety of published reports for the areas of interest within the HPIA (Table S7.5). Note that the LNAPL field data were not uniform in time or space; rather, measurements were collected intermittently in time and were located in an irregular pattern across the area of interest because they corresponded to existing monitor well locations. For each field observation, LNAPL thickness and groundwater elevation measurements are needed to accurately delineate the spatial LNAPL saturation profiles in the subsurface.

***Step 2. Interpolate field data:*** "Apparent" LNAPL thickness measurements collected from monitor wells typically differ from "actual" LNAPL thickness in the soil (American Petroleum Institute 2003). As such, calculations using the two thicknesses may produce different LNAPL volume estimates. In the interpolation and integration steps of this analysis, two calculation strategies are explored using the different thickness measurements (apparent versus actual). One strategy is to use the apparent LNAPL thickness measurements as point data to interpolate across the area of interest; the other strategy is to first convert the apparent LNAPL thicknesses into actual LNAPL thicknesses and then interpolate these point data across the area of interest. The Brooks-Corey equation (Brooks and Corey 1964, 1966) is used to define phase saturation-capillary pressure characteristics. Interpolation is conducted using kriging techniques within the Surfer software application (Golden Software 2011). Measured groundwater elevation data collected concurrently with LNAPL thickness data also are interpolated across the area of interest to determine the elevation of LNAPL in the aquifer.

***Step 3. Construct the spatial distribution of LNAPL saturation within a domain:*** Using interpolated apparent and actual LNAPL thicknesses, the parameters of $S_n$, $D_{nw}$, $D_{gn}$, $D_{gnw}$, $Z_{gn}$, and $Z_{gnw}$ are calculated at every interpolation point, and a vertical profile of LNAPL saturation is constructed over a horizontal plane across the HPIA domain. A spatial LNAPL-$S_n$ distribution is then developed by combining the vertical LNAPL-saturation profiles and groundwater elevation data.

***Step 4. Calculate LNAPL mass, volume, and distribution:*** Estimation of LNAPL mass and volume is accomplished using semi-analytical and numerical methods (Equations S7.15 and S7.26). The computations are conducted using the TechNAPLVol model code developed specifically for this analysis. The semi-analytical solution for LNAPL volume estimation, developed by Farr et al. (1990), uses apparent LNAPL thickness data. Semi-analytical and numerical solutions using actual LNAPL thickness are calculated using the TechNAPLVol model code. The TechNAPLVol code also generates vertical saturation profiles representing the distribution of LNAPL in the subsurface.

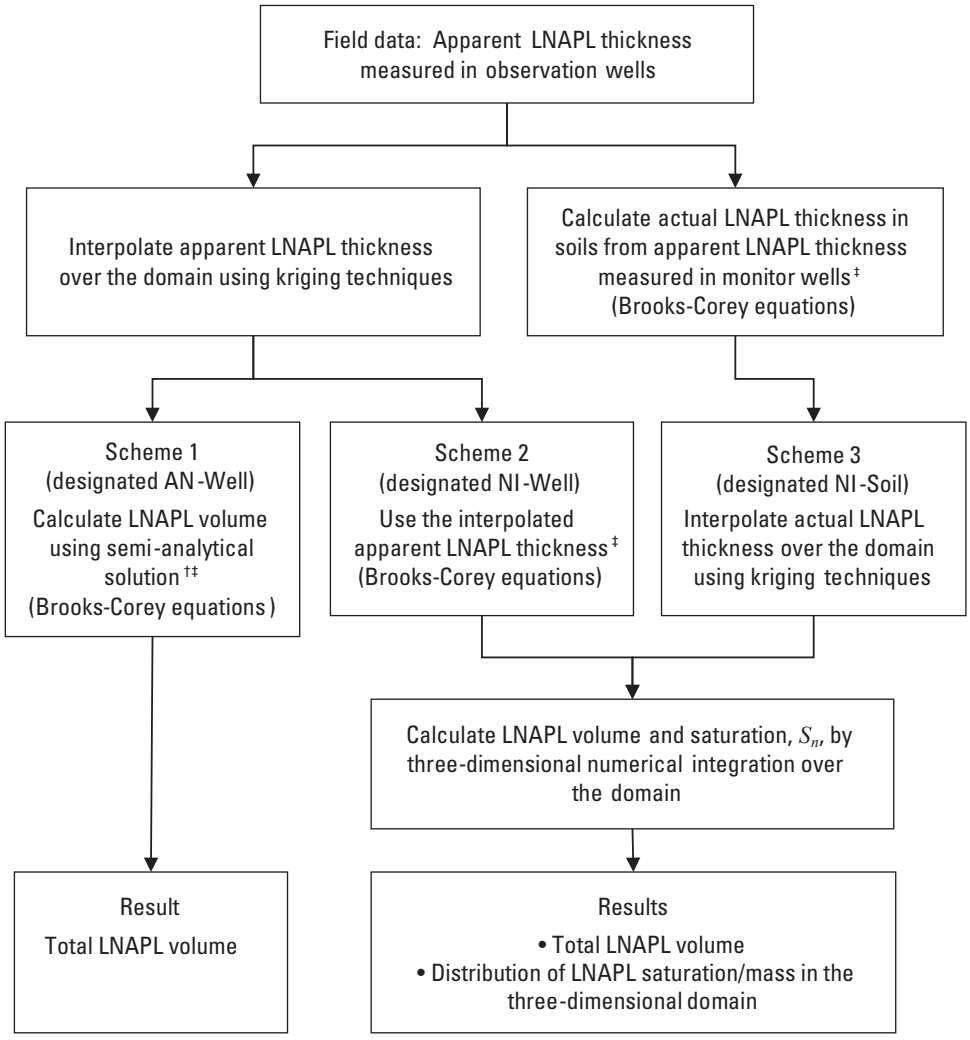


† Semi-analytical solution, developed by Farr et al. (1990)
‡ Incorporates hydrostatic equilibrium of fluids in a vertical direction (Brooks and Corey 1964, 1966)

**Figure S7.12.** Flowchart of step-wise process for estimating subsurface light nonaqueous phase liquid (LNAPL) volume and spatial distribution of LNAPL saturation distribution using the TechNAPLVol model code.

## Results

Interpolated results for actual LNAPL thickness in soil are shown in Figure S7.13. A relatively large area of free-phase LNAPL is in the HPFF area, and a relatively smaller area of free-phase LNAPL is in the Building 1613 area. The results are consistent with field data and historical information for these areas (Faye et al. 2010, 2012).

Soil porosity, which is the ratio of pore spaces or voids to soil matrix volume, can be an important factor in determining the total volume of free-phase LNAPL in the subsurface. A higher porosity translates into more pore space available to contain LNAPL. The effects of porosity and inter-phase surface tension on the estimates of LNAPL volume are presented in Table S7.6. For a baseline scenario with soil porosity of 0.2 and parameter values corresponding to fresh gasoline (scenario A1), LNAPL volume estimates for the three computation schemes ranged from 0.939 million gallons (Mgal) to 1.079 Mgal for the HPFF and Building 1613 areas combined. For a soil porosity of 0.3 (scenario A3), the LNAPL volume estimates for all three computation schemes increased by 50 percent over the baseline estimates. As expected from Equations S7.15 and S7.25, higher porosity results in higher estimates of LNAPL volume. Using Brooks-Corey equation parameter values corresponding to aged gasoline (scenario A4) rather than fresh gasoline (scenario A1) resulted in a 20-percent increase over the baseline LNAPL volume estimates for all three computation schemes. The LNAPL volume estimates calculated in this analysis for the baseline case (scenario A1, 0.939–1.079 Mgal) are in good agreement with historical model-derived estimates (0.4–1.1 Mgal; Table S7.4).

For a non-wetting phase such as LNAPL or gas to move into a soil pore space filled with a wetting phase (e.g., water), the capillary pressure between fluid phases should be greater than the displacement entry pressure of the soil. The effects of the air–water displacement (or entry) pressure, $\psi_d^{gw}$, and pore size distribution index, $\lambda$, of the Brooks-Corey equations on the estimates of LNAPL volume are presented in Table S7.7. LNAPL volume estimates for scenarios B1–B3 range from 0.901 Mgal to 1.253 Mgal.

In general, the LNAPL volume estimates using schemes 1 and 2, which both incorporate an interpolation of apparent LNAPL thickness, are in good agreement (Tables S7.6 and S7.7). The LNAPL volume estimates for scheme 3, which uses an interpolation of actual LNAPL thickness, are higher than the estimates developed using schemes 1 and 2. The LNAPL volume estimates developed in this analysis are consistent with historical model-derived estimates listed in Table S7.4.

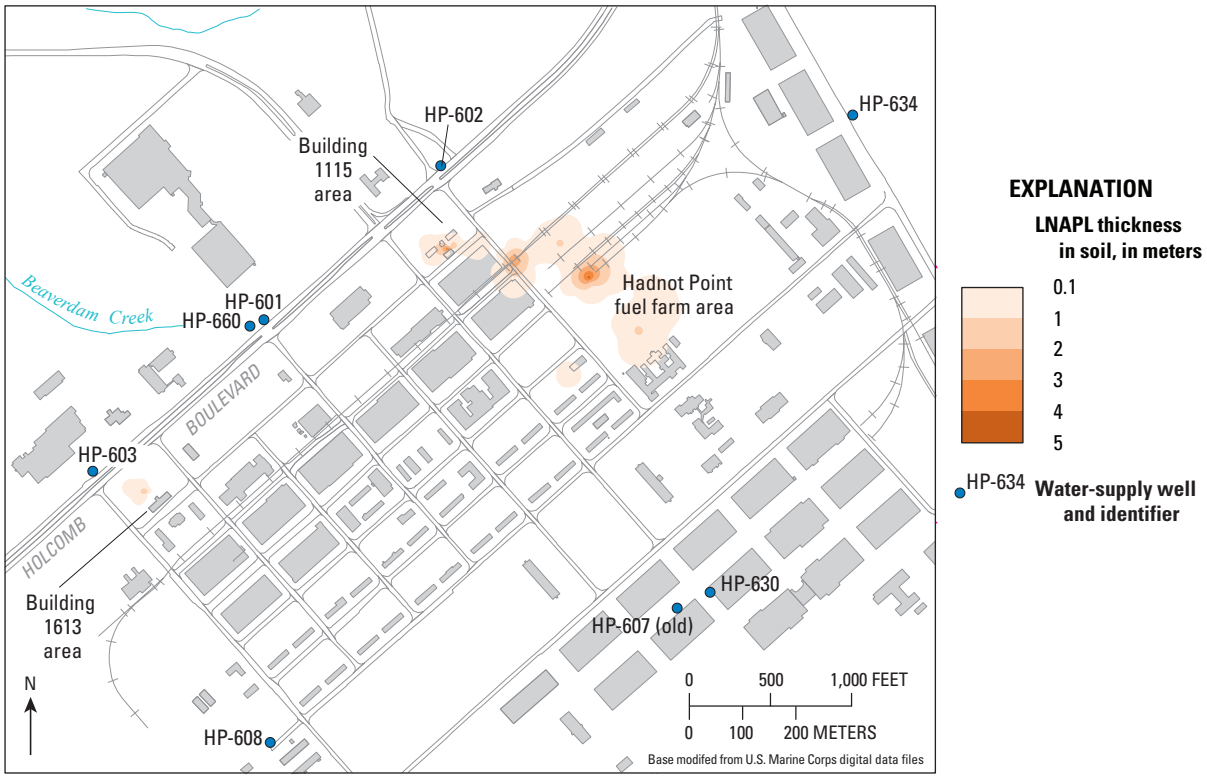


**Figure S7.13.** Interpolated actual light nonaqueous phase liquid (LNAPL) thickness in the soil at the Hadnot Point Industrial Area (HPIA), Hadnot Point–Holcomb Boulevard study area, U.S. Marine Corps Base Camp Lejeune, North Carolina.

**Table S7.6.** LNAPL volume estimates for three different soil porosities, Hadnot Point–Holcomb Boulevard study area, U.S. Marine Corps Base Camp Lejeune, North Carolina.

[LNAPL, light nonaqueous phase liquid; HPIA, Hadnot Point Industrial Area; HPFF, Hadnot Point fuel farm; Bldg, building]

| Scenario | Parameter values for Brooks-Corey equations[1] | Porosity, $\phi$ | Estimated LNAPL volume for HPIA areas of interest (HPFF, Bldg 1115, and Bldg 1613), in million gallons | | |
|---|---|---|---|---|---|
| | | | [2]Scheme 1 | [3]Scheme 2 | [4]Scheme 3 |
| A1 | [5]$\beta_{gn}$=1.60, 2.66 | 0.2 | 0.939 | 0.939 | 1.079 |
| A2 | [5]$\beta_{nw}$= 1.60, 2.66 | 0.25 | 1.174 | 1.174 | 1.348 |
| A3 | [6]$\beta_{gn}$=1.60, 2.66 | 0.3 | 1.408 | 1.409 | 1.618 |
| A4 | [6]$\beta_{nw}$= 1.44, 3.30 | 0.2 | 1.141 | 1.142 | 1.286 |

[1] In addition to the fluid-pair-dependent scaling factors shown for fresh and aged gasoline, the following parameter values were used in all cases: air-water displacement (or entry) pressure ($\psi_d^{gw}$), in meters of water, and pore size distribution index ($\lambda$)

[2] Semi-analytical solution (Farr et al. 1990) using interpolated apparent LNAPL thickness

[3] Numerical integration using interpolated apparent LNAPL thickness

[4] Numerical integration using interpolated actual LNAPL thickness

[5] Fluid-pair-dependent scaling factors for fresh gasoline (Farr et al. 1990)

[6] Fluid-pair-dependent scaling factors for aged gasoline (Farr et al. 1990)

**Table S7.7.** LNAPL volume estimates for different parameter values of the Brooks-Corey equation, Hadnot Point–Holcomb Boulevard study area, U.S. Marine Corps Base Camp Lejeune, North Carolina.

[LNAPL, light nonaqueous phase liquid; HPIA, Hadnot Point Industrial Area; HPFF, Hadnot Point fuel farm; m, meter; NAPL, nonaqueous phase liquid]

| Scenario | Parameter values for Brooks-Corey equations[1] | Porosity, $\phi$ | Estimated LNAPL volume for HPIA areas of interest (HPFF, Bldg 1115, and Bldg 1613), in million gallons | | |
|---|---|---|---|---|---|
| | | | [2]Scheme 1 | [3]Scheme 2 | [4]Scheme 3 |
| B1 | $\psi_d^{gw}$=0.068 m of water, $\lambda$=0.623 | 0.2 | 0.901 | 0.901 | 0.935 |
| B2 | $\psi_d^{gw}$=0.067 m of water, $\lambda$=1.27 | 0.2 | 1.138 | 1.139 | 1.190 |
| B3 | $\psi_d^{gw}$=0.064 m of water, $\lambda$=1.62 | 0.2 | 1.199 | 1.201 | 1.253 |

[1] The parameter values shown for air-water displacement (or entry) pressure ($\psi_d^{gw}$) and pore size distribution index ($\lambda$) are for well-graded soil (Al-Suwaiyan et al. 2002); the following additional parameter values were used in all cases: gas-LNAPL scaling factor, $\beta_{gn}$=1.60, and LNAPL-water scaling factor, $\beta_{nw}$=2.66, for fresh gasoline (Farr et al. 1990)

[2] Semi-analytical solution (Farr et al. 1990) using interpolated apparent LNAPL thickness

[3] Numerical integration using interpolated apparent LNAPL thickness

[4] Numerical integration using interpolated actual LNAPL thickness

# Fate and Transport of LNAPL Components

This analysis focuses on dissolution of individual contaminants from free-phase LNAPL source areas and subsequent fate and transport of dissolved phase contaminants in the groundwater system. Fate and transport processes included in this analysis are advection, mechanical dispersion, molecular diffusion, sorption, interphase mass transfer, and biological degradation. Interphase mass transfer of contaminants is assumed to occur among phases of water, LNAPL, and soil; this analysis does not consider interphase transfer of contaminants between water and gas phases.

Benzene and total xylenes were selected as specific contaminants of interest for this fate and transport analysis. Benzene is one of the most common contaminants found at contaminated sites and is classified as a known human carcinogen (U.S. Environmental Protection Agency 1998). Xylene, also known as dimethylbenzene, has three chemical isomer forms: *meta*-xylene (*m*-xylene), *ortho*-xylene (*o*-xylene), and *para*-xylene (*p*-xylene). The isomers are each composed of a benzene ring with two methyl groups attached and differ only in the arrangement of the methyl groups about the central benzene ring (ATSDR 2007). The physical and chemical properties of *p*-xylene are used in this study and are considered representative of all three isomers.

The contaminant fate and transport analysis described herein is conducted using the TechFlowMP model code. The groundwater-flow analysis upon which the fate and transport analysis is based was completed as a separate effort using the MODFLOW-2005 groundwater-flow model code (Suarez-Soto et al. 2013). Results from the MODFLOW groundwater-flow model were incorporated into the TechFlowMP contaminant fate and transport analysis. Further model details are provided in subsequent subsections.

## Methods

### Model Domain and Model Input Parameters

As part of the overall water-modeling project, a groundwater-flow model was developed for the entire HPHB study area (Figure S7.1). Within this larger model, two smaller subdomains were created to focus on contaminant fate and transport in specific local areas of interest, one of which is the HPIA. The groundwater-flow analyses for the larger HPHB model domain and the refined HPIA subdomain model are described in Suarez-Soto et al. (2013). Fate and transport of VOCs dissolved in groundwater within the HPIA model subdomain are described in Jones et al. 2013. For the purposes of the contaminant fate and transport analysis from subsurface dissolution of LNAPL, described herein, the focus is on the HPIA model subdomain.

To simulate three-dimensional groundwater flow and dissolved-phase contaminant migration, the HPIA model subdomain was discretized into 50-ft by 50-ft horizontal cells (Suarez-Soto et al. 2013, Jones et al. 2013). The TechfloMP computational grid also was constructed to be consistent with the groundwater-flow model grid of Suarez-Soto et al. (2013) (Figure S7.14). Description of the geohydrologic framework upon which the vertical descretization of the models is based is described in Faye (2012). The correlation between hydrogeologic units and model layers for the MODFLOW (groundwater flow) and TechFlowMP (contaminant fate and transport) models is presented in Table S7.8. MODFLOW considers only the water-saturated zone whereas TechFlowMP simulates contaminant transport in both the unsaturated (or variably saturated) and saturated zones. To facilitate contaminant transport modeling in the unsaturated and variably saturated zones, the upper layer of the TechFlowMP model is further vertically subdivided to form seven additional layers, designated as variably saturated zones (VSZs) 1–7 (Table S7.8). For the MODFLOW and TechFlowMP models, layer 1 is an unconfined aquifer, and layers 3, 5, and 7 are major water-bearing units and represent confined aquifers with relatively high hydraulic conductivities, ranging from 5 to 50 feet per day (ft/d). Model layers 2, 4, and 6 represent confining units (Table S7.8). In TechflowMP, the ratios of horizontal transverse and vertical transverse hydraulic conductivity to horizontal longitudinal hydraulic conductivity are 0.1 and 0.01, respectively. These parameter values for hydraulic conductivity were selected to be consistent with those used in the groundwater-flow analyses for the HPIA model subdomain described in Suarez-Soto et al. (2013).

Various physical, chemical, and biological parameter values used for the fate and transport analysis of benzene and total xylenes are listed in Table S7.9. The effective porosity of all aquifers for modeling purposes is 0.2. The horizontal longitudinal, horizontal transverse, and vertical transverse dispersivities implemented in the TechFlowMP model are 25, 2.5, and 0.25, respectively. These values also were selected to be consistent with those used in the fate and transport analyses for the HPIA model subdomain described in Jones et al. (2013). The rationale for selecting many of these parameter values was developed during work at the Tarawa Terrace study area of USMCB Camp Lejeune, as described in Faye (2008). As in the MODFLOW groundwater-flow model, the simulation period for the TechFlowMP contaminant fate and transport analysis is January 1942 through June 2008 (798 months). Variable-length time steps, or stress periods, are used in the TechFlowMP analysis.

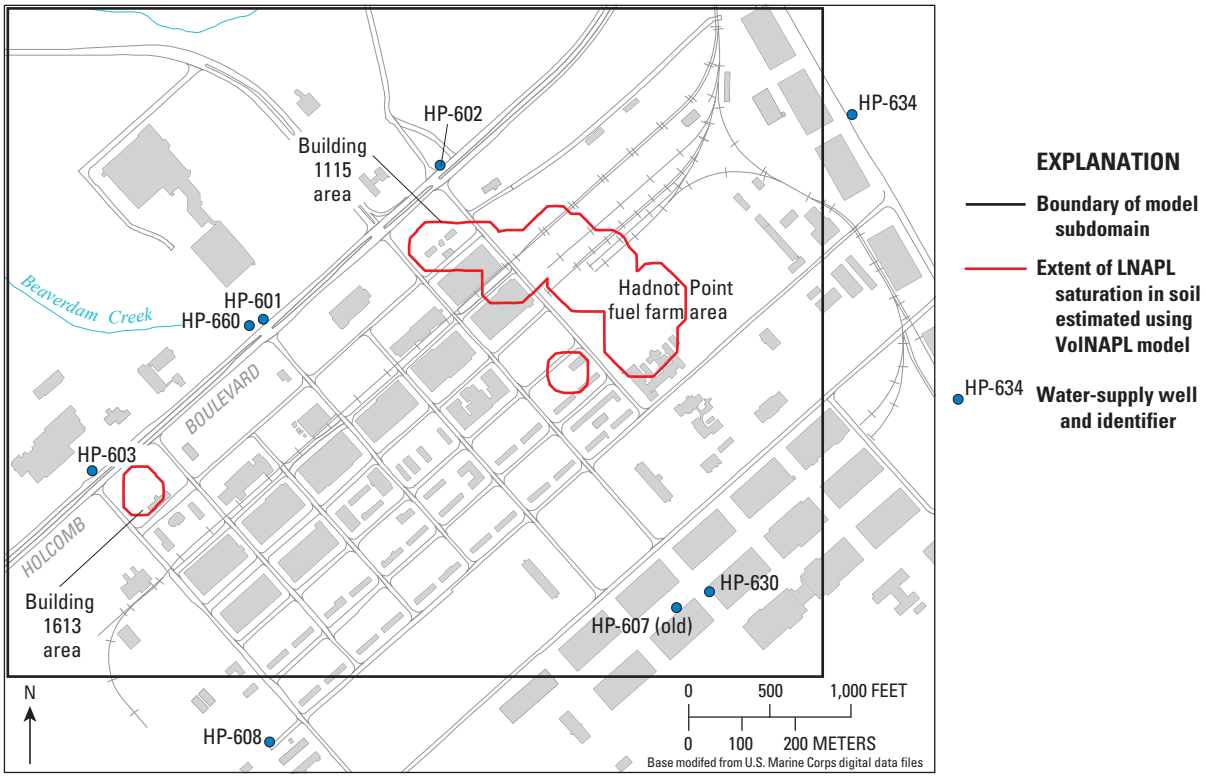


**Figure S7.14.** Hadnot Point Industrial Area (HPIA) model subdomain, Hadnot Point–Holcomb Boulevard study area, U.S. Marine Corps Base Camp Lejeune, North Carolina.

**Table S7.8.** Correlation between hydrogeologic units and model layers, Hadnot Point–Holcomb Boulevard study area, U.S. Marine Corps Base Camp Lejeune, North Carolina.

[MODFLOW, finite-difference groundwater-flow model code developed by U.S. Geological Survey; TechFLOWMP, finite element model code developed by the Multimedia Environmental Simulations Laboratory, Georgia Institute of Technology]

| Hydrogeologic unit[1] | Thickness range,[1] in feet | Model layer | |
|---|---|---|---|
| | | MODFLOW | TechFlowMP |
| Brewster Boulevard upper aquifer | 4 to 42 | 1 | [2]VSZ: 1–7 |
| Brewster Boulevard upper confining unit | 1 to 22 | | |
| Brewster Boulevard lower aquifer | 4 to 48 | | 1 |
| Brewster Boulevard lower confining unit | 2 to 30 | 2 | 2 |
| Tarawa Terrace aquifer (upper part) | 8 to 86 | 3 | 3 |
| Tarawa Terrace confining unit (middle and lower parts) | 4 to 40 | 4 | 4 |
| Upper Castle Hayne aquifer—River Bend unit | 16 to 70 | 5 | 5 |
| Local confining unit | 8 to 23 | | |
| Upper Castle Hayne aquifer—Lower unit | 10 to 48 | | |
| Middle Castle Hayne confining unit | 12 to 27 | 6 | 6 |
| Middle Castle Hayne aquifer | 62 to 122 | 7 | 7 |

[1] Units are listed from shallowest to deepest (Faye et al. 2012)

[2] VSZ: 1–7 indicates variably saturated zone model layers 1–7 used in the TechFlowMP model

**Table S7.9.** Soil and contaminant parameter values used in fate and transport analysis, Hadnot Point Industrial Area (HPIA) model subdomain, Hadnot Point–Holcomb Boulevard study area, U.S. Marine Corps Base Camp Lejeune, North Carolina.

[$m^2/s$, square meter per second; mg/L, milligram per liter; $cm^3/g$, cubic centimeter per gram; $d^{-1}$, per day; USEPA, U.S. Environmental Protection Agency; $K_{oc}$, partition coefficient with respect to organic fraction]

| Parameters | Benzene, $C_6H_6$ | *p*-xylene, $C_6H_4(CH_3)_2$ | Reference |
|---|---|---|---|
| Molecular weight | 78.11 | 106.16 | Cheremisinoff (2000) |
| Molecular diffusion in water | $7.77\times10^{-10}$ $m^2/s$ | $6.21\times10^{-10}$ $m^2/s$ | Calculated by Hayduk and Laudie method (Tucker and Nelken 1982) and from method outlined on USEPA Web site [1] |
| Aqueous solubility (at 25 degrees Celsius) | 1,780 mg/L | 181 mg/L | Lawrence 2007 |
| Equilibrium concentration in water | 16.8 mg/L | 7.9 mg/L | Calculated from method outlined by USEPA [1] |
| Decay rate (biodegradation rate) | 0.0001 $d^{-1}$ | 0.003 $d^{-1}$ | Selected based on literature review (Wilson et al. 1994; Wiedemeier 1995; U.S. Environmental Protection Agency 1999; Cozzarelli et al. 2010) |
| Sorption coefficient | 0.123 $cm^3/g$ | 0.8 $cm^3/g$ | Calculated using $K_{oc}$ values of 61.4 and 400 for benzene and *p*-xylene, respectively (U.S. Environmental Protection Agency 1996) |
| Mass transfer rate | 0.1 $d^{-1}$ | 0.1 $d^{-1}$ | Jang and Aral (2008a) |

[1] U.S. Environmental Protection Agency method available at *http://www.epa.gov/athens/learn2model/part-two/onsite*

## Water-Supply Wells in the HPIA

Historically, multiple water-supply wells operated within the HPIA (Figures S7.14, S7.15). Most of the water-supply wells within the HPIA have been out of service; only wells HP-606 and HP-642 were operating at the end of the study period (June 2008). Within the HPIA, water-supply wells extracted groundwater primarily from the Tarawa Terrace and Upper Castle Hayne aquifers, which correspond to model layers 3 and 5 (Table S7.8).

The water-supply wells closest to the LNAPL source areas in the HPIA are wells HP-602 and HP-603, constructed during November and December 1941, respectively; water-supply operations are estimated to have started during July 1942 (Sautner et al. 2013). Well HP-602 was constructed with multiple well screens open at various intervals from 70 to 160 ft below ground surface within the Tarawa Terrace and Upper Castle Hayne aquifer systems (Table S7.8). Well HP-603 was similarly constructed with multiple well screens open at intervals from 70 to 195 ft below ground surface. Construction details for these and other water-supply wells in the HPIA are provided in Faye et al. (2010).

In the TechFlowMP model, historical monthly operating schedules and pumping rates for water-supply wells in the HPIA during the simulation period correspond to the schedules and pumping rates used in the groundwater-flow analysis (Suárez-Soto et al. 2013). These well schedules and pumping rates were reconstructed from historical information and are described in detail in Sautner et al. 2013 and Telci et al. 2013. Wells HP-602 and HP-603 were reportedly shut down November 30, 1984, and June 1, 1996, respectively (Sautner et al. 2013). For model simulation, the corresponding timeframes for well shutdown are expressed as December 1984 and June 1996 because the model is discretized in monthly time steps or stress periods and water-supply wells are programmed as "on" or "off" for the entire stress period.

Reported concentrations of benzene and total xylenes for water samples collected from wells HP-602 and HP-603 during July 1984–September 1995 are listed in Table S7.10.

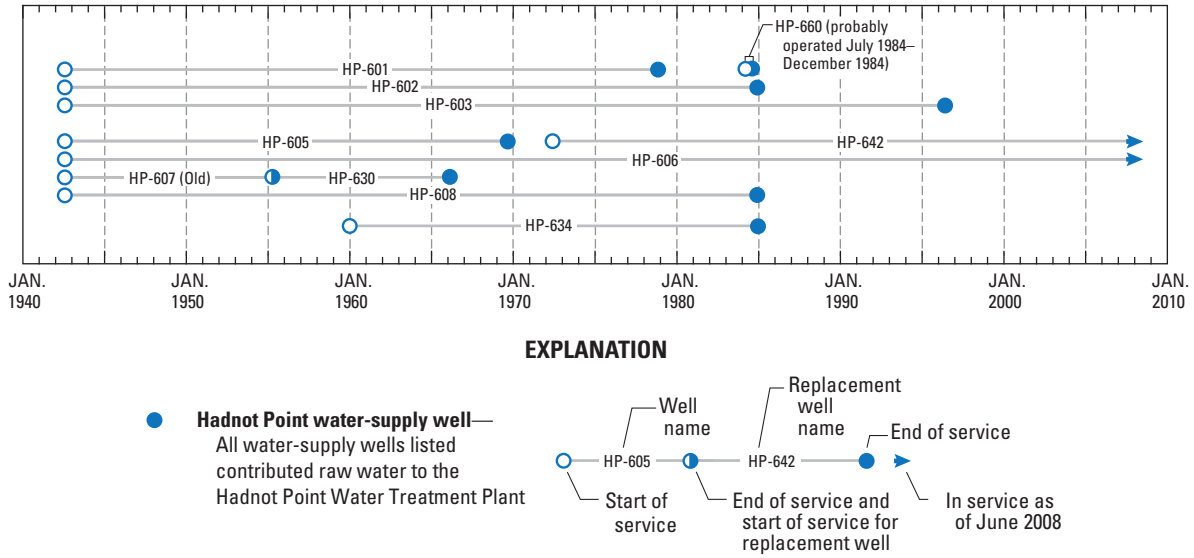


**Figure S7.15.** Operational chronology of water-supply wells within the Hadnot Point Industrial Area (HPIA) model subdomain, Hadnot Point–Holcomb Boulevard study area, U.S. Marine Corps Base Camp Lejeune, North Carolina (modified from Maslia et al. 2013, Figure A5).

**Table S7.10.** Reported concentrations of benzene and total xylenes in water-supply wells HP-602 and HP-603, Hadnot Point Industrial Area, Hadnot Point–Holcomb Boulevard study area, U.S. Marine Corps Base Camp Lejeune, North Carolina.[1]

[<, constituent is less than the detection limit. Number following the "<" is the detection limit; NA, constituent concentration not determined in laboratory analysis]

| Sample date | [2]Concentration, in micrograms per liter | |
|---|---|---|
| | Benzene | Total xylenes |
| Water-supply well HP-602 | | |
| 7/6/1984 | 380 | NA |
| 11/30/1984 | 120 | NA |
| 12/10/1984 | 720 | NA |
| 12/13/1984 | <1.0 | NA |
| 12/14/1984 | 230 | NA |
| 2/7/1985 | <10 | NA |
| 11/12/1986 | 50 | <12 |
| 1/22/1991 | 17 | <5.0 |
| Water-supply well HP-603 | | |
| 12/4/1984 | <10 | NA |
| 12/10/1984 | <10 | NA |
| 1/16/1985 | <10 | NA |
| 8/11/1988 | <10 | NA |
| 6/26/1990 | <5 | <5 |
| 1/22/1991 | <5 | <5 |
| 9/20/1995 | <0.50 | <0.50 |

[1] From Faye et al. (2010)

[2] Concentrations above the detection limit are highlighted in red font

## LNAPL Source Areas

LNAPL source areas defined for the HPIA model subdomain are shown in Figures S7.14 and S7.16. The LNAPL source areas correspond to the vertically variable LNAPL saturation profiles determined previously using the TechNAPLVol code and distribution of actual LNAPL thickness in soil (Figure S7.13). The LNAPL in the source areas is assumed to be stationary. This assumption is consistent with field data indicating very little migration of the footprint of LNAPL over time (Catlin Engineers and Scientists 2003).

The LNAPL source start dates for modeling purposes are set as January 1951 for the HPFF area and January 1964 for the Building 1613 area (Figure S7.16). Historical records delineating the start date of fuel spills or releases from the UST systems in these areas were not available. Consequently, a rationale for the source start date was formulated based on the installation date of UST systems and empirical data on the cause and timing of fuel leaks and releases from UST systems. In 1987, the USEPA published a report indicating that fuel delivery piping and spills/overfills accounted for more fuel releases (in terms of number of releases, not volume of release) than the associated storage tanks themselves (USEPA 1987). In fact, fuel piping and fittings were implicated in 80–85 percent of all releases from UST systems (USEPA 1987). In a separate study containing an analysis of 1,244 leak incident reports across the United States, the USEPA reported mean and median age for UST system piping leaks as 11 and 9 years, respectively (USEPA 1986). For this analysis, the median age of 9 years for UST piping leaks was used. The UST systems in the HPFF area were installed during 1941 and 1942; the UST system in the Building 1613 area was installed during the 1950s (O'Brien and Gere Engineers, Inc. 1988; Richard Catlin and Associates, Inc. 1996, 1998; CH2M HILL, Inc. 2001). Combining the UST installation dates of 1942 and 1955 (midpoint of installation date range) with the information indicating a 9-year median age of piping leaks yields the selected LNAPL source start dates of January 1951 for the HPFF area and January 1964 for the Building 1613 area used for modeling purposes.

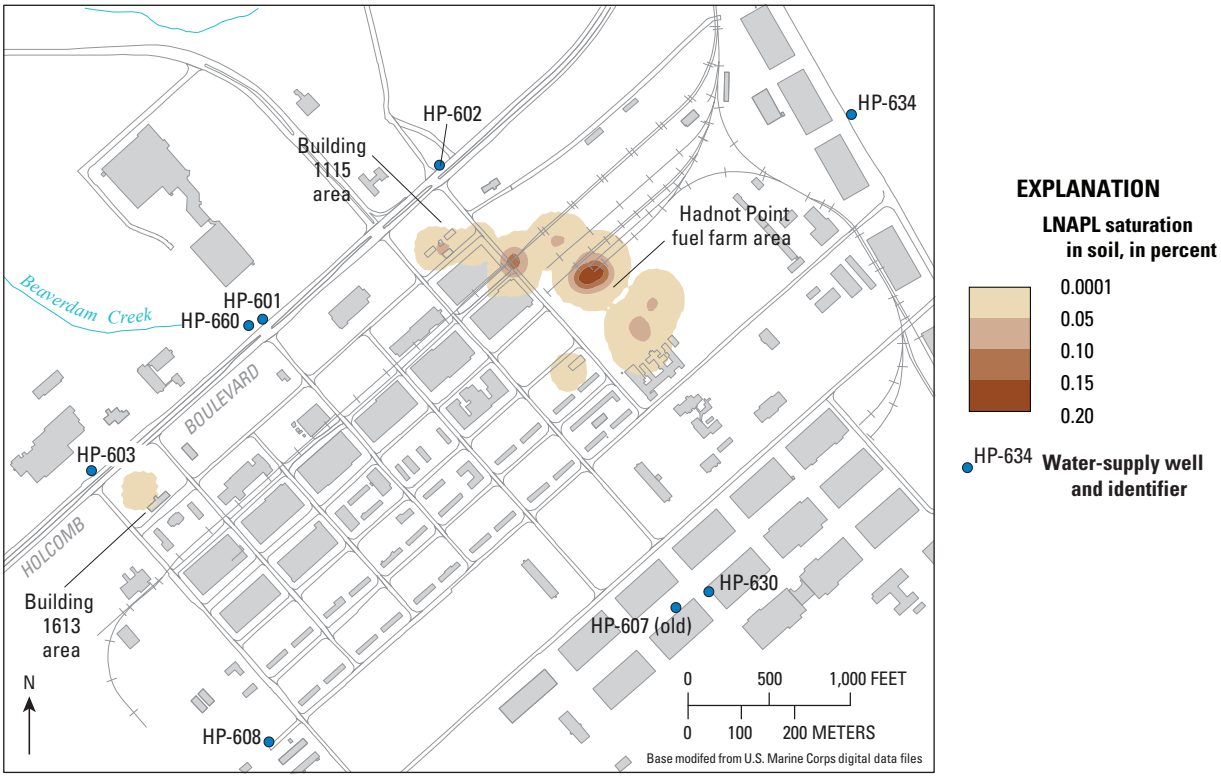


**Figure S7.16.** Estimated distribution of light nonaqueous phase liquid (LNAPL) saturation in the Hadnot Point fuel farm and Building 1613 areas, Hadnot Point–Holcomb Boulevard study area, U.S. Marine Corps Base Camp Lejeune, North Carolina.

## Groundwater Flow

Solution to the equation of multiphase flow in the subsurface (Equation 1) requires the temporal and spatial variation of the computed Darcy flux vector $\boldsymbol{q}_f$ for every cell (or element) in the model domain (i.e., the HPIA model subdomain, Figure S7.14). In multiphase flow, hydraulic conductivity is a function of fluid saturation, thereby resulting in a highly nonlinear equation for computing $\boldsymbol{q}_f$ (Equation 2). To reduce the computational burden when applying TechFlowMP to the HPIA, the Darcy velocities (specific discharges) computed using the MODFLOW model code were imported into the TechFlowMP code, thereby negating the need for TechFlowMP to compute groundwater-flow velocities. The velocities were obtained from the MODFLOW calibrated model described by Suárez-Soto et al. (2013) for every model layer (1–7) and every time step. To compute water saturations, the temporal and spatial variations of hydraulic heads derived by MODFLOW (Suárez-Soto et al. 2013) were also imported into TechFlowMP to solve the multiphase transport equation.

Contours of simulated hydraulic heads for model layers 3 and 5 in December 1961 and 1983 are presented in Figure S7.17. Generally, groundwater flow in the HPIA is from east to west/southwest, toward the New River. The areas where groundwater flow is depicted as radially inward represent the locations of water-supply wells that are withdrawing groundwater and subsequently lowering the hydraulic heads in the surrounding areas. The difference in hydraulic heads between model layers 3 and 5 indicates a vertical hydraulic gradient, or downward flow of groundwater.

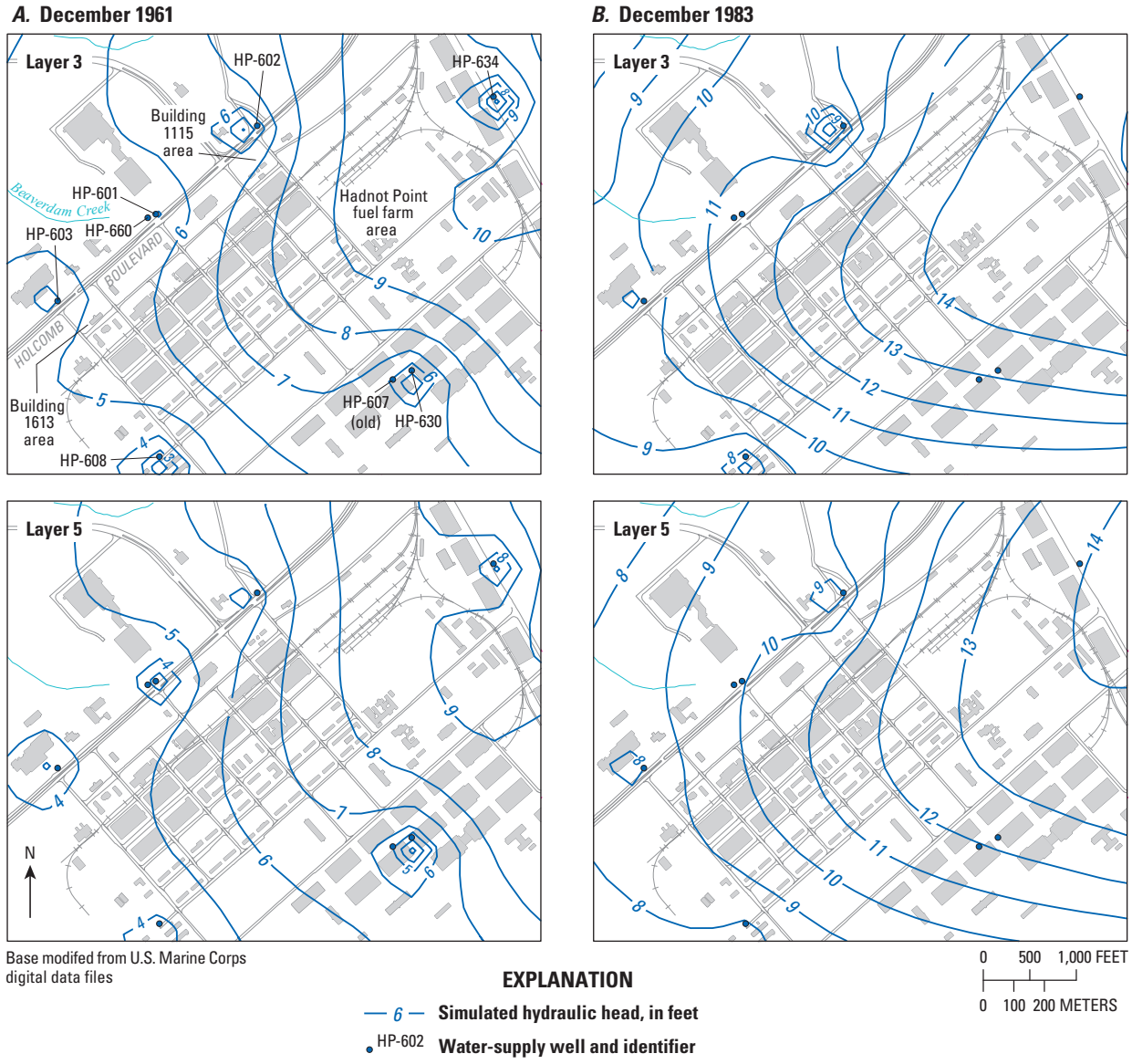


**Figure S7.17.** Simulated hydraulic heads for model layers 3 and 5 in the Hadnot Point Industrial area, Hadnot Point–Holcomb Boulevard study area, U.S. Marine Corps Base Camp Lejeune, North Carolina, *(A)* December 1961 and *(B)* December 1983.

The simulated hydraulic heads shown in Figure S7.17 are used to compute local water pressure heads and hydraulic gradients within TechFlowMP. Assuming gas pressure in the unsaturated zone is constant, the capillary pressure of water–gas is calculated and local water saturation is evaluated based on the saturation-capillary pressure relation. Within the LNAPL source zones (Figures S7.14 and S7.16), water saturation depends on both the capillary pressure of water–gas and LNAPL saturation because the presence of LNAPL in pore spaces may reduce local water saturation. The sum of water–gas and LNAPL saturations should not exceed 1 (Equation S7.5). The relative permeability of the groundwater is determined according to water saturation level, and then water saturation and Darcy velocity are used in the transport equation to model the migration of benzene and total xylenes.

## Numerical Techniques

The groundwater-flow analysis conducted by Suárez-Soto et al. (2013) uses various versions of the MODFLOW finite-difference model code developed by the USGS (McDonald and Harbaugh 1984; Harbaugh et al. 2000). The contaminant fate and transport analysis described herein uses the TechFlowMP model—a finite-element code. For contaminant transport modeling the MODFLOW finite-difference grid was imported into TechFlowMP and converted to a finite-element mesh. The TechFlowMP model uses a direct PARDISO sparse matrix solver with parallel computing and an iterative sparse matrix solver, IML++. A semi-implicit Crank-Nicolson technique is implemented for the numerical solution of the transport equation. Mass lumping of the time-derivative mass matrices is used to improve the stability of the solution of nonlinear flow equations (Frind 1982; Celia et al. 1990; Rathfelder and Abriola 1994; Jang and Aral 2006). An iterative scheme is used to handle nonlinear terms, including relative permeability. Mass balance calculations are conducted to determine temporal changes in contaminant mass within each phase and to verify that mass is conserved during simulations (Huyakorn and Pinder 1983).

# Results

The simulation period for this analysis is January 1942 through June 2008. Simulation results are presented and discussed in terms of

- the spatial and temporal variation of contaminant distributions in selected model layers,
- the temporal variation of dissolved phase contaminants that reach nearby water-supply wells HP-602 and HP-603, and
- the fate and distribution of contaminant mass within the overall model over time (mass balance accounting).

Timeframes for simulation results are stated in conventional calendar time and also occasionally in terms of the corresponding model stress period number. The first model stress period is January 1942 (Suárez-Soto et al. 2013, Table S4.6).

TechFlowMP simulation results for the distribution of dissolved phase benzene in model layers 1, 3, and 5 during December 1961 and December 1983 are shown in Figure S7.18. These results represent the dissolved phase benzene plumes in groundwater approximately 11 and 33 years after the HPFF source start date of January 1951. The dissolved benzene plume migrates laterally and downward from the LNAPL source area in the shallow aquifer (model layer 1), and its concentration decreases with depth. By December 1961 (Figure S7.18*A*), the simulated benzene plume reaches water-supply well HP-602, which is pumping from model layers 3 and 5—the primary water-bearing zones represented in the model (Table S7.8). The Building 1613 source start date is January 1964; therefore, dissolved phase benzene is not yet present in the Building 1613 area during 1961. By December 1983 (Figure S7.18*B*), simulation results show that a dissolved phase benzene plume has developed in both the HPFF and Building 1613 areas.

The temporal variation of dissolved benzene concentration in model layers 3–5 at water-supply wells HP-602 and HP-603 is shown in Figure S7.19. In well HP-602, simulated benzene concentrations in all three model layers increase over time until the well is shut down in the model in December 1984 (stress period 516). Once well HP-602 stops pumping, contaminant transport toward the well is reduced and the benzene concentrations in each model layer decrease rapidly.

Similar to well HP-602, simulated benzene concentrations for well HP-603 increase over time until well HP-603 is shut down in June 1996 (stress period 654). When well HP-603 is shut down, the benzene concentration in each model layer approaches a steady state, equilibrium value. Benzene concentrations in the two upper model layers (3 and 4) are higher than the equilibrium concentration when well HP-603 is shut down; therefore, the concentrations in layers 3 and 4 begin to decrease. When well HP-603 is shut down, the benzene concentration in model layer 5 is lower than the equilibrium concentration; therefore, the concentration in this layer increases.

At well HP-602, simulated benzene concentration is highest in all three model layers during November 1984 (stress period 515) (Figure S7.19). At well HP-603, simulated benzene concentration is highest during May 1996 (stress period 653). For both wells, flow-weighted concentrations can be calculated by combining simulated results from model layers 3–5. Recall that wells HP-602 and HP-603 were constructed with multiple well screens open to the Tarawa Terrace aquifer and the Upper Castle Hayne aquifer system (model layers 3–5). During actual well operation, the total volumetric flow at a water-supply well is the sum of contributions of groundwater from each individual well screen interval. Similarly, a flow-weighted concentration for the model results combines the individual flows and associated contaminant concentrations from each model layer to represent a total combined flow and concentration for the well of interest. The ratios of model layer flow to total flow for selected layers at wells HP-602 and HP-603 are listed in Table S7.11. Using these ratios, the flow-weighted concentration for benzene at

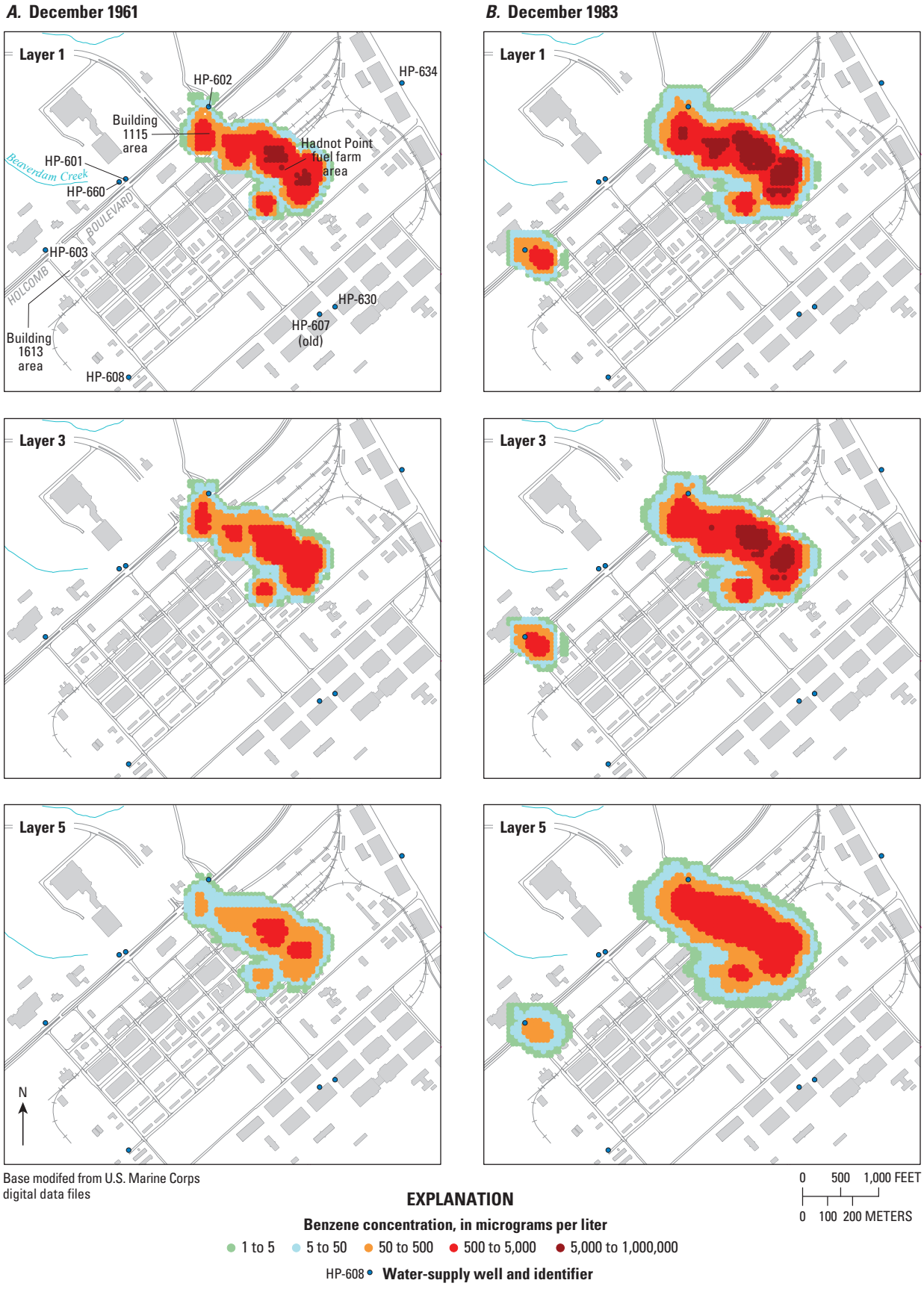


**Figure S7.18.** Simulated distribution of benzene within the Hadnot Point Industrial Area, model layers 1, 3, and 5, Hadnot Point–Holcomb Boulevard study area, U.S. Marine Corps Base Camp Lejeune, North Carolina, *(A)* December 1961 and *(B)* December 1983.

**Table S7.11.** Ratio of model layer flow to total flow for water-supply wells HP-602 and HP-603, Hadnot Point–Holcomb Boulevard study area, U.S. Marine Corps Base Camp Lejeune, North Carolina.

[—, no information presented for this model layer]

| Water-supply well identifier | [1]Ratio of model layer flow to total flow, in percent | | | | | | |
|---|---|---|---|---|---|---|---|
| | Layer 1 | Layer 2 | Layer 3 | Layer 4 | Layer 5 | Layer 6 | Layer 7 |
| HP-602 | — | — | 27.11 | 1.51 | 71.38 | — | — |
| HP-603 | — | — | 25.68 | 1.13 | 73.19 | — | — |

[1]The ratios shown are temporal averages calculated for the model simulation period January 1942–June 2008

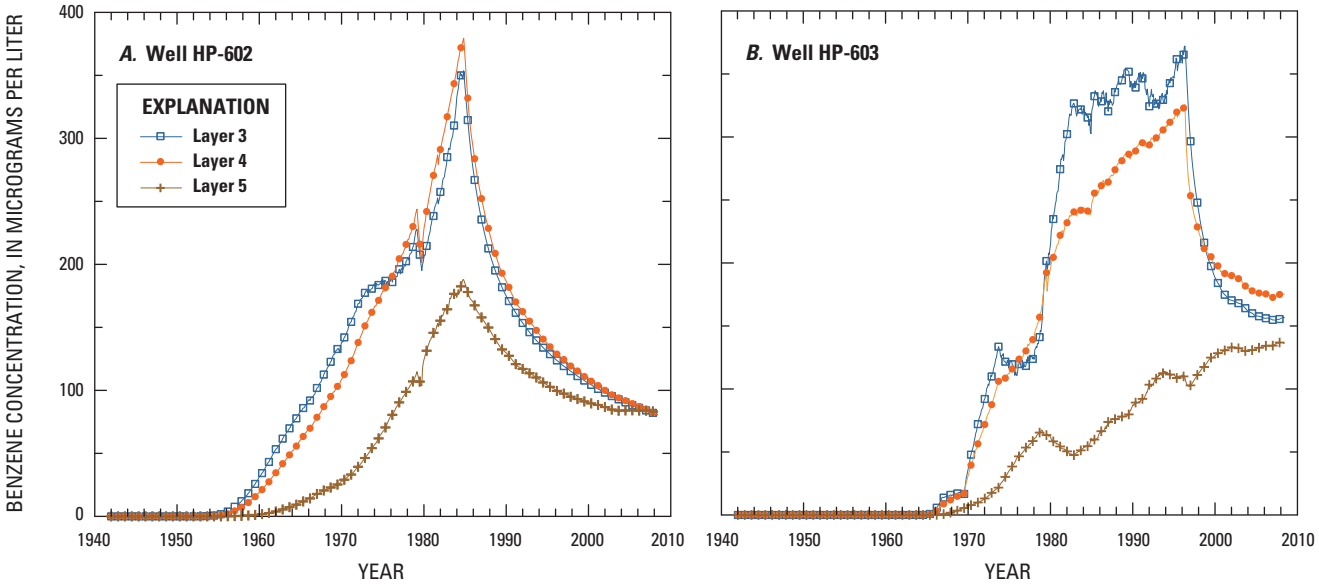


**Figure S7.19.** Simulated benzene concentration in model layers 3, 4, and 5 for water-supply wells *(A)* HP-602 and *(B)* HP-603, Hadnot Point Industrial area, Hadnot Point–Holcomb Boulevard study area, U.S. Marine Corps Base Camp Lejeune, North Carolina.

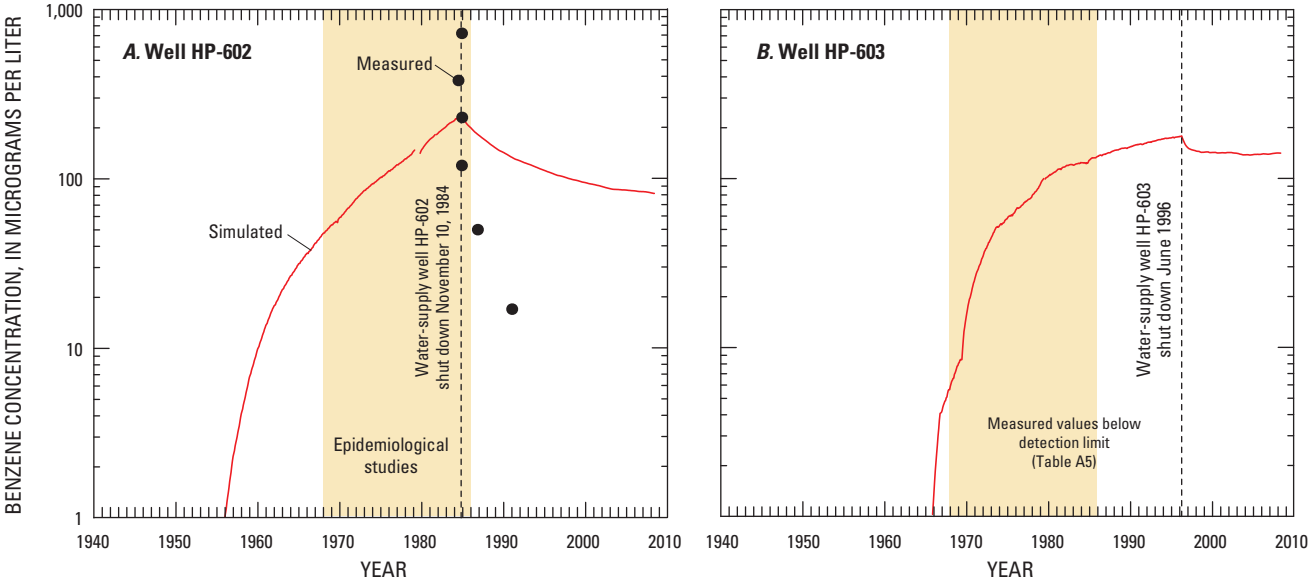


**Figure S7.20.** Simulated (flow-weighted) and measured concentrations of benzene at water-supply wells *(A)* HP-602 and *(B)* HP-603, Hadnot Point Industrial Area, Hadnot Point–Holcomb Boulevard study area, U.S. Marine Corps Base Camp Lejeune, North Carolina.

well HP-602 is calculated as 236 µg/L for November 1984. Similarly, the flow-weighted concentration for benzene at well HP-603 is calculated as 179 µg/L for May 1996. Flow-weighted simulation results for both wells HP-602 and HP-603 are presented in Figure S7.20.

Reported benzene concentrations for water samples collected from well HP-602 during July 1984–January 1991 are listed in Table S7.10. These measured data also are listed in Figure S7.20 for comparison to simulation results. The measured data show a sharper decrease than the simulated results after December 1984 when well HP-602 was shut down in the model. Reported benzene concentrations measured in water samples collected from well HP-603 during December 1984–September 1995 also are included in Table S7.10. The measured data at well HP-603 are all below laboratory detection limits that decrease over time from 10 µg/L to 0.5 µg/L.

Differences between measured data and simulation results at well HP-602 and particularly at well HP-603 may be due to a number of factors, including uncertainties and variability in field (measured) data due to sampling methods, analytical methods, and the inherent natural variation in environmental systems that are sampled over time. Such variability is apparent in the chronological listing of reported benzene concentrations in well HP-602 in Table S7.10. Other factors pertaining to water-supply well operation and sampling protocols (when and how long a particular water-supply well had operated before sample collection) also may account for differences between measured data and simulation results. A more detailed discussion of how water-supply well operation may affect measured sample data is provided on page C63 of Faye et al. (2010). Additionally, as discussed in Maslia et al (2013), differences in the local hydraulic, fate, and transport characteristics in the vicinity of Building 1613 compared to the average hydraulic, fate, and transport properties represented by the model may also contribute to the disparity between simulation and sampled benzene concentrations at well HP-603.

Simulation results for the distribution of dissolved phase total xylenes in model layers 1, 3, and 5 during December 1961 and December 1983 are shown in Figure S7.21. These results represent the dissolved phase plumes of total xylenes in groundwater approximately 11 and 33 years after the source start date of January 1951 in the HPFF area. The concentrations of dissolved phase xylenes are much lower than the concentrations of benzene for the same timeframes due to the difference in chemical properties of the two contaminants. The equilibrium concentration of xylenes (7.9 µg/L) is less than that of benzene (16.8 µg/L), which means that xylenes have a lower dissolution rate (and ultimately a smaller total mass transfer) from the LNAPL source areas into the groundwater. The sorption coefficient and decay rate of xylenes are greater than the corresponding values for benzene, which translates into relatively less xylenes in the dissolved phase in groundwater and relatively more xylenes being degraded or sorbing to soil.

By December 1961 (Figure S7.21*A*), the simulated total xylenes plume reaches water-supply well HP-602. By December 1983 (Figure S7.21*B*), simulation results show a dissolved phase plume of total xylenes has developed in both the HPFF and Building 1613 areas.

The temporal variation of dissolved total xylenes concentrations in model layers 3, 4, and 5 at wells HP-602 and HP-603 is shown in Figure S7.22. Simulated concentrations of total xylenes increase over time at both wells until they are shut down during December 1984 (stress period 516) and June 1996 (stress period 654). Concentrations of total xylenes decrease in each well after shutdown.

The fate of benzene and total xylenes in the TechFlowMP model simulation is illustrated in Figure S7.23 in terms of a mass balance representing the relative amount of contaminant over time in the dissolved and sorbed phases as well as the relative amount of contaminant removed from the system through biodegradation and withdrawal by water-supply wells. Contaminant mass is added to the system through the dissolution of benzene and total xylenes from the LNAPL source areas. The mass of contaminant in various states is presented as a percent of the total mass in the system (from LNAPL dissolution). The cumulative mass balance error is less than 0.7 percent over the simulation period.

The fate and transport of benzene and total xylenes in the model is consistent with their respective physical and chemical properties (Table S7.9). For much of the simulation period, the ratio of sorbed mass is similar to the ratio of dissolved mass for benzene (Figure S7.23*A*). As benzene is transferred into the groundwater through dissolution, contaminant mass in both the dissolved and sorbed phases increases steadily over time. Because xylenes have a higher sorption coefficient than benzene and a relatively low aqueous solubility (an order of magnitude lower than that of benzene), more xylenes tend to exist in the sorbed phase rather than in the dissolved phase (Figure S7.23*B*). Xylenes have a higher biodegradation (decay) rate; therefore, relatively more total xylenes than benzene are removed from the system over time. Relatively little contaminant mass is removed from the system through groundwater pumping by water-supply wells HP-602 and HP-603. It is interesting to note that the dissolution of benzene and total xylenes from the LNAPL source areas over the entire simulation period reduces the source area LNAPL mass by only 1.7 percent.

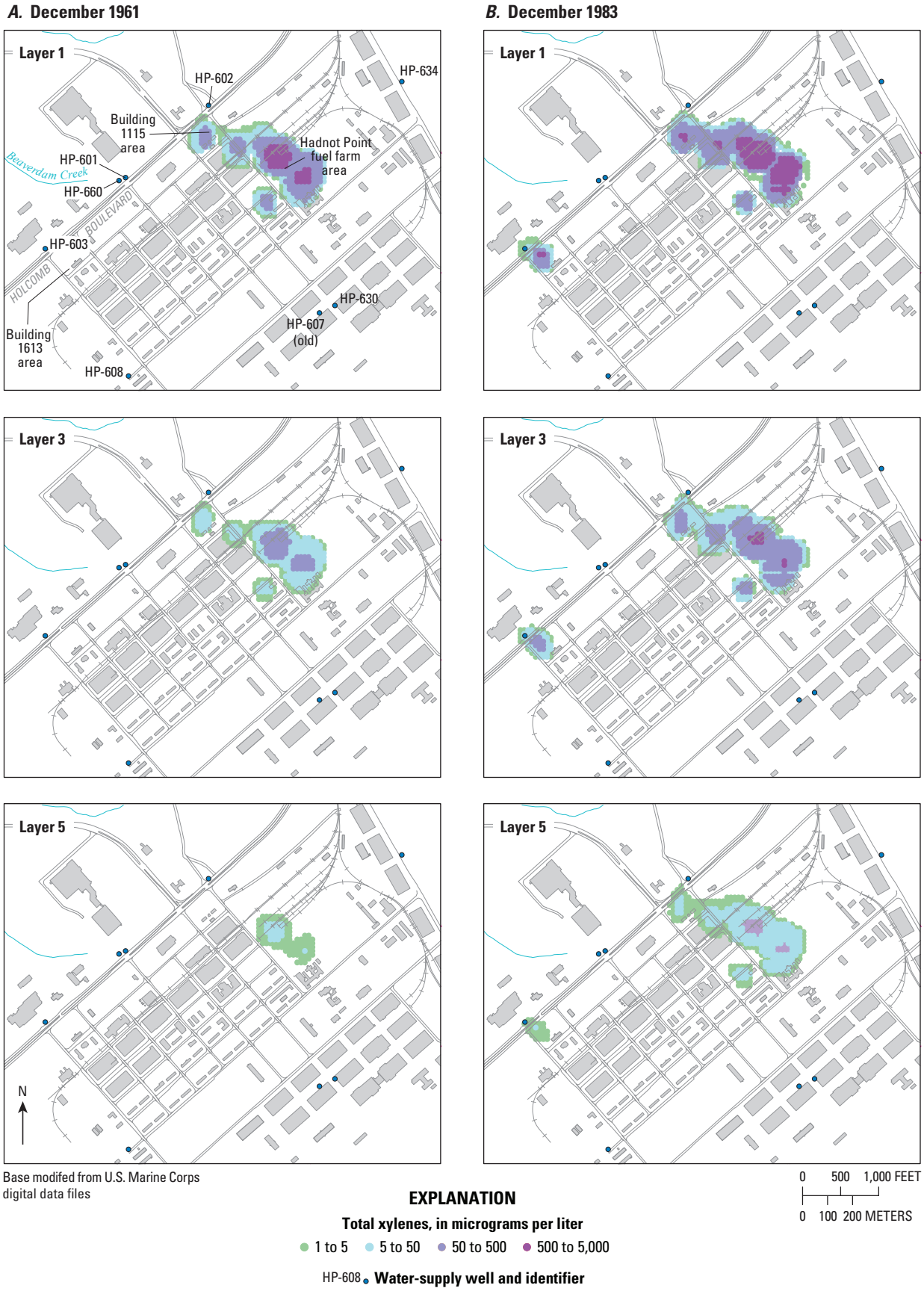


**Figure S7.21.** Reconstructed (simulated) distribution of total xylenes within the Hadnot Point Industrial Area fate and transport model subdomain, model layers 1, 3, and 5, Hadnot Point–Holcomb Boulevard study area, U.S. Marine Corps Base Camp Lejeune, North Carolina, *(A)* December 1961 and *(B)* December 1983.

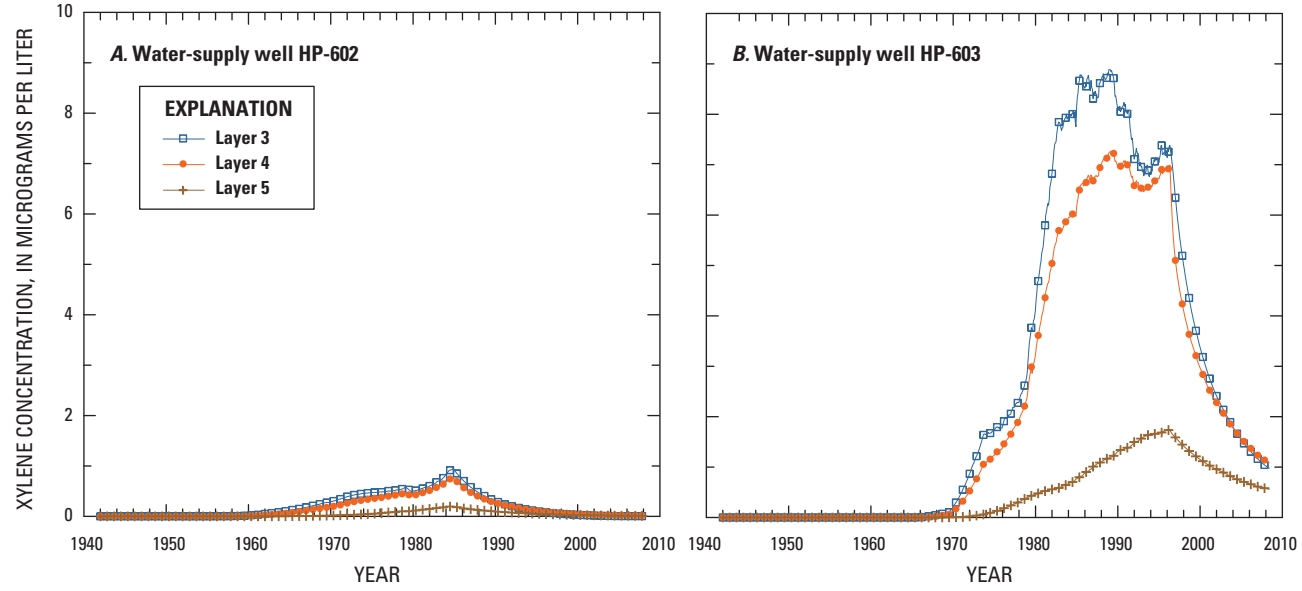


**Figure S7.22.** Simulated total xylenes concentrations in model layers 3, 4, and 5 for water-supply wells *(A)* HP-602 and *(B)* HP-603, Hadnot Point Industrial area, Hadnot Point–Holcomb Boulevard study area, U.S. Marine Corps Base Camp Lejeune, North Carolina.

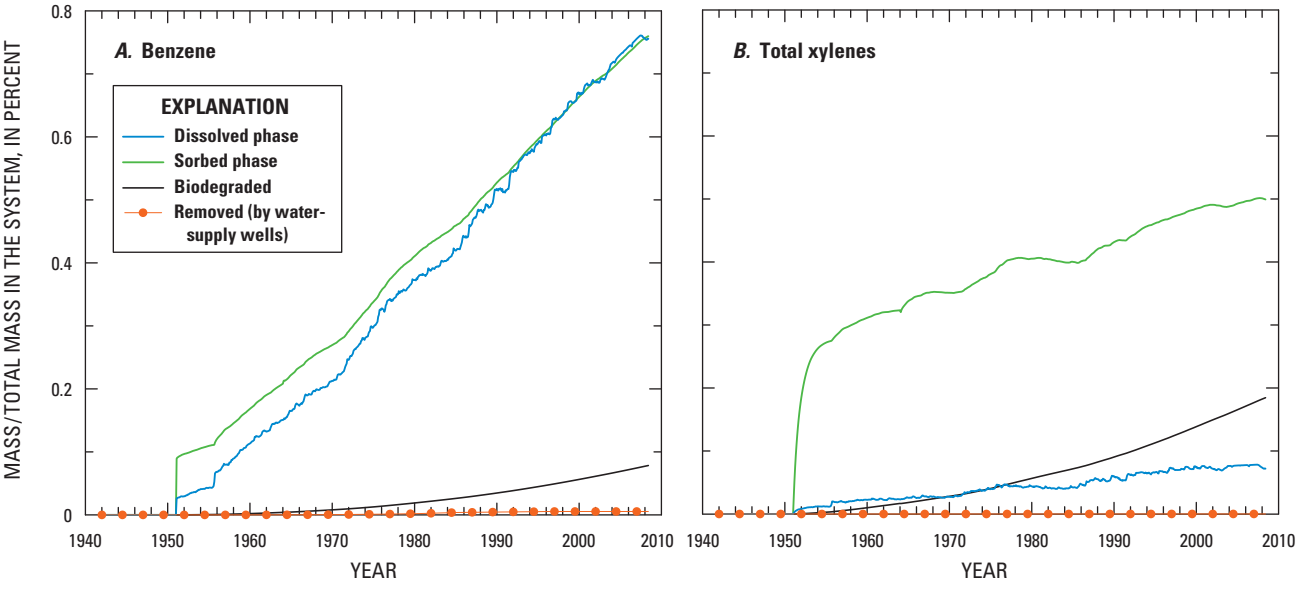


**Figure S7.23.** Fate of *(A)* benzene and *(B)* total xylenes during the TechFlowMP model simulation period, within the Hadnot Point Industrial area fate and transport model subdomain, Hadnot Point–Holcomb Boulevard study area, U.S. Marine Corps Base Camp Lejeune, North Carolina.

## Sensitivity Analysis

Numerous physical, chemical, and biological parameters, such as aquifer hydraulic conductivity and dispersivity, contaminant reaction rates, and distribution (sorption) coefficients, are needed to characterize system behavior in a fate and transport analysis of contaminants in groundwater. Uncertainties exist in the physical system as well as in the model analysis due to the inherent randomness of natural processes, scarcity of data to fully characterize model input parameters, and the incomplete mathematical formulation of complex natural processes (Aral 2010). As discussed in Maslia et al. (2013), there are numerous methods for characterizing a model's sensitivity and uncertainty based on variations of calibrated parameter values (ASTM 1994, Cullen and Frey 1999, Saltelli et al. 2000, Tung and Yen 2005, Hill and Tiedeman 2007). These methods are generally classified into two groups: (1) sensitivity analysis, wherein calibrated model parameter values are varied one at a time (either manually or through some automated and objective parameter estimation method) and (2) probabilistic uncertainty analysis, wherein probabilistic methods are used to characterize and quantify the input and output parameter variation and uncertainty. Both general types of methods are illustrated in previous work at Camp Lejeune for the Tarawa Terrace study area (Maslia et al. 2009). Although the analysis in this study utilizes some probabilistic components, it is designated a sensitivity analysis within the framework, and definitions are provided in Maslia et al. (2013).

The analysis in this study is focused on contaminant reaction rate (decay rate) and distribution (sorption) coefficient. These two parameters are key factors in determining the total mass and distribution of contaminant in the groundwater system. The relative likelihood or statistical distribution of these parameters can be generated by using a variety of sampling techniques, including Monte Carlo (MC) simulation and Latin hypercube sampling (Frey and Patil 2002). MC simulation is used herein to generate random values that approximate probability density functions (PDFs) of contaminant reaction rate and sorption coefficient.

Because benzene is classified as a known human carcinogen (National Toxicology Program 2011), it is a contaminant of concern and of primary interest to the ATSDR health studies. Therefore, the sensitivity analysis reported herein focuses on benzene. The definition and input statistics for benzene reaction rate and distribution coefficient PDFs were developed based on literature values (USEPA 1999, 1996) and some site-specific refinement using model simulations and available field data. For this analysis, the PDF for benzene decay rate is expressed as a log-normal distribution with a mean value of $1\times10^{-4}$ per day ($d^{-1}$) and minimum, maximum, and standard deviation of $2.0\times10^{-5}d^{-1}$, $2.2\times10^{-4}d^{-1}$, and $0.54\,d^{-1}$, respectively. The distribution coefficient of benzene is expressed as a Gaussian (normal) distribution with a mean of 0.123 and minimum, maximum, and standard deviation of 0.024 cubic centimeter per gram ($cm^3/g$), 0.221 $cm^3/g$, and 0.024 $cm^3/g$, respectively. The PDFs generated using 500 MC realizations for reaction rate and distribution coefficient are shown in Figure S7.24. Descriptive statistics for these PDFs, including the 5th and 95th percentile values, are listed in Table S7.12.

The 5th and 95th percentile values from the PDFs for benzene reaction rate and distribution coefficient (Figure S7.24, Table S7.12) are used in the model to estimate the range of results for benzene concentration (i.e., upper and lower limits of benzene concentration) in the groundwater system. Simulation results for the upper and lower limits of dissolved benzene concentration at layers 3, 4, and 5 are shown in Figure S7.25. At the location of water-supply well HP-602, simulated benzene concentration peaks during November 1984 (stress period 515). During this peak period, the ranges (upper and lower limits) of simulated benzene concentration in model layers 3, 4, and 5 are 220–530 µg/L, 230–580 µg/L, and 110–320 µg/L, respectively. At water-supply well HP-603, simulated benzene concentration peaks during May 1996 (stress period 653). During this peak period, the ranges (upper and lower limits) of simulated benzene concentration in model layers 3 and 4 are 250–465 µg/L and 230–395 µg/L, respectively. Expressed in terms of flow-weighted averages that combine results for model layers 3–5, the ranges of simulated total benzene concentration at peak periods are 138–378 µg/L in well HP-602 during November 1984 and 124–218 µg/L in well HP-603 during May 1996.

**Table S7.12.** Descriptive statistics for Monte Carlo-generated probability density functions for benzene reaction rate and distribution coefficient.

[$d^{-1}$, per day; $cm^3/g$, cubic centimeter per gram]

| Model parameter | Mean[1] | Standard deviation[1] | 5th percentile[1] | 95th percentile[1] | Random number generation method |
|---|---|---|---|---|---|
| Benzene reaction rate ($d^{-1}$) | $9.22\times10^{-5}$ | 0.49 | $3.311\times10^{-5}$ | $1.853\times10^{-4}$ | Monte Carlo simulation using lognormal distribution[2] |
| Benzene distribution coefficient ($cm^3/g$) | 0.123 | 0.024 | 0.075 | 0.169 | Monte Carlo simulation using normal distribution |

[1] Statistical data obtained from 500 Monte Carlo realizations

[2] Log-normal distribution selected based on data reported in U.S. Environmental Protection Agency (1999)

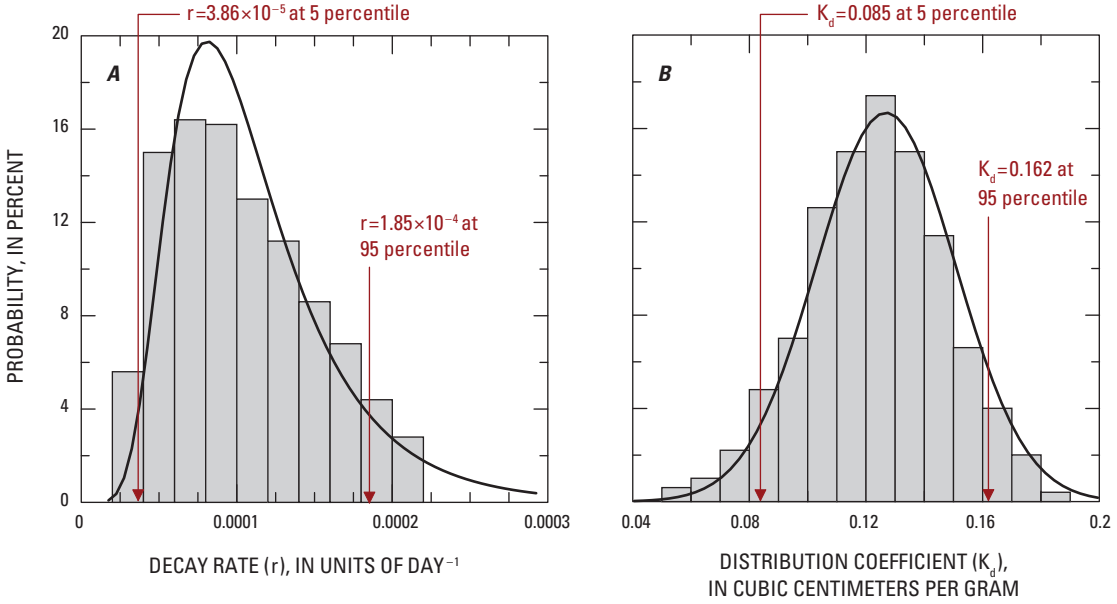


**Figure S7.24.** Probability density functions generated using 500 Monte Carlo realizations for *(A)* benzene decay rate and *(B)* benzene distribution coefficient, Hadnot Point Industrial Area fate and transport model subdomain, Hadnot Point–Holcomb Boulevard study area, U.S. Marine Corps Base Camp Lejeune, North Carolina.

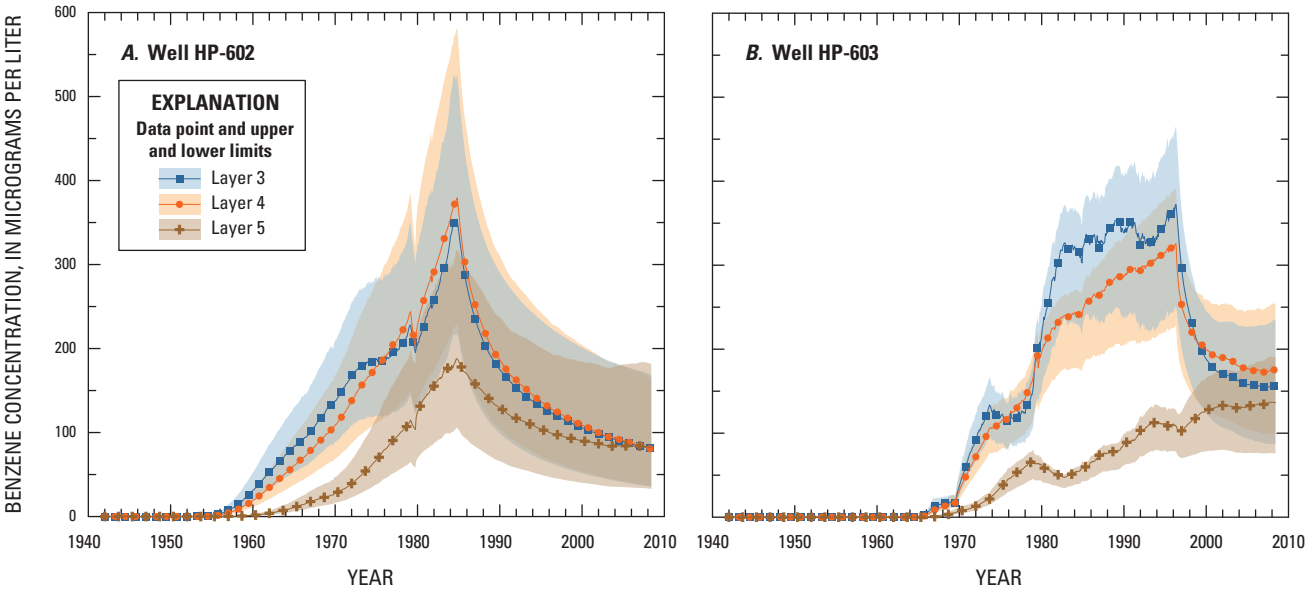


**Figure S7.25.** Sensitivity analysis results (upper and lower limits) for simulated benzene concentration in model layers 3, 4, and 5 at water-supply wells *(A)* HP-602 and *(B)* HP-603, Hadnot Point–Holcomb Boulevard study area, U.S. Marine Corps Base Camp Lejeune, North Carolina.

# Summary and Conclusions

The subsurface migration of LNAPL through the unsaturated zone and into a dissolved phase in groundwater is often oversimplified in environmental modeling. In fact, the downward migration of LNAPL through soil pore spaces of variable saturation involves complex, simultaneous, multiphase fluid flow of water, LNAPL, and air. Lateral migration of LNAPL at a fluctuating soil-water interface is likewise complicated. The multiphase flow that characterizes these scenarios depends on many parameters, including soil porosity, pore size, surface tension of the mobile fluid, and fluid capillary pressures. The migration of free-phase LNAPL and the behavior and dimensions of an LNAPL lens at the water table play a critical role in the subsequent dissolution or mass flux of LNAPL components into the groundwater.

In this study, the migration of free-phase LNAPL in soil was first explored using a semi-analytical model (HSSM) and a numerical model (TechFlowMP) for several idealized subsurface scenarios that approximate the conditions of interest at the HPIA. A dense model grid was used to analyze the downward movement of LNAPL through the unsaturated zone and subsequent lateral spreading of LNAPL at the water table. A coarse model grid was used to examine the development and expansion of an LNAPL lens at the water table. The temporal and spatial profiles of LNAPL saturation generated using the TechFlowMP and HSSM models showed good agreement.

Three computation schemes for LNAPL volume estimation were developed using apparent LNAPL measurements in monitor wells and calculated actual LNAPL thicknesses in soil and applying a semi-analytical solution as well as numerical integration techniques. The uncertainties associated with soil porosity and variations in Brooks-Corey equation parameter values (e.g., fluid-dependent scaling factors and saturation-capillary pressure characteristics) were explored using all three computation schemes. Overall, the LNAPL volume estimates ranged from 0.901 to 1.618 Mgal for the HPFF and Building 1613 areas combined. For a baseline scenario with soil porosity of 0.2 and parameter values corresponding to fresh gasoline, LNAPL volume estimates for the three computation schemes ranged from 0.939 Mgal to 1.079 Mgal for the combined areas. For a soil porosity of 0.3, the LNAPL volume estimates for all three computation schemes increased by 50 percent over the baseline estimates. Using Brooks-Corey equation parameter values corresponding to aged gasoline rather than fresh gasoline resulted in a 20-percent increase over the baseline LNAPL volume estimates for all three computation schemes. The LNAPL volume estimates calculated in this analysis for the baseline case (0.939–1.079 Mgal) are in good agreement with historical model-derived estimates (0.4–1.1 Mgal).

The TechNAPLVol model used to implement the computation schemes and estimate total LNAPL volume at the site was also used to generate a spatial profile of LNAPL saturation in the subsurface. This LNAPL saturation profile was programmed into the TechFlowMP model as the contaminant source for a fate and transport analysis of dissolved LNAPL components in groundwater at the HPIA. Benzene and total xylenes were selected as specific contaminants of interest for this analysis. Fate and transport processes included in the analysis were advection, mechanical dispersion, molecular diffusion, sorption, interphase mass transfer, and biological degradation. Flow-weighted simulation results indicate maximum dissolved benzene concentrations of 236 micrograms per liter (µg/L) in November 1984 and 179 µg/L in May 1996 at water-supply wells HP-602 and HP-603,[7] respectively. Sensitivity analyses for benzene transport indicate the associated ranges (upper and lower limits) of benzene concentration at these peak times are 138–378 µg/L for well HP-602 and 124–218 µg/L for well HP-603.

Reconstructed results for well HP-602 are consistent with reported benzene concentrations in water samples collected from the well during July 1984–January 1991. Reconstructed results for well HP-603 are not as consistent with reported benzene concentrations from water samples collected during December 1984–January 1995. Flow-weighted results for well HP-603 indicate a maximum benzene concentration of 365 µg/L; measured data are all below laboratory detection limits of 0.5–10 µg/L.

Differences between measured data and simulation results at well HP-602 and particularly well HP-603 may be due to a number of factors, including limitations of the numerical model and associated assumptions, uncertainties and variability in field (measured) data due to sampling methods, analytical methods, and the inherent natural variation in environmental systems and processes over time. Such variability is apparent in the reported benzene concentrations for well HP-602 that ranged from 720 µg/L to <1.0 µg/L to 230 µg/L during a 4-day period in 1984 (Table S7.10). Other factors pertaining to water-supply well operation and sampling protocols (when and how long a particular water-supply well had operated before sample collection) also may account for differences between measured data and simulation results. Additionally, it should be noted that the actual source start dates—the timeframe when fuel releases occurred—is unknown (undocumented) for the Building 1613 and HPFF areas. The source concentration and size of the source areas during much of the period of simulation are likewise uncertain.

The analyses developed and presented herein contain useful information about the subsurface migration of LNAPL and the dissolution and transport of benzene and total xylenes in the groundwater within the HPIA. The results from these analyses contribute to an understanding of the site contaminants and should be considered and integrated with results of other models developed as part of the overall project objective to produce estimates and uncertainty bounds for the concentration of contaminants over time in water-distribution systems of interest to the ATSDR health studies at USMCB Camp Lejeune.

[7] Wells HP-602 and HP-603 were reportedly shut down on November 30, 1984, and June 1, 1996, respectively (Sautner et al. 2013).

# References[8]


Abriola LM. Modeling Multiphase Migration of Organic Chemicals in Groundwater Systems—A Review and Assessment. Environmental Health Perspectives. 1989;83:117–143.

Abriola LM and Pinder GF. A Multiphase Approach to the Modeling of Porous Media Contamination by Organic Compounds. 1. Equation Development. Water Resources Research. 1985;21(1):11–18.

Agency for Toxic Substances and Disease Registry. Toxicological Profile for Gasoline. U.S. Department of Health and Human Services, Agency for Toxic Substances and Disease Registry; 1995.

Agency for Toxic Substances and Disease Registry. Toxicological Profile for Toluene. U.S. Department of Health and Human Services, Agency for Toxic Substances and Disease Registry, Public Health Service; 2000.

Agency for Toxic Substances and Disease Registry. Toxicological Profile for Xylene. U.S. Department of Health and Human Services, Agency for Toxic Substances and Disease Registry, Public Health Service, 2007.

Al-Suwaiyan MS, Bashir K, Aiban SA, and Ishaq AM. Analytical Model to Quantify Crude Oil Spill Volume in Sandy Layered Aquifers. Journal of Environmental Engineering. 2002;128(4):320–326.

Alagappan G and Cowan RM. Effect of Temperature and Dissolved Oxygen on the Growth Kinetics of Pseudomonas putida F1 Growing on Benzene and Toluene. Chemosphere. 2004;54(8):1255–1265.

American Petroleum Institute. Answers to Frequently Asked Questions about Managing Risk at LNAPL Sites. API Soil and Groundwater Research Bulletin Number 18. Washington DC; 2003; Available from *http://www.api.org/ehs/groundwater/upload/18_bull_hires.pdf* .

Andreoni V and Gianfreda L. Bioremediation and Monitoring of Aromatic-Polluted Habitats. Applied Microbiology and Biotechnology. 2007;76(2):287–308.

Aral MM. Environmental Modeling and Health Risk Analysis (Acts/Risk). Springer; 2010.

ASTM. Standard Guide for Conducting a Sensitivity Analysis for a Ground-Water Flow Model Application. ASTM Guide D5611-94 (Reapproved 2002). West Conshohocken, PA: ASTM; 1994.

ASTM. Standard Guide for Development of Conceptual Site Models and Remediation Strategies for Light Nonaqueous-Phase Liquids Released to the Subsurface, Designation: E2531–06. ASTM Committee E50 on Environmental Assessment, Risk Management and Corrective Action, DOI: 10.1520/E2531-06E01; 2007.

Auer LH, Rosenberg ND, Birdsell KH, and Whitney EM. The effects of barometric pumping on contaminant transport. Journal of Contaminant Hydrology. 1996;24(2):145–166.

Baker Environmental, Inc. Groundwater and Subsurface Petroleum Product Evaluation at the Former Hadnot Point Fuel Farm and Building 1115 Areas, Marine Corps Base, Camp Lejeune, North Carolina: A Preliminary Draft Report; 1996. Contained in UST Management Web Portal file #01185; p. 526–562.

Baker Environmental, Inc. Final Five-Year Review, Marine Corps Base Camp Lejeune, North Carolina; 1999. Contract Task Order 0099, Contract No.: N62470-89-D-4814 (CERCLA Administrative Record File #2332).

Barbaro JR, Barker JF, Lemon LA, and Mayfield CI. Biotransformation of BTEX under Anaerobic, Denitrifying Conditions—Field and Laboratory Observations. Journal of Contaminant Hydrology. 1992;11(3–4):245–272.

Bear J. Dynamics of Fluids in Porous Media. Environmental Science Series. American Elsevier; 1972.

Borden RC and Kao CM. Evaluation of Groundwater Extraction for Remediation of Petroleum-Contaminated Aquifers. Water Environment Research. 1992;64(1):28–36.

Brooks RH and Corey AT. Hydraulic Properties of Porous Media. Hydrology Paper 3. Fort Collins, Colorado: Colorado State University; 1964, 27 p.

Brooks RH and Corey AT. Properties of Porous Media Affecting Fluid Flow. Journal of the Irrigation and Drainage Division, American Society of Civil Engineers, IR2. 1966:61–88.

Brost EJ and DeVaull GE. Non-Aqueous Phase Liquid (NAPL) Mobility Limits in Soil.American Petroleum Institute Soil & Groundwater Research Bulletin. 2000;(9).

Catlin Engineers and Scientists. Well Sampling Report, Hadnot Point Fuel Farm, Volumes I&II, Marine Corps Base Camp Lejeune, North Carolina; 2001. Contract No.: N62470-95-D-6009 (UST Management Web Portal File #468).


[8] Certain documents have been provided to ATSDR by the Department of the Navy (Headquarters Marine Corps, Eastern Area Counsel Office, and Marine Corps Base Camp Lejeune) under terms of "For Official Use Only" (FOUO) documents. Some of these documents are not releasable by ATSDR under the terms of FOUO.

Catlin Engineers and Scientists. Revised Corrective Action Plan (CAP) for Hadnot Point Fuel Farm, Marine Corps Base Camp Lejeune, North Carolina; 2003. Contract No.: N62470-01-D-3009 (UST Management Web Portal File #418).

Celia MA, Bouloutas ET, and Zarba RL. A General Mass-Conservative Numerical Solution for the Unsaturated Flow Equation. Water Resources Research. 1990;26(7):1483–1496.

CH2M HILL, Inc.. Hadnot Point Fuel Farm/Building 1101, Remediation Assessment Report, Marine Corps Base Camp Lejeune, North Carolina; 2001. Contract No.: N62470-95-D-6007 (UST Management Web Portal File #670).

Charbeneau R and Adamski M. 2008. Developments in LNAPL Understanding, presented at the September 14, 2008, Site Assessment and Mitigation (SAM) forum organized by the San Diego County Department of Environmental Health. San Diego, CA. [cited 2012 February 29]; Available from *http://www.sdcounty.ca.gov/deh/water/docs/sam_forum_part_1_adamski.pdf*; 2011.

Cheremisinoff NP. Handbook of Hazardous Chemical Properties. Elsevier; 2000.

Chiang CY, Loos KR, and Klopp RA. Field Determination of Geological/Chemical Properties of an Aquifer by Cone Penetrometry and Headspace Analysis. Ground Water. 1992;30(3):428–436.

Cozzarelli IM, Bekins BA, Eganhouse RP, Warren E, and Essaid HI. In Situ Measurements of Volatile Aromatic Hydrocarbon Biodegradation Rates in Groundwater. Journal of Contaminant Hydrology. 2010;111(1–4):48–64.

Cullen AC and Frey HC. Probabilistic Techniques in Exposure Assessment: A Handbook for Dealing with Variability and Uncertainty in Models and Inputs. Plenum Press; 1999.

Davis JW, Klier NJ, and Carpenter CL. Natural Biological Attenuation of Benzene in Ground Water Beneath a Manufacturing Facility. Ground Water. 1994;32(2):215–226.

Deska I and Malina G. Estimation of Actual Free Product Thickness on the Groundwater Table Based on Soil and LNAPL Properties. In: Waclawek M, editor. Proceedings of ECOpole 2008, Volume 2. Proceedings of ECOpole. Opole: Opole University; 2008. p. 303–308.

Environmental Systems & Technologies. SpillCAD User and Technical Guide, ES&T Software, Ltd. Blacksburg, VA: ES&T; 1993.

Falta RW, Javandel I, Pruess K, and Witherspoon PA. Density-Driven Flow of Gas in the Unsaturated Zone Due to the Evaporation of Volatile Organic Compounds. Water Resources Research. 1989;25(10):2159–2169.

Farr AM, Houghtalen RJ, and McWhorter DB. Volume Estimation of Light Nonaqueous Phase Liquids in Porous Media. Ground Water. 1990;28(1):48–56.

Faust CR. Transport of Immiscible Fluids within and Below the Unsaturated Zone—A Numerical Model. Water Resources Research. 1985;21(4):587–596.

Faye RE. Analyses of Groundwater Flow, Contaminant Fate and Transport, and Distribution of Drinking Water at Tarawa Terrace and Vicinity, U.S. Marine Corps Base Camp Lejeune, North Carolina: Historical Reconstruction and Present-Day Conditions—Chapter F: Simulation of the Fate and Transport of Tetrachloroethylene (PCE). Atlanta, GA: Agency for Toxic Substances and Disease Registry; 2008.

Faye RE. Analyses and Historical Reconstruction of Groundwater Flow, Contaminant Fate and Transport, and Distribution of Drinking Water Within the Service Areas of the Hadnot Point and Holcomb Boulevard Water Treatment Plants and Vicinities, U.S. Marine Corps Base Camp Lejeune, North Carolina—Chapter B: Geohydrologic Framework of the Brewster Boulevard and Castle Hayne Aquifer Systems and the Tarawa Terrace Aquifer. Atlanta, GA: Agency for Toxic Substances and Disease Registry; 2012.

Faye RE, Anderson BA, Suárez-Soto RJ, and Sautner JB. Analyses and Historical Reconstruction of Groundwater Flow, Contaminant Fate and Transport, and Distribution of Drinking Water Within the Service Areas of the Hadnot Point and Holcomb Boulevard Water Treatment Plants and Vicinities, U.S. Marine Corps Base Camp Lejeune, North Carolina—Chapter C: Occurrence of Selected Contaminants in Groundwater at Installation Restoration Program Sites. Atlanta, GA: Agency for Toxic Substances and Disease Registry; 2010.

Faye RE, Suárez-Soto RJ, and Maslia ML. Analyses and Historical Reconstruction of Groundwater Flow, Contaminant Fate and Transport, and Distribution of Drinking Water Within the Service Areas of the Hadnot Point and Holcomb Boulevard Water Treatment Plants and Vicinities, U.S. Marine Corps Base Camp Lejeune, North Carolina—Chapter D: Occurrence of Selected Contaminants in Groundwater at Above-Ground and Underground Storage Tank (AST/UST) Sites. Atlanta, GA: Agency for Toxic Substances and Disease Registry; 2012.

Forsyth PA, Unger AJA, and Sudicky EA. Nonlinear iteration methods for nonequilibrium multiphase subsurface flow. Advances in Water Resources. 1998;21(6):433–449.

Frey CH and Patil SR. Identification and Review of Sensitivity Analysis Methods. Risk Analysis. 2002;22(3):553–578.

Frind EO. Simulation of long-term transient density-dependent transport in groundwater. Advances in Water Resources. 1982;5(2):73–88.

Golden Software I. Surfer version 10 Manual. Golden, CO; 2011.

Golder Associates. Guidance on Assessment of Light Non-Aqueous Phase Liquid Mobility for Site Classification Purposes in British Columbia, Report Submitted to BC Ministry of Environment, October 9, 2008; 45 p.

Harbaugh AW, Banta ER, Hill MC, and McDonald MG. MODFLOW-2000, the U.S. Geological Survey Modular Ground-Water Model—User Guide to Modularization Concepts and the Ground-Water Flow Process. U.S. Geological Survey Open-File Report 00–92; 2000. 121 p.

Harbaugh AW. MODFLOW-2005, The U.S. Geological Survey Modular Ground-Water Model—The Ground-Water Flow Processes. Reston, VA: U.S. Geological Survey Techniques and Methods 6-A16; 2005.

Hawthorne JM and Kirkman AJ. Residual, Mobile and Migrating LNAPL. Applied NAPL Science Review. 2011;1(10).

Hill MC, and Tiedeman CR. Effective Groundwater Model Calibration. Hoboken: John Wiley & Sons, Inc.; 2007.

Huntley D and Beckett GD. Evaluating Hydrocarbon Removal from Source Zones and Its Effect on Dissolved Plume Longevity and Magnitude. American Petroleum Institute, Publication Number 4715; 2002.

Huyakorn PS and Pinder GF. Computational Methods in Subsurface Flow: Academic Press; 1983.

Jang W and Aral MM. Three-Dimensional Multiphase Flow and Multi-Species Transport Model, TechFlowMP. Report No. MESL-02-05. Multimedia Environmental Simulations Laboratory, School of Civil and Environmental Engineering, Georgia Institute of Technology, Atlanta, GA; 2005.

Jang W and Aral MM. Modeling of Multiphase Flow and Contaminant Removal under In-Situ Air Sparging. Air & Waste Management Association's 99th Annual Conference & Exhibition, June 20–23, 2006. New Orleans, LA; 2006.

Jang W and Aral MM. Density-Driven Transport of Volatile Organic Compounds and Its Impact on Contaminated Groundwater Plume Evolution. Transport in Porous Media. 2007;67(3):353–374.

Jang W and Aral MM. Effect of Biotransformation on Multispecies Plume Evolution and Natural Attenuation. Transport in Porous Media. 2008a;72(2):207–226.

Jang W and Aral MM. Analyses of Groundwater Flow, Contaminant Fate and Transport, and Distribution of Drinking Water at Tarawa Terrace and Vicinity, U.S. Marine Corps Base Camp Lejeune, North Carolina: Historical Reconstruction and Present-Day Conditions—Chapter G: Simulation of Three-Dimensional Multispecies, Multiphase Mass Transport of Tetrachloroethylene (PCE) and Associated Degradation By-Products. Atlanta, GA: Agency for Toxic Substances and Disease Registry; 2008b.

Jones LE, Suárez-Soto RJ, Anderson BA, and Maslia ML. Characterization and Simulation of Fate and Transport of Selected Volatile Organic Compounds in the Vicinities of the Hadnot Point Industrial Area and Landfill—Supplement 6. In: Maslia ML, Suárez-Soto RJ, Sautner JB, Anderson BA, Jones LE, Faye RE, Aral MM, Guan J, Jang W, Telci IT, Grayman WM, Bove FJ, Ruckart PZ, and Moore SM. Analyses and Historical Reconstruction of Groundwater Flow, Contaminant Fate and Transport, and Distribution of Drinking Water Within the Service Areas of the Hadnot Point and Holcomb Boulevard Water Treatment Plants and Vicinities, U.S. Marine Corps Base Camp Lejeune, North Carolina—Chapter A: Summary and Findings. Atlanta, GA: Agency for Toxic Substances and Disease Registry; 2013.

Kaluarachchi JJ and Parker JC. An Efficient Finite-Element Method for Modeling Multiphase Flow. Water Resources Research. 1989;25(1):43–54.

Kechavarzi C, Soga K, and Wiart P. Multispectral Image Analysis Method to Determine Dynamic Fluid Saturation Distribution in Two-Dimensional Three-Fluid Phase Flow Laboratory Experiments. Journal of Contaminant Hydrology. 2000;46(3–4):265–293.

Lawrence SJ. Analyses of Groundwater Flow, Contaminant Fate and Transport, and Distribution of Drinking Water at Tarawa Terrace and Vicinity, U.S. Marine Corps Base Camp Lejeune, North Carolina: Historical Reconstruction and Present-Day Conditions—Chapter D: Properties of Degradation Pathways of Common Organic Compounds in Groundwater. Atlanta, GA: Agency for Toxic Substances and Disease Registry; 2007.

Lenhard RJ and Parker JC. Estimation of Free Hydrocarbon Volume from Fluid Levels in Monitoring Wells. Ground Water. 1990;28(1):57–67.

Lundegard PD and Mudford BS. LNAPL Volume Calculation: Parameter Estimation by Nonlinear Regression of Saturation Profiles. Ground Water Monitoring & Remediation. 1998;18(3):88–93.

Maslia ML, Suárez-Soto RJ, Wang J, Aral MM, Sautner JB, and Valenzuela C. Analyses of Groundwater Flow, Contaminant Fate and Transport, and Distribution of Drinking Water at Tarawa Terrace and Vicinity, U.S. Marine Corps Base Camp Lejeune, North Carolina: Historical Reconstruction and Present-Day Conditions—Chapter I: Parameter Sensitivity, Uncertainty, and Variability Associated with Model Simulations of Groundwater Flow, Contaminant Fate and Transport, and Distribution of Drinking Water. Atlanta, GA: Agency for Toxic Substances and Disease Registry; 2009.

Maslia ML, Suárez-Soto RJ, Sautner JB, Anderson BA, Jones LE, Faye RE, Aral MM, Guan J, Jang W, Telci IT, Grayman WM, Bove FJ, Ruckart PZ, and Moore SM. Analyses and Historical Reconstruction of Groundwater Flow, Contaminant Fate and Transport, and Distribution of Drinking Water Within the Service Areas of the Hadnot Point and Holcomb Boulevard Water Treatment Plants and Vicinities, U.S. Marine Corps Base Camp Lejeune, North Carolina—Chapter A: Summary and Findings. Atlanta, GA: Agency for Toxic Substances and Disease Registry; 2013.

Mayer A and Hassanizadeh SM. Soil and Groundwater Contamination: Nonaqueous Phase Liquids. American Geophysical Union, Water Resources Monograph; 2005.

McDonald MG and Harbaugh AW. A Modular Three-Dimensional Finite-Difference Groundwater-Flow Model. U.S. Geological Survey Open-File Report 83–875; 1984.

Mendoza CA and Frind EO. Advective-Dispersive Transport of Dense Organic Vapors in the Unsaturated Zone. 1. Model Development. Water Resources Research. 1990;26(3):379–387.

Mercer JW and Cohen RM. A Review of Immiscible Fluids in the Subsurface: Properties, Models, Characterization and Remediation. Journal of Contaminant Hydrology. 1990;6(2):107–163.

Millington RJ and Quirk JP. Permeability of Porous Solids. Transactions of the Faraday Society. 1961;57:1200–1207.

Moroizumi T and Sasaki Y. Estimating the Nonaqueous-Phase Liquid Content in Saturated Sandy Soil Using Amplitude Domain Reflectometry. Soil Science Society of America Journal. 2008;72(6):1520–1526.

National Toxicology Program. Report on Carcinogens, Twelfth. Research Triangle Park, NC: U.S. Department of Health and Human Services, Public Health Service, 2011.

Newell CJ, Acree SD, Ross RR, and Huling SG. Light Nonaqueous Phase Liquids. U.S. Environmental Protection Agency, EPA/540/S-95/500; 1995.

O'Brien and Gere Engineers, Inc. Final Report, Contaminated Ground Water Study, Marine Corps Base Camp Lejeune, North Carolina, Hadnot Point Area; 1988. Contract No.: N62470-86-C-8740 (CERCLA Administrative Record File #417; UST Management Web Portal File #669).

O'Brien and Gere Engineers, Inc. Preliminary Engineering Report, Product Recovery System Design, Hadnot Point Fuel Farm, Marine Corps Base Camp Lejeune, North Carolina; 1990. Contract No.: N62470-88-D-5825 (CERCLA Administrative Record File #382).

OHM Remediation Services Corp. Annual Monitoring Report, Building 1613, Marine Corps Base Camp Lejeune, Onslow County, North Carolina; 2000. Contract No.: N62470-97-5000 (UST Management Web Portal File #547).

OHM Remediation Services Corp. Final Closeout Report for Removal or Abandonment of Underground Fuel Oil Pipeline, Hadnot Point Fuel Farm/Buildings 1115, 1502, 1601, Marine Corps Base, Camp Lejeune, North Carolina; 2001. Contract No.: N62470-97-D-5700 (UST Management Web Portal File #417).

Parker JC and Lenhard RJ. Vertical Integration of Three-Phase Flow Equations for Analysis of Light Hydrocarbon Plume Movement. Transport in Porous Media. 1989;5(2):187–206.

Parker JC, Lenhard RJ, and Kuppusamy T. A Parametric Model for Constitutive Properties Governing Multiphase Flow in Porous Media. Water Resources Research. 1987;23(4):618–624.

Rathfelder K and Abriola LM. Mass Conservative Numerical Solutions of the Head-Based Richards Equation. Water Resources Research. 1994;30(9):2579–2586.

Rathfelder KM, Lang JR, and Abriola LM. A Numerical Model (MISER) for the Simulation of Coupled Physical, Chemical and Biological Processes in Soil Vapor Extraction and Bioventing Systems. Journal of Contaminant Hydrology. 2000;43(3–4):239–270.

Richard Catlin and Associates, Inc. Final Leaking Underground Storage Tank Comprehensive Site Assessment, Building 1613, USTs 1613 1–4, Marine Corps Base Camp Lejeune, North Carolina, Volumes I&II; 1996. Contract No. N62470-93-D-4020 (CERCLA Administrative Record File #90; UST Management Web Portal File #548).

Richard Catlin and Associates, Inc. Leaking Underground Storage Tank Corrective Action Plan, USTs 1613 1–4, Marine Corps Base Camp Lejeune, North Carolina; 1998. Contract No.: N62470-95-D-6009 (UST Management Web Portal File #546).

Sale T. Methods for Determining Inputs to Environmental Petroleum Hydrocarbon Mobility and Recovery Models. API Publication Number 4711; 2001.

Saltelli A, Chan K, and Scott EM, editors. Sensitivity Analysis. Chichester, England: John Wiley & Sons, Ltd.; 2000.

Sautner JB, Anderson BA, Suárez-Soto RJ, and Maslia ML. Descriptions and Characterizations of Data Pertinent to Water-Supply Well Capacities, Histories, and Operations—Supplement 1. In: Maslia ML, Suárez-Soto RJ, Sautner JB, Anderson BA, Jones LE, Faye RE, Aral MM, Guan J, Jang W, Telci IT, Grayman WM, Bove FJ, Ruckart PZ, and Moore SM. Analyses and Historical Reconstruction of Groundwater Flow, Contaminant Fate and Transport, and Distribution of Drinking Water Within the Service Areas of the Hadnot Point and Holcomb Boulevard Water Treatment Plants and Vicinities, U.S. Marine Corps Base Camp Lejeune, North Carolina—Chapter A: Summary and Findings. Atlanta, GA: Agency for Toxic Substances and Disease Registry; 2013.

Shaw Environmental, Inc. Final 2008–2009 Monitoring Report, Hadnot Point Fuel Farm/Building 1115 Sites, Marine Corps Base, Camp Lejeune, Onslow County, North Carolina; 2009. Contract No.: N62470-02-D-3260 (UST Management Web Portal File #HPFF_2009FinalAMR_Shaw).

Shoop S, Berini C, and Guyer R. Development of a Continuously Monitoring Resistivity Probe for Free-Phase Petroleum Hydrocarbons. In: Proceedings of the Symposium on the Application of Geophysics to Engineering and Environmental Problems; 1996. p. 11–20.

Sleep BE and Sykes JF. Modeling the Transport of Volatile Organics in Variably Saturated Media. Water Resources Research. 1989;25(1):81–92.

Suárez-Soto RJ, Jones LE, and Maslia ML. Simulation of Three-Dimensional Groundwater Flow—Supplement 4. In: Maslia ML, Suárez-Soto RJ, Sautner JB, Anderson BA, Jones LE, Faye RE, Aral MM, Guan J, Jang W, Telci IT, Grayman WM, Bove FJ, Ruckart PZ, and Moore SM. Analyses and Historical Reconstruction of Groundwater Flow, Contaminant Fate and Transport, and Distribution of Drinking Water Within the Service Areas of the Hadnot Point and Holcomb Boulevard Water Treatment Plants and Vicinities, U.S. Marine Corps Base Camp Lejeune, North Carolina—Chapter A: Summary and Findings. Atlanta, GA: Agency for Toxic Substances and Disease Registry; 2013.

Telci IT, Sautner JB, Suárez-Soto RJ, Anderson BA, Maslia ML, and Aral. Development and Application of a Methodology to Characterize Present-Day and Historical Water-Supply Well Operations—Supplement 2. In: Maslia ML, Suárez-Soto RJ, Sautner JB, Anderson BA, Jones LE, Faye RE, Aral MM, Guan J, Jang W, Telci IT, Grayman WM, Bove FJ, Ruckart PZ, and Moore SM. Analyses and Historical Reconstruction of Groundwater Flow, Contaminant Fate and Transport, and Distribution of Drinking Water Within the Service Areas of the Hadnot Point and Holcomb Boulevard Water Treatment Plants and Vicinities, U.S. Marine Corps Base Camp Lejeune, North Carolina—Chapter A: Summary and Findings. Atlanta, GA: Agency for Toxic Substances and Disease Registry; 2013.

Tucker WA and Nelken LH. Diffusion Coefficients in Air and Water Handbook of Chemical Property Estimation Methods: American Chemical Society; 1982.

Tung Y-K and Yen B-C. Hydrosystems Engineering Uncertainty Analysis. McGraw-Hill; 2005.

U.S. Environmental Protection Agency. Underground Motor Fuel Storage Tanks: A National Survey. Washington, DC: U.S. Environmental Protection Agency, EPA-560/5-86-013; 1986.

U.S. Environmental Protection Agency. Causes of Release From UST Systems. Washington, DC: U.S. Environmental Protection Agency, EPA 510-R-92-702; 1987.

U.S. Environmental Protection Agency. Soil Screening Guidance. U.S. Environmental Protection Agency, Technical Background Document, EPA/540/R-95/128; 1996.

U.S. Environmental Protection Agency. Carcinogenic Effects of Benzene: An Update. Washington, DC: U.S. Environmental Protection Agency, EPA/600/P-97/001F; 1998.

U.S. Environmental Protection Agency. Anaerobic Biodegradation Rates of Organic Chemicals in Groundwater: A Summary of Field and Laboratory Studies; 1999.

U.S. Environmental Protection Agency. Reregistration Eligibility Decision for Xylene, List C, Case No. 3020. Arlington, VA: U.S. Environmental Protection Agency; 2005.

UST Management Web Portal File, (file number and title vary and not consecutively available), provided to ATSDR in digital format by the Department of the Navy (Headquarters Marine Corps and Marine Corps Base Camp Lejeune) under terms of “For Official Use Only” (FOUO) documents, accessed 2010–2012.

van Genuchten MT. A Closed-Form Equation for Predicting the Hydraulic Conductivity of Unsaturated Soils. Soil Science Society of America Journal. 1980;44(5):892–898.

Water and Air Research, Inc. Initial Assessment Study of Marine Corps Base Camp Lejeune, North Carolina. Prepared for Naval Energy and Environmental Support Activity; 1983.

Weaver JW, Charbeneau RJ, Tauxe JD, Lien BK, and Provost JB. The Hydrocarbon Spill Screening Model (HSSM) Volume 1 User's Guide (Version 1.1 Rev. October 1996). Athens, GA: U.S. Environmental Protection Agency Office of Research and Development; 1996.

Weber WJ and DiGiano FA. Process Dynamics in Environmental Systems. Environmental Science and Technology: A Wiley-Interscience Series of Texts and Monographs; 1996.

Wiedemeier TH, Swanson MA, Wilson JT, Kampbell DH, Miller RN, and Hansen JE. Patterns of Intrinsic Bioremediation at Two United States Air Force Bases. In: Hinchee RE, Wilson JT, and Downey DC, editors. Intrinsic Bioremediation. Columbus, OH: Battelle Press; 1995. p. 31–51.

Wilson JT, Kampbell DH, and Armstrong J. Natural Bioreclamation of Alkylbenzenes (BTEX) from a Gasoline Spill in Methanogenic Groundwater. In: Hinchee RE, Miller RN, and Hoeppel RE, editors. Hydrocarbon Bioremediation. Boca Raton, FL: Lewis Publishers; 1994. p. 201–218.

Wu Y-S and Forsyth PA. On the Selection of Primary Variables in Numerical Formulation for Modeling Multiphase Flow in Porous Media. Journal of Contaminant Hydrology. 2001;48(3–4):277–304.

Zhu JT and Sykes JF. Simple Screening Models of NAPL Dissolution in the Subsurface. Journal of Contaminant Hydrology. 2004;72(1–4):245–258.

ATSDR
AGENCY FOR TOXIC SUBSTANCES AND DISEASE REGISTRY

# Analyses and Historical Reconstruction of Groundwater Flow, Contaminant Fate and Transport, and Distribution of Drinking Water Within the Service Areas of the Hadnot Point and Holcomb Boulevard Water Treatment Plants and Vicinities, U.S. Marine Corps Base Camp Lejeune, North Carolina—Chapter A–Supplement 7: Source Characterization and Simulation of the Migration of Light Nonaqueous Phase Liquids (LNAPLs) in the Vicinity of the Hadnot Point Industrial Area